Modélisation des espaces d’agriculture en environnement contrôlé à haute densité

par

Gilbert LAROCHELLE MARTIN

THÈSE PAR ARTICLES PRÉSENTÉE À L’ÉCOLE DE TECHNOLOGIE SUPÉRIEURE COMME EXIGENCE PARTIELLE À L’OBTENTION DU DOCTORAT EN GÉNIE
Ph.D.

MONTRÉAL, LE 1 AOÛT 2024

ÉCOLE DE TECHNOLOGIE SUPÉRIEURE
UNIVERSITÉ DU QUÉBEC

PRÉSENTATION DU JURY

CETTE THÈSE A ÉTÉ ÉVALUÉE

PAR UN JURY COMPOSÉ DE :

Mme Danielle Monfet, directrice de thèse
Département de génie de la construction à l'École de technologie supérieure

M. Stanislaw Kajl, président du jury
Département de génie mécanique à l'École de technologie supérieure

M. Daniel Rousse, membre du jury
Département de génie mécanique à l'École de technologie supérieure

M. Étienne Chantoiseau, examinateur externe
Département milieu physique, paysage, territoire à l'Institut Agro Rennes-Angers

ELLE A FAIT L'OBJET D'UNE SOUTENANCE DEVANT JURY ET PUBLIC

LE 24 JUILLET 2024

À L'ÉCOLE DE TECHNOLOGIE SUPÉRIEURE

REMERCIEMENTS

Je tiens à remercier les membres du jury de leurs commentaires et suggestions visant l'amélioration de cette thèse. J'aimerais remercier ma directrice, Mme Danielle Monfet, pour son soutien, sa disponibilité et sa patience qui ont permis de m'orienter vers la voie de la réussite en recherche. Je tiens également à remercier mes collègues du laboratoire des technologies de l'énergie pour leur appui lors de la rédaction de cette thèse.

La réalisation de cette thèse n'a pas été sans obstacle. De nombreux défis se sont présentés sur mon parcours, mais j'ai pu les surmonter grâce au soutien indéfectible de ma famille et de mes amis. Je suis reconnaissant pour leur patience, leurs encouragements et leur présence tout au long de ces années.

Modélisation des espaces d'agriculture en environnement contrôlé à haute densité

Gilbert LAROCHELLE MARTIN

RÉSUMÉ

L'agriculture en environnement contrôlé (AEC), tel que les serres, et l'agriculture en environnement contrôlé à haute densité (AEC-HD), aussi connu sous les termes « *plant factory* » ou « *vertical farm* », visent à augmenter la productivité en découplant le microclimat de production des aléas de la météo, ce qui augmente considérablement la consommation d'énergie. De plus, l'uniformité du microclimat de production est essentielle pour obtenir un produit uniforme et mitiger l'apparition de maladies. Actuellement, les modèles énergétiques d'espaces d'AEC, souvent développés pour une application précise, ne sont pas assez flexibles pour un usage général et ne sont pas disponibles publiquement. Il n'existe pas actuellement d'outils de simulation énergétiques validés permettant de modéliser adéquatement les interactions énergétiques des espaces d'AEC, et par extension des espaces d'AEC-HD qui permettent de quantifier l'impact de différentes enceintes, systèmes énergétiques et contrôles.

Ainsi, l'objectif principal des travaux de recherche de cette thèse est de développer une méthode de modélisation énergétique des espaces d'AEC-HD basé sur l'utilisation d'outils de simulation de la performance énergétique du bâtiment (BPS) en tenant compte de l'uniformité du microclimat de production. La méthodologie utilisée est basée sur la modification d'outils existants de dynamique des fluides numériques (CFD) et de BPS, c.-à-d. ANSYS Fluent et EnergyPlus, afin d'y intégrer les phénomènes physiques associés aux plantes cultivées. Cette thèse par article aborde plusieurs facettes de la modélisation des espaces d'agriculture en environnement contrôlé à haute densité (AEC-HD) tel que le bilan d'énergie à la feuille, la photosynthèse, la résistance à l'écoulement et l'impact des coefficients de transfert de chaleur convectifs des surfaces internes sur les résultats de simulation.

Cette thèse apporte trois contributions originales soit : (1) une méthode d'optimisation de la distribution de l'air dans un espace d'AEC-HD tenant compte de l'uniformité du microclimat de production, (2) l'intégration de la résolution du bilan d'énergie à la feuille dans un outil de BPS à l'aide d'une interface graphique simplifiée et (3) l'évaluation des algorithmes de calcul des coefficients de transfert de chaleur convectifs (CHTCs) des surfaces internes à partir de valeurs de références issues d'un modèle CFD pour leur utilisation dans un outil BPS. Ces trois contributions viennent épauler les professionnels du domaine de la mécanique du bâtiment qui pourront améliorer leur processus de modélisation, de conception et d'opération des espaces d'AEC-HD et des systèmes énergétiques associés à ces espaces.

Mots-clés: Dynamique numérique des fluides (CFD), simulation énergétique du bâtiment (BPS), agriculture en environnement contrôlé à haute densité (AEC-HD), modèle de plante, optimisation, coefficients de transfert de chaleur convectifs (CHTCs)

High-density controlled environment agriculture spaces modelling

Gilbert LAROCHELLE MARTIN

ABSTRACT

Controlled environment agriculture (CEA), such as greenhouses, and high-density controlled environment agriculture (CEA-HD), also known as « *plant factory* » or « *vertical farm* », aim to raise yield by decoupling the production microclimate from weather variations, which raises considerably the energy consumption. Furthermore, the production microclimate uniformity is essential to obtain a uniform product and mitigate diseases. Currently, CEA energy models are often developed for a specific application, are not flexible enough and are not available publicly. Currently, no validated energy modelling software is capable of accurately simulating the complex energy interactions within CEA production spaces and, consequently, CEA-HD facilities. This hinders quantifying energy consumption impacts associated with various wall constructions, energy systems, and control implementations.

Therefore, the main objective of this research thesis is to develop an energy modelling method for CEA-HD spaces based on the use of building performance simulation (BPS) tools while considering the production microclimate uniformity. The methodology used is based on modifying existing computational fluid dynamics (CFD) and BPS tools, i.e., ANSYS Fluent and EnergyPlus, and integrating the physical phenomena associated with the crops cultivated. This article-based thesis addresses several aspects of high-density controlled environment agriculture (CEA-HD) space modelling, such as leaf energy balance, photosynthesis, flow resistance, and the impact of internal surface convective heat transfer coefficients on simulation results.

This thesis makes three original contributions: (1) a method for optimizing air distribution in CEA-HD spaces while considering the production microclimate uniformity, (2) the integration of a leaf energy balance resolution algorithm into a BPS tool using a simplified graphical interface and (3) an internal surface convective heat transfer coefficients (CHTCs) algorithms evaluation based on reference values from a CFD model for their use in a BPS tool.

These three contributions will support building engineering professionals, enabling them to enhance their CEA-HD spaces and associated energy systems modelling, design, and operation.

Keywords: Computational fluid dynamics (CFD), building performance simulation (BPS), high-density controlled environment agriculture (CEA-HD), crop model, optimization, convective heat transfer coefficients (CHTCs)

TABLE DES MATIÈRES

Page

LISTE DES TABLEAUX

Page

LISTE DES FIGURES

LISTE DES ABRÉVIATIONS, SIGLES ET ACRONYMES

ACH	« *air changes per hour* »
AEC	agriculture en environnement contrôlé
AEC-HD	agriculture en environnement contrôlé à haute densité
API	interface de programmation
BEM	« *building energy model* »
BI-CEA	« *building integrated controlled environment agriculture* »
BPS	performance énergétique du bâtiment
CAC	« *cultivation area cover* »
CD	« *cultivated density* »
CEA	« *controlled environment agriculture* »
CEA-HD	« *high-density controlled environment agriculture* »
CFD	dynamique des fluides numériques
CHTC	coefficient de transfert de chaleur convectif
COV	covariance
CV	« *coefficient of variation* »
CVCA	chauffage, ventilation et conditionnement de l'air
CV-RMSE	« *coefficient of variation of the root mean square error* »
DLI	« *Daily Light Integral* »
EMS	« *energy management system* »
ePAR	« *extended photosynthetically active radiation* »
GUI	« *graphical user interface* »
HPS	sodium haute pression

HVAC	« *Heating, Ventilation and Air Conditioning* »
LAD	« *Leaf Area Density* »
LAI	indice foliaire, « *Leaf Area Index* »
LED	diodes électroluminescentes
NFT	« *nutrient film technique* »
NMBE	« *normalised mean bias error* »
PAR	« *photosynthetically active radiation* »
PIV	« *particle image velocimetry* »
PPFD	densité du flux de photon photosynthétique
RANS	« *Reynolds Averaged Navier Stokes* »
UDF	fonction définie par l'utilisateur
VPD	déficit de pression de vapeur

LISTE DES SYMBOLES ET UNITÉS DE MESURE

A_i	aire de la surface	[m^2]
ACH	changements d'air par heure	[ACH]
CAC	« cultivation area cover »	[-]
C_D	coefficient de trainée	[-]
C_p	chaleur spécifique à pression constante	[$J \cdot kg^{-1} \cdot K^{-1}$]
C_z	capacité thermique de la zone	[$J \cdot m^3 \cdot K^{-1}$]
D_h	diamètre hydraulique	[m]
D_T	diffusivité turbulente	[$m^{-2} \cdot s^{-1}$]
E_{ij}	composante de vitesse de déformation	[s^{-1}]
f_v	fraction visible	[-]
$\boldsymbol{F}$	vecteur des forces externes	[N]
$\boldsymbol{g}$	vecteur de gravité	[$m \cdot s^{-2}$]
Gr	nombre de Grashof	[-]
H	flux de chaleur sensible	[$W \cdot m^{-2}$]
H	hauteur caractéristique	[m]
h_c	coefficients de transfert de chaleur convectifs	[$W \cdot m^{-2} \cdot K^{-1}$]
h_{ci}	coefficients de transfert de chaleur convectifs	[$W \cdot m^{-2} \cdot K^{-1}$]
h_i	coefficients de transfert de chaleur convectifs	[$W \cdot m^{-2} \cdot K^{-1}$]
h_j	enthalpie	[$kJ \cdot kg^{-1}$]
I_s	rayonnement à ondes courtes	[$W \cdot m^{-2}$]
J	flux de diffusion	[$kg \cdot m^{-2} \cdot s^{-1}$]

k	énergie cinétique turbulente	$[m^2 \cdot s^{-2}]$
K	perméabilité	$[m^2]$
K_1	perméabilité inertielle	[m]
k_{eff}	conductivité effective	$[W \cdot m^{-1} \cdot K^{-1}]$
L	longueur caractéristique	[m]
LAD	«*Leaf Area Density*»	$[m^{-1}]$
LAI	Indice foliaire, « Leaf Area Index »	[-]
LE	flux de chaleur latent	$[W \cdot m^{-2}]$
$\dot{m}_i$	débit massique interzone	$[kg \cdot s^{-1}]$
$\dot{m}_{inf}$	débit massique d'infiltration	$[kg \cdot s^{-1}]$
n_{tiers}	nombre d'étages du système de production	[-]
P_{cell}	taux de photosynthèse net	$[\mu mol \cdot s^{-1}]$
P_{el}	densité de puissance électrique d'éclairage	$[W \cdot m^{-2}]$
PPE	« photosynthetic photon efficiency »	$[\mu mol \cdot J^{-1}]$
PPFD	densité de flux de photons photosynthétiques	$[\mu mol \cdot s^{-1} \cdot m^{-2}]$
Pr	nombre de Prandtl	[-]
p_{ws}	pression de vapeur à saturation	[Pa]
q	flux de fluide	$[m \cdot s^{-1}]$
$q''_{LWX,plt}$	rayonnement à ondes longues	$[W \cdot m^{-2}]$
$q''_{SW,plt}$	rayonnement à ondes courtes	$[W \cdot m^{-2}]$
$q''_{conv,plt}$	flux de chaleur convectif sensible	$[W \cdot m^{-2}]$
$q''_{latent,plt}$	flux de chaleur latent	$[W \cdot m^{-2}]$

q_s	« surface adjacent cell heat flux »	$[W\cdot m^{-2}]$
$\overline{q}_s$	« surface average heat flux »	$[W\cdot m^{-2}]$
q''_{soil}	conduction par le sol	$[W\cdot m^{-2}]$
$\dot{Q}_i$	gains convectifs de la zone	[W]
$\dot{Q}_{sys}$	flux d'énergie des systèmes CVCA	[W]
$r_{X,Y}$	coefficient de corrélation de Pearson	[-]
r_a	résistance aérodynamique	$[s\cdot m^{-1}]$
r_s	résistance stomatale	$[s\cdot m^{-1}]$
r_{sl}	résistance stomatale	$[s\cdot m^{-1}]$
Ra	nombre de Rayleigh	[-]
Re	nombre de Reynolds	[-]
R_i	taux de production net	$[kg\cdot m^{-3}\cdot s^{-1}]$
R_n	rayonnement net	$[W\cdot m^{-2}]$
s	vitesse de l'écoulement d'air	$[m\cdot s^{-1}]$
S_h	source de chaleur volumétrique	$[W\cdot m^{-3}]$
Sc_t	nombre de Schmidt turbulent	[-]
S_i	source d'espèce	$[kg\cdot m^{-3}\cdot s^{-1}]$
t	temps	[s]
T	température	[K]
T_∞	température de l'air extérieur	[ºC]
T_{SA}	température de soufflage	[ºC]
T_a	température de l'air ambiant	[ºC]
T_{air}	température de l'air	[ºC]

T_{plt}	température de la feuille	[ºC]
$\widehat{T_{plt}}$	estimé de la température de la feuille	[ºC]
T_{si}	température de la surface	[ºC]
T_z	température de la zone	[ºC]
T_{zi}	température de la zone adjacente	[ºC]
$u_{x,y}$	vélocité cartésienne	[m·s^{-1}]
$\boldsymbol{V}$	vecteur de la vitesse d'écoulement	[m·s^{-1}]
VPD	déficit de pression de vapeur	[Pa]
$\boldsymbol{x}$	vecteur position $[x, y, z]$	[m]
y^+	distance de la paroi adimensionnelle	[-]
Y_i	fraction de masse locale	[kg·kg^{-1}]

Lettres grecques

γ	constante psychrométrique	[Pa·ºC^{-1}]
Δ	pente de la pression de vapeur de saturation	[Pa·ºC^{-1}]
ΔP	perte de charge	[Pa]
ΔT	différence de température	[ºC]
Δx	longueur du média poreux	[m]
ε	slope of the saturation function curve	[-]
ε	taux de dissipation de l'énergie cinétique turbulente	[m^2·s^{-3}]
η_t	viscosité turbulente	[Pa·s^{-1}]
θ	angle de la surface	[º]

λ	chaleur latente d'évaporation	$[J \cdot g^{-1}]$
μ	moyenne	
μ	viscosité	$[Pa \cdot s^{-1}]$
μ_T	viscosité de turbulence	$[kg \cdot m^{-1} \cdot s^{-1}]$
ρ	densité	$[kg \cdot m^{-3}]$
$\rho_{a\cdot}$	densité de l'air	$[kg \cdot m^{-3}]$
ρ_{plt}	réflectivité de la feuille	[-]
ρ_r	réflectivité de la feuille	[-]
σ	écart type	
$\bar{\bar{\tau}}$	tenseur des contraintes	[Pa]
$\bar{\bar{\tau}}_{eff}$	tenseur déviatorique des contraintes	[Pa]
τ_{plt}	transmissivité de la feuille	[-]
τ_w	contrainte de cisaillement à la paroi	[Pa]
χ_a	concentration de vapeur dans l'air ambiant	$[g \cdot m^{-3}]$
χ_s	concentration de vapeur à la surface de la feuille	$[g \cdot m^{-3}]$
ω_n	humidité absolue	$[kg \cdot kg^{-1}]$

INTRODUCTION

La population mondiale devrait atteindre 9.7 milliards d'habitants d'ici 2050 (UN, 2015). Cette augmentation de la population mondiale engendrera une demande plus élevée de 50 % pour les produits de l'agriculture à l'horizon 2050. De plus, la pandémie de SARS-Cov-2 causant la maladie COVID-19 a remis en question la résilience des chaînes d'approvisionnement globales et renouvelé l'intérêt public et scientifique face à l'amélioration de la souveraineté alimentaire.

L'une des solutions envisagées afin d'adresser cette problématique est l'augmentation de la production de fruits et légumes en environnement contrôlé. L'agriculture en environnement contrôlé (AEC) est une méthode de production agricole définie par : (1) l'utilisation d'une enceinte de production découplant le microclimat de production des aléas de la météo et (2) la régulation de ce microclimat par un système énergétique actif. La régulation du microclimat de production contrôle la température, l'humidité, la concentration de CO_2, la vitesse de l'écoulement d'air et le niveau d'éclairement à des niveaux adaptés pour la plante cultivée. L'objectif de cette régulation est de maximiser le rendement de production, la qualité du produit et l'efficacité d'utilisation des ressources en plus de minimiser les stress abiotiques et l'apparition de maladies. La production effectuée en AEC se décline en trois groupes principaux : (1) la production maraîchère (fruits et légumes), (2) la production horticole (fleurs) et (3) la production de cannabis. La production maraîchère en serre au Québec en 2021 représente 151 ha et 624 compagnies. Les plantes produites en serre au Québec sont principalement : la tomate (69 ha), du concombre (42), la laitue (15 ha) et le poivron (8 ha) (Gouvernement du Québec, 2024). Plusieurs changements ont été apportés à l'environnement économique québécois de la production maraîchère en environnement contrôlé au début des années 2020. En effet, le gouvernement du Québec a adopté une stratégie de croissance de la production en serres à l'horizon 2020-2025 visant à doubler le volume de la culture de fruits et des légumes en serre (Gouvernement du Québec, 2020). À l'aube de 2024, le volume de production a déjà presque doublé avec une augmentation des superficies cultivées de 66 ha (Cameron, 2023). De plus, la consommation d'énergie électrique associée au chauffage des espaces destinés à la culture de végétaux est désormais (depuis 2020) admissible au tarif préférentiel de 6.164 ¢·kWh^{-1} en plus de l'éclairage de photosynthèse. Le tarif est dit interruptible puisque le tarif grimpe à 58.168 ¢·kWh^{-1} lors des périodes de grande demande typiquement d'une centaine d'heures par année.

De plus, ce tarif s'applique aussi à d'autres types d'enceintes de production en AEC encore en émergence, telle que les espaces d'agriculture en environnement contrôlé à haute densité (AEC-HD), aussi connue sous la terminologie de fermes verticales («*vertical farm*» ou «*Plant Factory*») qui est effectuée sous un éclairage complètement artificiel dans des bâtiments très isolés thermiquement. Ces espaces sont munis de systèmes de production où plusieurs plants de culture sont agencés de façon à occuper l'espace le plus efficacement possible. Ce type d'AEC comporte plusieurs avantages tels qu'une utilisation plus efficace des ressources, une productivité par unité de surface supérieure, une production sans pesticides et une production prévisible de haute qualité (Kozai, 2018). Ces installations engendrent toutefois une consommation énergétique importante. En effet, les installations industrielles d'AEC-HD ont actuellement une puissance entre 6 à 8 MW, avec une consommation énergétique pouvant atteindre 70 000 MWh par an. De plus grandes installations sont également en cours de planification (EPRI, 2018).

0.1 Problématique

Un des obstacles importants à la commercialisation de l'AEC est la consommation énergétique associée à l'éclairage et au maintien du microclimat de production (Scott et al., 2005). Des modèles énergétiques d'espaces d'AEC ont été proposés dans la littérature pour améliorer la prédiction de l'appel de puissance et de la consommation énergétique de ces espaces (Deltour et al., 1985; Pieters & Deltour, 1999; Roy et al., 2002; Graamans et al., 2017; Iddio et al., 2020; Weidner et al., 2021). Toutefois, ces modèles sont souvent développés spécifiquement pour une application précise, ne sont pas assez flexibles pour un usage général et ne sont pas disponibles publiquement. Par conséquent, il est nécessaire de déployer des outils permettant le développement d'un modèle énergétique pour les espaces d'AEC prenant en compte les variables du microclimat de production et quantifiant l'impact de différent type d'enceintes, de systèmes énergétiques et de contrôles.

Les outils logiciels développés pour le domaine de la modélisation de la performance des bâtiments (BPS) pourraient contribuer à résoudre une partie de ce problème. En effet, ces outils sont utilisés par divers professionnels pour la modélisation énergétique de bâtiments destinés à différents usages en prenant en compte différentes géométries et la modélisation de systèmes énergétiques diversifiés. Cependant, il n'existe actuellement pas d'outils de BPS permettant de modéliser nativement les interactions énergétiques des espaces d'AEC, et par extension des espaces d'AEC-HD, incluant la contribution des plantes comme source interne de pertes ou gains (Talbot & Monfet, 2020). La contribution des plantes varie selon les conditions de l'environnement intérieur et peut grandement influencer les besoins en refroidissement, déshumidification, chauffage et humidification des espaces d'AEC-HD (Talbot & Monfet, 2024). En plus de la modélisation adéquate des échanges énergétiques, l'uniformisation du microclimat de production reste un défi présent pour les systèmes de production en AEC-HD (Jiang et al., 2018a). En effet, le poids des plantes récolté peut varier en fonction de leur position dans l'espace en raison d'une mauvaise uniformité (Chang et al., 2011). De plus, l'écoulement de l'air altère l'épaisseur de la couche limite à la feuille, ce qui influence les taux de diffusion de la chaleur, de la vapeur d'eau et du dioxyde de carbone (Zhang & Kacira, 2022). La distribution spatiale du microclimat de production exerce donc une influence sur la consommation énergétique, l'apparition de maladies et la qualité des produits. Ainsi, la modélisation spatiale de l'environnement de l'AEC pourrait mener à une conception et un contrôle plus efficace des systèmes CVCA de ces espaces, résultant en des économies de ressources, d'énergie et de moyens (Boulard et al., 2002). L'uniformisation du microclimat de production est donc interreliée avec la performance énergétique d'une production en AEC.

0.2 Objectifs

L'objectif principal de cette thèse est de développer une méthode de modélisation énergétique des espaces d'AEC basée sur l'utilisation d'outils de simulation de la performance énergétique du bâtiment (BPS) en tenant compte de l'uniformité du microclimat de production. Cet objectif est décliné en plusieurs sous-objectifs :

(1) Optimiser la distribution de l'air afin d'uniformiser la distribution spatiale des variables du microclimat de production;

(2) Intégrer le calcul du bilan d'énergie à la feuille dans un logiciel de simulation énergétique du bâtiment supporté, validé, gratuit et publiquement disponible;

(3) Évaluer la performance des algorithmes de calcul des coefficients de transfert de chaleur convectifs (CHTCs) du logiciel de simulation énergétique du bâtiment sélectionné pour la distribution de l'air optimisée.

Cette thèse se limite aux aspects énergétiques et de mécanique des fluides des espaces d'AEC-HD. Plusieurs autres considérations agronomiques peuvent exercer une influence sur les décisions de production et ne sont pas abordées dans cette thèse. Bien qu'étroitement reliées à la modélisation des espaces d'AEC-HD, la modélisation énergétique et de la mécanique des fluides des serres ne sont pas explicitement réalisées dans cette thèse. Toutefois, plusieurs principes peuvent être appliqués, avec des modifications mineures, à la modélisation énergétique et de la dynamique des fluides des serres. Cette thèse par article est scindée en huit sections : (1) revue de la littérature scientifique permettant de contextualiser les contributions des articles, (2) méthodologie globale utilisée dans la réalisation de ce travail de recherche, (3) méthode d'optimisation de la distribution de l'air dans les espaces d'AEC-HD par l'utilisation de la CFD et d'un algorithme d'optimisation évolutionnaire (article #1), (4) méthode de modélisation de la transpiration dans un outil de simulation de la performance des bâtiments (article #2), (5) impact de l'utilisation des algorithmes de calcul des coefficients de convection des surfaces internes des outils de BPS pour la modélisation énergétique des espaces d'AEC-HD (article #3), (6) discussion des résultats obtenus et (7) conclusion suivie de (8) recommandations pour les prochaines initiatives de recherche au sujet de la modélisation des espaces d'AEC-HD.

CHAPITRE 1

REVUE DE LITTÉRATURE

Cette section présente une revue de la littérature complémentaire à celles des trois articles scientifiques de cette thèse. Ce complément vise à introduire différentes notions essentielles à la compréhension de cet ouvrage et à mettre en contexte les contributions scientifiques. Ce chapitre se décline donc par une introduction aux trois principaux domaines abordés soit : (1) la simulation énergétique du bâtiment, (2) la modélisation énergétique des espaces d'agriculture en environnement contrôlé (AEC) et (3) la dynamique des fluides numérique (CFD).

1.1 Simulation énergétique du bâtiment

Les outils de modélisation énergétique du bâtiment («*Building Energy Modelling*» (BEM)) ou de la simulation de la performance des bâtiments («*Building Performance Simulation*» (BPS)) sont des outils logiciels utilisant une représentation thermique simplifiée d'un immeuble, de ses systèmes énergétiques et de ses occupants afin d'effectuer des analyses énergétiques. Ces outils évaluent les transferts d'énergie effectués à travers l'enveloppe du bâtiment, au sein de ses zones thermiques et par ses systèmes de chauffage, ventilation et conditionnement d'air (CVCA). Une zone thermique peut être définie comme un espace ou un regroupement d'espaces d'un bâtiment ayant les mêmes points de consignes et besoins de régulation. Le domaine de la simulation énergétique des bâtiments est un domaine scientifique mature dont les avancées techniques sont utilisées par différents professionnels tels que les ingénieurs en mécanique du bâtiment et les architectes. Les outils de simulation énergétiques sont nombreux et variés. En effet, certains sont très simplifiés (p. ex. SIMEB (Millette et al., 2011), HOT2000 (Bradley & Riley, 1991)) tandis que d'autres sont très complexes et essentiellement réservés à la recherche (p. ex. ESP-R (Strachan et al., 2008), Spawn (Wetter et al., 2023)). Dans cette thèse, l'outil de modélisation utilisé est le logiciel EnergyPlus (Crawley et al., 2001) et des résultats de simulation issus du logiciel TRNSYS (Fiksel et al., 1995) sont utilisés pour fins de comparaison.

Le logiciel EnergyPlus est un logiciel gratuit, développé par plusieurs laboratoires de recherche américains et supporté par le département de l'énergie américain (DOE). La modélisation avec le logiciel EnergyPlus est basée sur l'utilisation de fichiers textes pour établir une représentation thermique simplifiée du bâtiment et de ses systèmes énergétiques. Des interfaces de développeurs tiers peuvent être utilisées pour faciliter la construction de ces fichiers textes. Des configurations typiques de systèmes énergétiques sont proposées par le logiciel permettant de modéliser facilement des dispositions de systèmes CVCA typiques en plus de permettre la modélisation par composantes pour des dispositions particulières. Ce logiciel est utilisé pour plusieurs usages tels que la recherche (plus de 1800 citations de l'article original), l'évaluation de la conformité (CNÉB-2015 QC, ASHRAE 90.1), la conception (DesignBuilder, OpenStudio) et l'optimisation (JePlus, BEopt) de bâtiments.

Le logiciel TRNSYS est un logiciel payant utilisant une approche de modélisation par composantes, appelées types, qui sont reliées entre elles à l'aide d'une interface graphique, appelée studio. Une méthode d'itération successive est utilisée par le logiciel pour assurer une convergence entre les différents types utilisés dans le modèle énergétique à chaque pas de temps de simulation. Plusieurs types, variant en complexité, sont disponibles dans le logiciel pour modéliser les différents aspects énergétiques du bâtiment allant des charges thermiques au contrôle des systèmes CVCA. L'approche de modélisation par types utilisée par le logiciel TRNSYS facilite l'ajout de capacités de modélisation par l'utilisateur en lui permettant d'ajouter ses propres types au logiciel. TRNSYS ne propose pas de configurations typiques de systèmes CVCA et repose exclusivement sur la modélisation par composantes.

Une description détaillée des capacités de modélisation et des principales hypothèses de modélisation utilisées par les logiciels EnergyPlus, TRNSYS et par d'autres logiciels de simulation énergétique du bâtiment populaires a été proposée par Crawley et al. (2008). Pour la suite de cette revue de littérature, l'accent est porté sur l'outil de modélisation énergétique du bâtiment utilisé dans cette thèse : EnergyPlus.

Le logiciel EnergyPlus regroupe plusieurs modules pour modéliser divers aspects énergétiques du bâtiment. La Figure 1.1 illustre les liens entre les principaux modules de simulation du logiciel EnergyPlus.

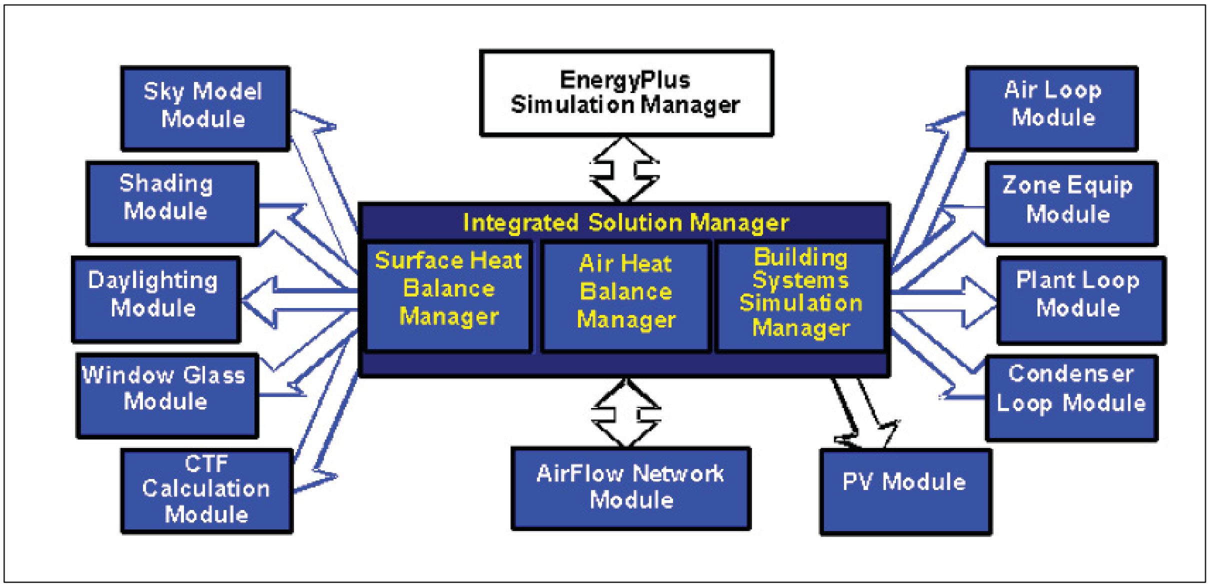

Figure 1.1 Diagramme général des différents modules de simulation du logiciel EnergyPlus
Tirée de la documentation du logiciel EnergyPlus

Les modules à la gauche de la Figure 1.1 sont associés à la modélisation du rayonnement solaire et de la conduction à travers l'enveloppe tandis que les modules à la droite de la Figure 1.1 sont associés à la modélisation de la performance des systèmes de chauffage, ventilation et conditionnement d'air (CVCA). Les modules au centre de la Figure 1.1 sont utilisés pour effectuer le bilan thermique des surfaces internes et externes du bâtiment modélisé, de l'air de la zone thermique ainsi que des charges comblées par les systèmes CVCA. Pour l'ajout de sources internes, tel que l'effet des plantes, l'élément le plus important est le «*Air Heat Balance Manager*». Cet élément représente l'application de la méthode du bilan thermique sur un nœud d'une zone thermique. L'état de l'air de la zone thermique est usuellement représenté par un seul nœud en utilisant l'hypothèse d'une zone thermique parfaitement brassée («*well stired hypothesis*»). La Figure 1.2 illustre la méthode du bilan thermique utilisée dans le logiciel EnergyPlus.

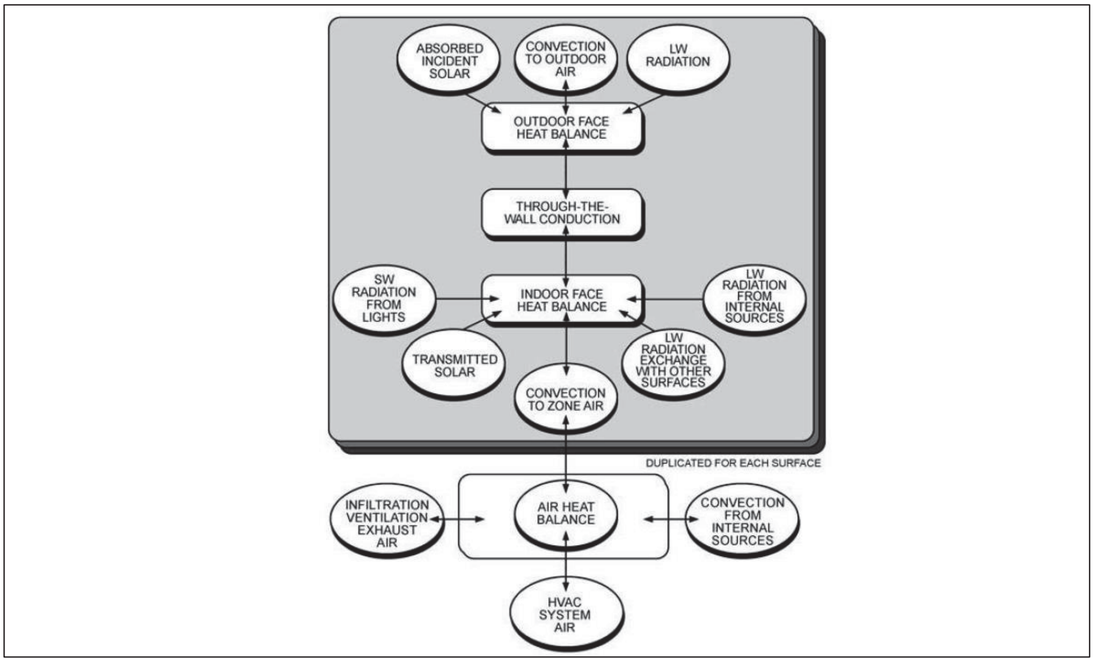

Figure 1.2 Diagramme de la méthode du bilan thermique
Tirée de American Society of Heating and Air-Conditioning Engineers (2021)

Le bilan d'énergie de la modélisation des plantes (section 1.2.3.1) ajoute une dimension supplémentaire au bilan thermique de la zone. De plus, les coefficients de transfert de chaleur convectif (CHTCs) calculé par la dynamique des fluides numérique (CFD) et par les algorithmes du logiciel de simulation énergétique (voir Chapitre 5) exercent une influence directe sur le flux de chaleur convectif entre l'air de la zone thermique et les surfaces internes. L'équation (1.1) est l'équation différentielle à résoudre pour obtenir la prédiction de la température d'une zone thermique dans le logiciel EnergyPlus. La méthode numérique couramment utilisée pour résoudre cette équation est une expansion en série de Taylor du troisième ordre vers l'arrière. Avec cette approche, l'équation (1.2) est utilisée comme approximation de la dérivée partielle. L'équation de mise à jour de la température de la zone est obtenue en substituant l'équation (1.2) dans l'équation (1.1). L'équivalent de l'équation (1.1) et (1.2) est aussi effectué pour le bilan de masse de vapeur d'eau dans la zone. Le bilan d'énergie à la feuille de la modélisation des plantes ajoute aussi un terme à l'équation du bilan de masse de la zone.

$$C_z \frac{dT_z}{dt} = \sum_{i=1}^{N_{\dot{Q}}} \dot{Q}_i + \sum_{i=1}^{N_{surfaces}} h_i A_i (T_{si} - T_z) + \sum_{i=1}^{N_{zones}} \dot{m}_i C_p (T_{zi} - T_z) + \dot{m}_{inf} C_p (T_\infty - T_z) + \dot{Q}_{sys} \quad (1.1)$$

Où : C_z = capacité thermique de la zone ($J \cdot m^3 \cdot K^{-1}$)

T_z = température de la zone (°C)

t = temps (s)

$\dot{Q}_i$ = gains convectifs de la zone (W)

h_i = coefficients de transfert de chaleur convectifs ($W \cdot m^{-2} \cdot K^{-1}$)

A_i = aire de la surface (m^2)

T_{si} = température de la surface (°C)

$\dot{m}_i$ = débit massique interzone ($kg \cdot s^{-1}$)

C_p = chaleur spécifique à pression constante ($J \cdot kg^{-1} \cdot K^{-1}$)

T_{zi} = température de la zone adjacente (°C)

$\dot{m}_{inf}$ = débit massique d'infiltration ($kg \cdot s^{-1}$)

T_∞ = température de l'air extérieur (°C)

$\dot{Q}_{sys}$ = flux d'énergie des systèmes CVCA (W)

$$\left.\frac{dT_z}{dt}\right|_t \approx (\partial t^{-1}) \left(\frac{11}{6} T_z^t - 3 T_z^{t-\partial t} + \frac{3}{2} T_z^{t-2\partial t} - \frac{1}{3} T_z^{t-3\partial t} \right) + O(\partial t^3) \quad (1.2)$$

Cette brève introduction à la méthode du bilan thermique, utilisée dans le logiciel EnergyPlus, permettra de mettre en contexte les similarités des outils de simulation énergétiques du bâtiment avec les modèles énergétiques spécifiquement développés pour les espaces d'agriculture en environnement contrôlé (AEC). Bien que d'autres aspects de la modélisation des plantes soient abordés dans la prochaine section, la méthode du bilan thermique ainsi que les modules de simulation des systèmes énergétiques couvrent une bonne partie des besoins de modélisation énergétiques des espaces d'AEC.

1.2 Modélisation des espaces d'agriculture en environnement contrôlé

La modélisation des espaces d'AEC englobe plusieurs domaines tels qu'illustrés à la Figure 1.3. Certains domaines touchent directement l'ingénierie (p. ex., systèmes énergétiques, contrôles, etc.) et d'autres sont de nature agronomiques (p. ex. croissance de plantes, rendement, etc.). Ces domaines sont toutefois interdépendants de plusieurs façons, ce qui rend impossible la dissociation entre les différentes expertises. Les modèles d'ingénierie doivent donc prendre en compte des contraintes de nature agronomique tandis que les modèles agronomiques doivent tenir compte des contraintes d'ingénierie. Pour mieux comprendre les éléments à considérer pour la modélisation d'espaces d'AEC, trois facettes seront approfondies : (1) la modélisation énergétique, (2) l'éclairage et (3) la modélisation des plantes.

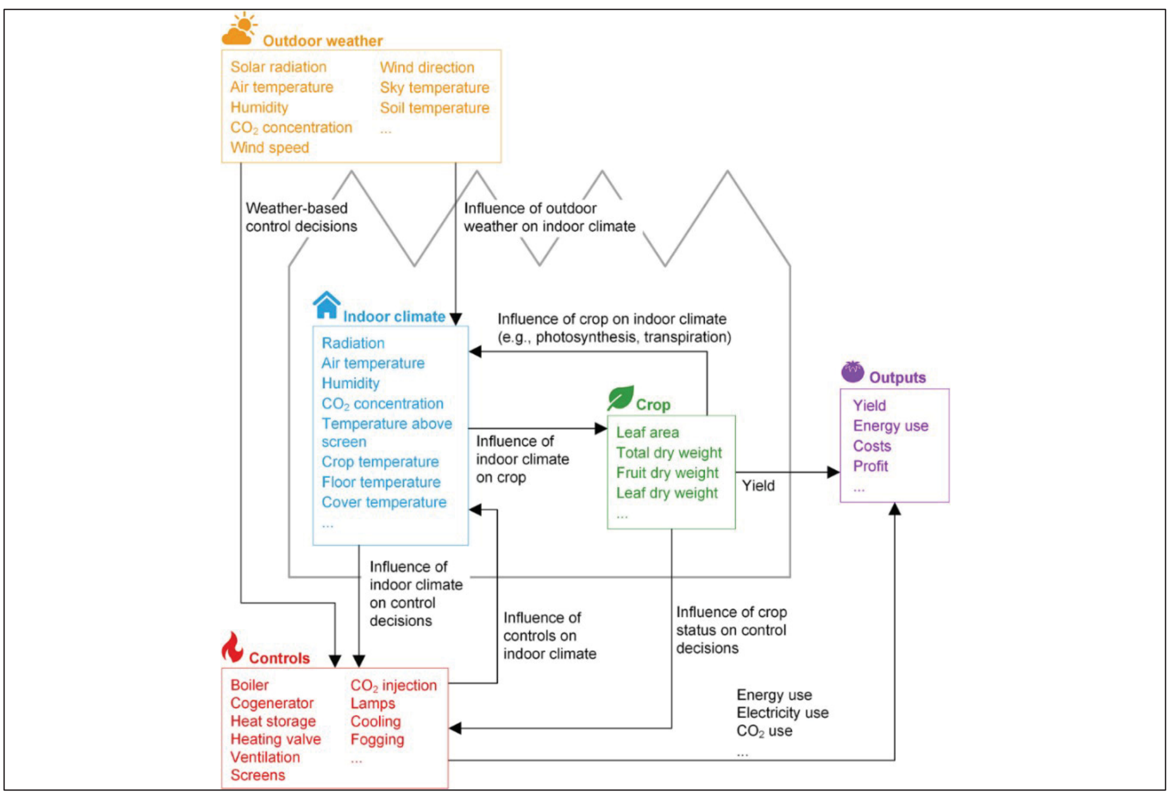

Figure 1.3 Relations entre les différents domaines de la modélisation des espaces d'AEC
Tirée de Katzin et al. (2022)

1.2.1 Modélisation énergétique

La modélisation énergétique des espaces d'agriculture en environnement contrôlé (AEC) vise à prédire les flux thermiques et massiques issus des différents bilans énergétiques de ces espaces afin d'en prédire le microclimat et la consommation énergétique. Ainsi, les charges sensibles et latentes des espaces d'AEC peuvent être déterminées par la modélisation des échanges thermiques par conduction, convection et rayonnement ainsi que des échanges massiques dus à la transpiration des plantes et à l'évaporation du sol. La Figure 1.4 illustre ces différents flux touchant la convection avec l'air de la zone, la conduction dans le sol, le rayonnement à ondes longues, le rayonnement solaire et les flux de vapeur d'eau.

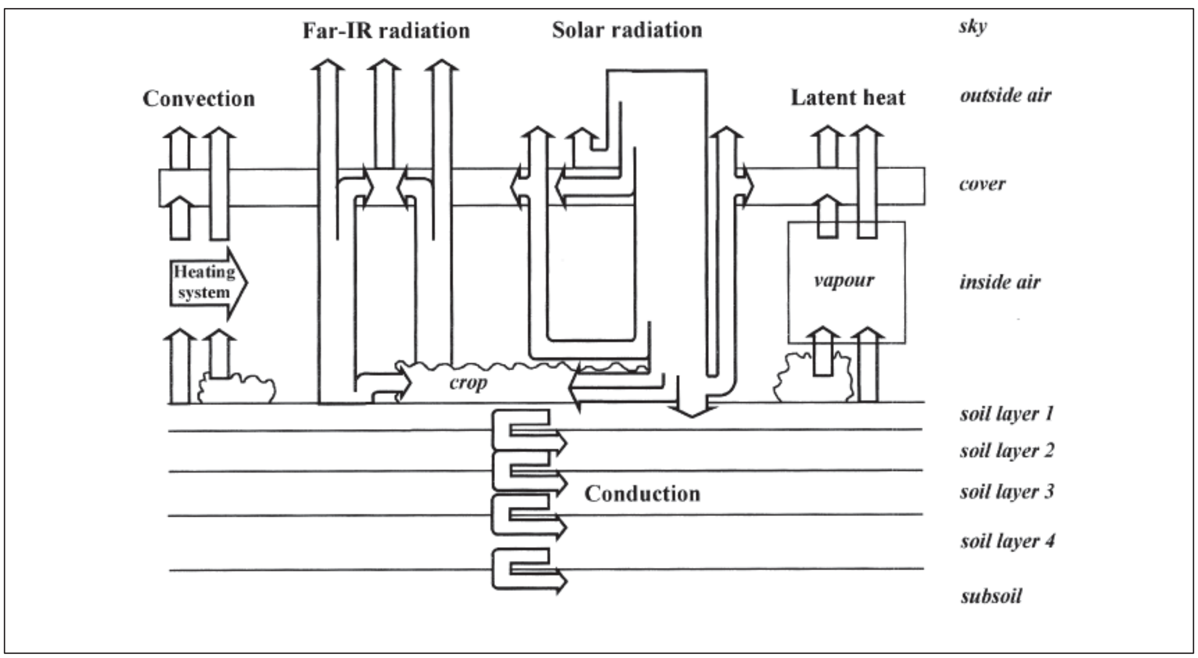

Figure 1.4 Schéma énergétique de la modélisation thermique d'une serre
Tirée de Pieters and Deltour (1999)

Plusieurs modèles énergétiques ont été proposés dans la littérature basés sur la méthode du bilan thermique (voir Choab et al. (2019)). Ces modèles utilisent typiquement comme variable d'état la température et l'humidité du microclimat de production. Ces deux variables sont combinées dans le calcul du déficit de pression de vapeur (VPD) indiquant le potentiel d'évaporation à la feuille de la plante effectuée. Le VPD est calculé selon l'équation (1.4) en fonction de la pression de vapeur à saturation (équation (1.3) (American Society of Heating & Air-Conditioning Engineers, 2021)) et l'humidité relative.

$$\ln p_{ws} = \frac{C_1}{T} + C_2 + C_3 \cdot T + C_4 \cdot T^2 + C_5 \cdot \mathrm{T}^3 + C_6 \cdot \ln T \tag{1.3}$$

Où : p_{ws} = Pression de vapeur à saturation (Pa)

T = Température (K)

C_1 = −5.8002206e03

C_2 = 1.3914993e00

C_3 = −4.8640239e−02

C_4 = 4.1764768e−05

C_5 = −1.4452093e−08

C_6 = 6.5459673e00

$$\mathrm{VPD} = p_{ws} - p_{ws} \cdot RH \tag{1.4}$$

Où : VPD = Déficit de pression de vapeur (Pa)

p_{ws} = Pression de vapeur à saturation (Pa)

RH = Humidité relative

Différentes combinaisons de température et d'humidité relative sont donc associées au même VPD. La modulation judicieuse du point de consigne de température et d'humidité dans des séquences de contrôle optimisées permet de maintenir un VPD idéal dans l'espace de production tout en minimisant la consommation des systèmes énergétiques (Körner & Challa, 2003). Les modèles énergétiques ont été utilisés dans la littérature pour de nombreuses applications telles que l'évaluation de la performance d'une serre avec des matériaux à changement de phase (Berroug et al., 2011), l'intégration de systèmes photovoltaïques (Nayak & Tiwari, 2008) et l'évaluation des effets croisés liés au remplacement de l'éclairage (Katzin et al., 2021).

1.2.2 Éclairage

La lumière est essentielle à la croissance des plantes. Elle agit à la fois comme signal qui orchestre les différentes facettes de leur croissance et comme source d'énergie indispensable à la photosynthèse (voir section 1.2.3.2). Le spectre électromagnétique utile pour la photosynthèse, le rayonnement photosynthétique actif («*photosynthetically active radiation*» (*PAR*)) se situe entre 400 et 700 nm (McCree, 1971). Plus récemment, les effets synergétiques de la lumière dans l'infrarouge lointain (≈700–750 nm) ont entraîné l'utilisation du terme spectre électromagnétique étendu utile pour la photosynthèse («*extended PAR*» (*ePAR*))(Zhen et al., 2021) afin de distinguer cet ajout du spectre PAR usuellement utilisé. Ces spectres électromagnétiques étant différents de la lumière visible par l'œil humain (entre 360 nm-400 nm et 760 nm–830 nm (Sliney, 2016)), les termes ainsi que les unités utilisées pour décrire l'éclairage dans des espaces d'agriculture en environnement contrôlé (AEC) sont différents de l'éclairage dans les bâtiments. Le Tableau 1.1 présente les distinctions importantes entre les définitions utilisées pour l'éclairage des plantes et l'éclairage pour la vision humaine.

Tableau 1.1 Termes utilisés pour l'éclairage des plantes et pour la vision humaine
Adapté de la documentation du logiciel Agi 32

	Lumière Humain	**Lumière Plante**
Radiant power	*Lumens*	*Photosynthetic Photon Flux (PPF)*
Light falling onto a surface	*Illuminance*	*Photosynthetic Photon Flux Density (PPFD)*
Units	*Lux*	*Micromoles per second per sq.meter* ($\mu mol \cdot s^{-}1 \cdot m^{-2}$)

Le niveau d'éclairement est mesuré dans les espaces d'AEC par la densité du flux de photon (PPFD ($\mu mol \cdot m^{-2} \cdot s^{-1}$)) et la quantité journalière de photons requise par la plante par la DLI («*Daily Light Integral*» ($mol \cdot m^{-2} \cdot$jour)). Ces deux quantités sont les métriques établies pour la conception et l'exploitation des systèmes d'éclairage artificiel. L'éclairage artificiel est utilisé dans les serres pour complémenter l'éclairage naturel afin d'assurer la production en période hivernale. Pour la production dans des espaces d'AEC-HD, l'éclairage artificiel est essentiel puisque l'enceinte de production est opaque. La lumière rose, caractéristique des espaces de production en AEC, est le résultat d'un taux élevé de photosynthèse grâce à l'abondance de lumière bleue et rouge, telle qu'illustrée à la Figure 1.5.

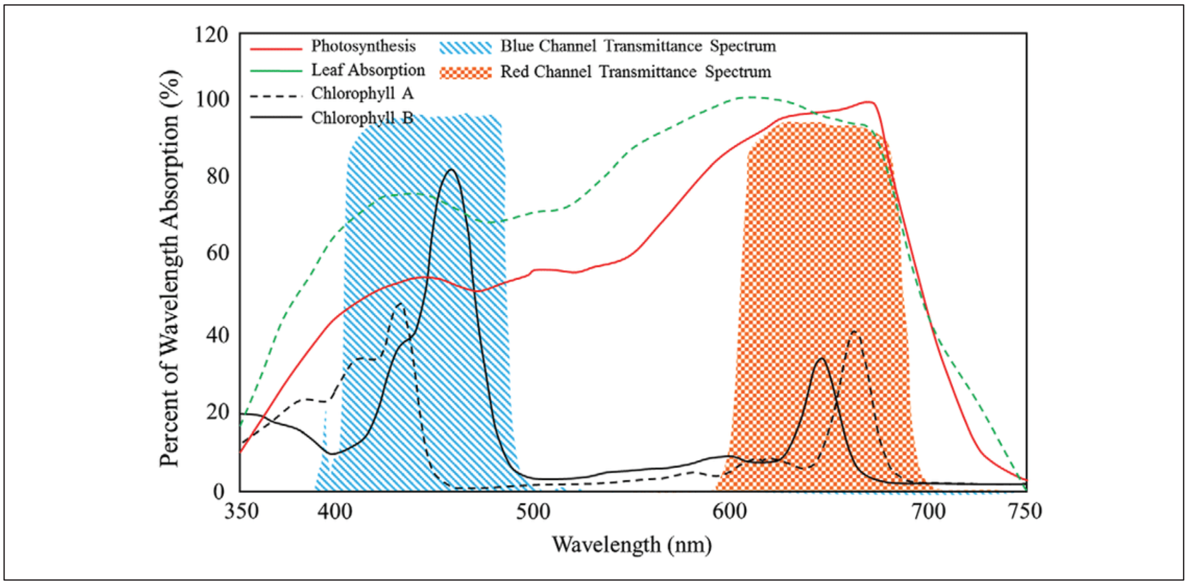

Figure 1.5 Absorption relative en fonction du spectre électromagnétique de la photosynthèse, de la feuille, de la chlorophylle A et B
Tirée de Zhang et al. (2019b)

L'effet de la quantité de lumière sur la croissance est souvent quantifié par la règle du pouce qui associe 1% plus de lumière à 1% plus de production (Marcelis et al., 2006). La qualité de l'éclairage, déterminée par la distribution du spectre électromagnétique, ainsi que l'éclairage dynamique, basé sur le cycle circadien et la modulation dynamique du spectre, sont des domaines de recherche actuellement actifs (Pocock, 2016; Marie et al., 2022).

La performance énergétique des technologies d'éclairage a aussi connu une évolution importante depuis le début du 21e siècle par l'augmentation rapide de l'efficacité des diodes électroluminescentes (LEDs). Le Tableau 1.2 présente l'efficacité de plusieurs technologies d'éclairage.

Tableau 1.2 Efficacité des types de lampes utilisées en AEC
Adapté de Nelson and Bugbee (2014)

Type de Lampes	**Efficacité ($\mu mol \cdot J^{-1}$)**	**Décennie**
Fluorescent	0.84 – 0.95	1940s
Ceramic Metal Halide	1.25 – 1.46	1970s
High Pressure Sodium (HPS)	0.94 – 1.70	1970s
Light emitting diodes (LED)	0.89 – 1.70	2000s

Les avancements technologiques récents permettent d'atteindre une efficacité de 3.4 $\mu mol \cdot J^{-1}$. La limite théorique des diodes électroluminescentes est estimée à 3.76 $\mu mol \cdot J^{-1}$ pour la lumière bleue (450 nm) et 5.1 $\mu mol \cdot J^{-1}$ pour la lumière rouge (660 nm) (Kusuma et al., 2020). Bien que plus efficace, ce type d'éclairage nécessite toujours un investissement initial plus élevé que les lampes au sodium haute pression. De plus, les effets croisés (c.-à-d., l'augmentation de la charge de chauffage liée à l'amélioration de l'efficacité de l'éclairage) ne sont pas toujours mis de l'avant par les manufacturiers. Les économies d'énergies liées au remplacement de lampes HPS par des luminaires DEL peuvent être estimées par l'équation (1.5) proposée par Katzin et al. (2021).

$$y = 0.37 \cdot x - 5.41 \tag{1.5}$$

Où : y = Économies d'énergie (%)

x = Proportion d'énergie utilisée pour l'éclairage HPS (%)

1.2.3 Modélisation des plantes

Tel que présenté à la Figure 1.3, la modélisation des plantes est l'un des domaines importants de la modélisation des espaces d'AEC. Cette section aborde et résume brièvement trois facettes essentielles de la modélisation des plantes, soit : (1) le bilan d'énergie à la feuille, (2) la photosynthèse et (3) la résistance à l'écoulement.

1.2.3.1 Bilan d'énergie à la feuille

Le bilan d'énergie est utilisé au niveau de la feuille pour déterminer les flux thermiques et massiques en fonction du rayonnement net reçu. Ainsi, l'énergie apportée par rayonnement à ondes courtes se convertit en flux de chaleur sensible, sous forme convective, et en transpiration (flux de chaleur latent) tel que présenté dans le bilan d'énergie de l'équation (1.6). Ce bilan néglige le rayonnement à ondes longues, l'énergie absorbée par photosynthèse au sein de la plante et la capacité thermique de la feuille.

$$q''_{SW,plt} = q''_{conv,plt} + q''_{latent,plt} \tag{1.6}$$

Où : $q''_{SW,plt}$ = rayonnement ondes courtes ($W \cdot m^{-2}$)
$q''_{conv,plt}$ = flux de chaleur convectif sensible ($W \cdot m^{-2}$)
$q''_{latent,plt}$ = flux de chaleur latent ($W \cdot m^{-2}$)

Le rayonnement à ondes courtes considéré dans le bilan d'énergie au niveau du canopé de la plante est obtenu en considérant les caractéristiques spectrales de la feuille (équation (1.7)).

$$q''_{SW,plt} = \left(1 - \tau_{plt} - \rho_{plt}\right) \cdot I_s \tag{1.7}$$

Où : τ_{plt} = transmissivité de la feuille
ρ_{plt} = réflectivité de la feuille
I_s = rayonnement à ondes courtes ($W \cdot m^{-2}$)

Le flux de chaleur sensible transmis vers l'espace de production par convection est calculé en fonction du différentiel de température entre la surface de la feuille et la température de l'espace de production tel que présenté par l'équation (1.8). Cette équation prend en compte la résistance aérodynamique associée à la couche limite de l'écoulement d'air sur la feuille.

$$q^{"}_{conv,plt} = \frac{\rho_a . c_p}{r_a} \cdot \left(T_{plt} - T_a\right) \tag{1.8}$$

Où : $\rho_a.$ = densité de l'air ($kg \cdot m^{-3}$)

c_p = chaleur spécifique de l'air ($J \cdot kg^{-1} \cdot {}^{o}C^{-1}$)

r_a = résistance aérodynamique ($s \cdot m^{-1}$)

T_{plt} = température de la plante (°C)

T_a = température de l'air ambiant (°C)

Le flux de chaleur latente associé à la transpiration des plantes est décrit par l'équation (1.9) qui est basée sur la différence de concentration de vapeur d'eau à la surface de la feuille et dans l'air ambiant. En plus de la résistance aérodynamique, la résistance de la diffusion de la vapeur d'eau à l'intérieur des stomates est prise en compte par l'ajout de la résistance stomatale.

$$q^{"}_{latent,plt} = \lambda \cdot \frac{(\chi_s - \chi_a)}{r_a + r_s} \tag{1.9}$$

Où : λ = chaleur latente d'évaporation ($J \cdot g^{-1}$)

r_s = résistance stomatale ($s \cdot m^{-1}$)

χ_s = concentration de vapeur à la surface de la feuille ($g \cdot m^{-3}$)

χ_a = concentration de vapeur dans l'air ambiant ($g \cdot m^{-3}$)

Ce bilan d'énergie à la surface d'une feuille utilisant la pente de la courbe de pression de vapeur en fonction de la température a été proposé initialement par Penman (1948). Le calcul de l'évapotranspiration de plantes a été développé par la suite dans l'équation de Penman-Monteith (Monteith, 1981) (équation (1.10)).

$$q''_{latent,plt} = \frac{\Delta\left(q''_{SW,plt} - q''_{soil}\right) + \rho_a \cdot c_p \cdot \mathrm{VPD} \cdot {r_a}^{-1}}{\Delta + \gamma \cdot (1 + r_s/r_a)} \tag{1.10}$$

Où : q''_{soil} = conduction par le sol (W·m^{-2})

Δ = pente de la pression de vapeur de saturation (Pa·ºC^{-1})

ρ_a = densité de l'air (kg·m^{-3})

c_p = chaleur spécifique de l'air (J·kg^{-1}·ºC^{-1})

VPD = déficit de pression de vapeur (Pa)

γ = constante psychrométrique (Pa·ºC^{-1})

Le modèle de Stanghellini (1987) adapte le modèle de Penman-Monteith au niveau de la canopée des plantes produites par l'introduction de l'indice foliaire, le «*Leaf Area Index*» (LAI). Le LAI est défini par la surface totale des feuilles, en considérant un seul côté, par unité de surface horizontale. L'équation (1.11) présente le modèle proposé par Stanghellini.

$$q''_{latent,plt} = \frac{\Delta}{\Delta + \gamma^*}\left(q''_{SW,plt} - q''_{soil}\right) + \frac{\gamma}{\Delta + \gamma^*} 2 \cdot \mathrm{LAI} \cdot \rho_a \cdot \lambda \cdot \frac{\mathrm{VPD}}{r_a} \tag{1.11}$$

Où : LAI = Indice foliaire, *Leaf Area Index*

γ^* $= \gamma(1 + r_s/r_a)$

Villarreal-Guerrero et al. (2012) ont comparé la performance de ces deux modèles pour la prédiction de la transpiration dans une serre de recherche et ont conclu que le modèle de Penman-Monteith (Monteith, 1981) avait une tendance à surestimer et que le modèle Stanghellini (Stanghellini, 1987) était plus performant sans toutefois relever de différences statistiquement significatives entre les deux modèles. Ainsi, la transpiration des plantes à l'intérieur des espaces d'AEC est un bilan de masse ayant un impact énergétique important en plus d'influencer la régulation du microclimat de production. Toutefois, la production de vapeur d'eau n'est pas le seul bilan de masse à prendre place au sein de l'espace de production. L'absorption par les plantes de dioxyde de carbone dans le processus de photosynthèse est un autre bilan massique important ayant un impact direct sur la production dans des espaces d'AEC.

1.2.3.2 Photosynthèse

La croissance des plantes s'effectue par le processus de photosynthèse. La photosynthèse est le processus par lequel le rayonnement est converti par la plante en sucres et en oxygène par le cycle de Calvin. L'équation stœchiométrique (1.12) résume ce processus, soit la combinaison d'eau, de dioxyde de carbone et d'énergie lumineuse pour la création d'oxygène et de sucres.

$$6 \cdot CO_2 + 12 \cdot H_2O + \text{Énergie lumineuse} = C_6H_{12}O_6 + 6 \cdot O_2 + 6 \cdot H_2O \qquad (1.12)$$

Ainsi, la concentration de dioxyde de carbone est souvent régulée dans les espaces d'AEC afin d'optimiser la croissance des plantes. La relation entre la photosynthèse et la concentration ambiante de dioxyde de carbone est non linéaire avec peu de bénéfices au-dessus d'une concentration de 700 ppm (Allen et al., 2004). D'un autre côté, la respiration cellulaire («*dark respiration*» ou «*mitochondrial respiration*») est un processus qui oxyde des sucres pour les convertir en énergie biochimique (adénosine triphosphate) tout en rejetant du dioxyde de carbone. De plus, la photorespiration est un processus lié à la photosynthèse consommant de l'oxygène et libérant du dioxyde de carbone ainsi que de l'ammoniac. Le bilan entre la photosynthèse, consommant du dioxyde de carbone, et la respiration cellulaire additionnée de la photorespiration, produisant du dioxyde de carbone, est appelé taux de photosynthèse net (Wohlfahrt & Gu, 2015). La photosynthèse peut être définie selon différentes formulations. À titre d'exemple, la corrélation empirique proposée par Okayama et al. (2008a) (équation (1.13)), spécifiquement développée pour les espaces d'AEC-HD, est utilisée pour modéliser le taux de photosynthèse net en fonction de la vitesse de l'écoulement d'air.

$$P_{cell} = 1.4 \cdot \left(1 - e^{-12.8 \cdot s}\right) + 1.52 \qquad (1.13)$$

Où : P_{cell} = taux de photosynthèse net ($\mu mol \cdot s^{-1}$)

s = vitesse de l'écoulement d'air ($m \cdot s^{-1}$)

1.2.3.3 Résistance à l'écoulement

Les plantes dans les espaces d'AEC exercent une influence sur l'écoulement au sein de l'espace de production. L'impact de celles-ci sur la conservation de la quantité de mouvement de l'écoulement peut être modélisé par les équations associées aux médias poreux. Les plantes peuvent donc être représentées par une géométrie rectangulaire ayant des caractéristiques homogènes (Fatnassi et al., 2023). Koch et al. (2019) ont effectué la validation expérimentale de l'utilisation du modèle de Darcy–Forchheimer (équation (1.14)) pour la modélisation d'un écoulement d'air à travers des plantes. Ils ont conclu qu'il s'agit d'une méthode simple et robuste de modélisation indépendante de la morphologie de la plante modélisée.

$$\frac{\Delta P}{\Delta x} = -\left(\frac{\mu}{K}\right) q - \left(\frac{\rho}{K_1}\right) q^2 \tag{1.14}$$

Où : ΔP = perte de charge (Pa)
Δx = longueur du média poreux (m)
μ = viscosité (Pa·s^{-1})
K = perméabilité (m^2)
q = Flux de fluide (m·s^{-1})
ρ = densité (kg·m^{-3})
K_1 = perméabilité inertielle (m)

Pour des vitesses d'écoulement faibles, Fatnassi et al. (2023) ont utilisé l'équation (1.15) négligeant ainsi le terme linéaire de l'équation (1.14). Ils ont rapporté des coefficients de trainée (C_D) entre 0.2 et 0.32 pour différentes plantes.

$$\frac{\Delta P}{\Delta x} = -LAD \cdot C_D \cdot q^2 \tag{1.15}$$

Où : LAD = «*Leaf Area Density*» (m^{-1})
C_D = coefficient de trainée

1.3 Dynamique des fluides numériques

La dynamique des fluides newtoniens est décrite par les équations de Navier-Stokes qui ajoutent les stress liés à la viscosité aux équations d'Euler. Ainsi, la dynamique des fluides numérique («*Computational Fluid Dynamics*» (CFD)) vise la résolution des équations de Navier-Stokes par l'utilisation de méthodes numériques puisque la résolution analytique de ces équations est toujours complexe. Les équations de conservation de la masse (équation (1.16)), du momentum (équation (1.17)) ainsi que de l'énergie (équation (1.18)) sont donc résolues numériquement afin d'obtenir une prédiction de la distribution spatiale des différentes variables d'état de l'écoulement.

$$\frac{\partial \rho}{\partial t} + \nabla \cdot (\rho \cdot \boldsymbol{V}) = 0 \tag{1.16}$$

$$\frac{\partial (\rho \cdot \boldsymbol{V})}{\partial t} + \nabla \cdot (\rho \cdot \boldsymbol{V} \cdot \boldsymbol{V}) = -\nabla p + \nabla(\bar{\bar{\tau}}) + \rho \cdot \boldsymbol{g} + \boldsymbol{F} \tag{1.17}$$

$$\frac{\partial (\rho \cdot E)}{\partial t} + \nabla \cdot \big(\boldsymbol{V}(\rho \cdot E + p)\big) = \nabla \cdot \left(k_{eff} \cdot \nabla T - \sum_j h_j \cdot J_j + \left(\bar{\bar{\tau}}_{eff} \cdot \boldsymbol{V}\right)\right) + S_h \tag{1.18}$$

Où :
ρ = densité du fluide ($kg{\cdot}m^{-3}$)
t = temps (s)
∇ ≡ Opérateur Nabla $\left[\frac{\partial}{\partial x}\ \frac{\partial}{\partial y}\ \frac{\partial}{\partial z}\right]$
$\boldsymbol{V}$ = vecteur de la vitesse d'écoulement ($m{\cdot}s^{-1}$)
p = pression (Pa)
$\bar{\bar{\tau}}$ = tenseur des contraintes (Pa)
$\bar{\bar{\tau}}_{eff}$ = tenseur déviatorique des contraintes (Pa)
$\boldsymbol{g}$ = vecteur de gravité ($m{\cdot}s^{-2}$)
$\boldsymbol{F}$ = vecteur des forces externes (N)
k_{eff} = conductivité effective ($W{\cdot}m^{-1}{\cdot}K^{-1}$)
h_j = enthalpie ($kJ{\cdot}kg^{-1}$)
T = température (K)
J = flux de diffusion ($kg{\cdot}m^{-2}{\cdot}s^{-1}$)
S_h = source de chaleur volumétrique ($W{\cdot}m^{-3}$)

Pour les écoulements turbulents, la résolution d'équations supplémentaires est nécessaire. En effet, en substituant l'équation (1.19) dans les équations de conservations (c.-à-d. (1.16), (1.17) et (1.18)) on obtient les équations de Navier-Stokes moyennées (*Reynolds Averaged Navier Stokes* (RANS) (Reynolds, 1895)), base de plusieurs modèles de turbulences.

$$V(\boldsymbol{x},t) = \bar{V}(\boldsymbol{x}) + V'(\boldsymbol{x},t) \tag{1.19}$$

Où : $\boldsymbol{x}$ = vecteur position $[x,y,z]$

$\bar{V}(\boldsymbol{x})$ = moyenne temporelle de la vitesse ($m \cdot s^{-1}$)

$V'(\boldsymbol{x},t)$ = fluctuation de la vitesse ($m \cdot s^{-1}$)

Au cours de cette substitution, un nouveau terme apparait dans l'équation temporellement moyennée du momentum : le stress de Reynolds (terme à gauche de l'équation (1.20)). Ce terme ajoute neuf variables inconnues au lot d'équations à résoudre. Cette inéquation entre le nombre de variables et le nombre d'équations est connue sous le problème de la fermeture des équations RANS. Plusieurs modèles de turbulence ont été proposés dans la littérature (voir Wilcox (1993)). Pour la modélisation CFD des espaces d'AEC (voir chapitre 3), le modèle k-ε développé par Launder and Spalding (1974) est utilisé pratiquement par tous les auteurs. Ce modèle ajoute deux équations aux dérivées partielles ((1.21) et (1.22)) visant à calculer la viscosité de turbulence (μ_T) en utilisant l'hypothèse que le tenseur des contraintes anisotropes est proportionnel au tenseur des taux d'élongations moyens (Boussinesq, 1877). Cette hypothèse réduit le tenseur des stress de Reynolds à la formulation présentée par l'équation (1.20). Les constantes $C_{1\varepsilon}$, $C_{2\varepsilon}$, C_{μ}, σ_{ε}, et σ_k, sont obtenues en calibrant le modèle avec des données expérimentales.

$$-\rho\overline{V_i'V_j'} = \mu_T\left(\frac{\partial \bar{V}_i'}{\partial x_j} + \frac{\partial \bar{V}_j'}{\partial x_i}\right) - \frac{2}{3}\delta_{ij}k \tag{1.20}$$

Où : μ_T = viscosité de turbulence ($kg \cdot m^{-1} \cdot s^{-1}$)

δ_{ij} = delta de Kronecker

k = énergie cinétique turbulente ($m^2 \cdot s^{-2}$)

$$\frac{\partial(\rho k)}{\partial t} + \nabla \cdot (\rho k \boldsymbol{V}) = \nabla \cdot \left[\frac{\mu_t}{\sigma_k} \nabla \mathrm{k}\right] + 2\mu_t E_{ij} E_{ij} - \rho\varepsilon \tag{1.21}$$

$$\frac{\partial(\rho\varepsilon)}{\partial t} + \nabla \cdot (\rho\varepsilon \boldsymbol{V}) = \nabla \cdot \left[\frac{\mu_t}{\sigma_\varepsilon} \nabla \varepsilon\right] + C_{1\varepsilon} \frac{\varepsilon}{k} 2\mu_t E_{ij} E_{ij} - C_{2\varepsilon} \rho \frac{\varepsilon^2}{k} \tag{1.22}$$

Où : ε = taux de dissipation de l'énergie cinétique turbulente ($m^2 \cdot s^{-3}$)

E_{ij} = composante de vitesse de déformation (s^{-1})

D'autres modèles linéaires de la viscosité turbulente (p. ex. k-ω (Wilcox, 1988), ¸SST k-ω (Menter, 1993), etc.) ont été proposés dans la littérature ainsi que d'autres méthodes plus coûteuses au niveau informatique (p. ex. *Reynolds Stress Models*, *Large Eddy Simulation* et *Direct Numerical Simulation*). La modélisation des écoulements avec la CFD comprend beaucoup d'autres aspects tels que les méthodes de discrétisation des opérateurs différentiels, de définitions des différentes conditions limites, de modélisation du traitement des surfaces frontières, de définition du maillage, etc.

1.4 Constats

Le corpus de connaissances scientifiques identifié dans le cadre de la réalisation de cette thèse par articles comporte certaines lacunes. En effet, aucune méthode d'optimisation de la distribution de l'air pour uniformiser la distribution spatiale des variables du microclimat de production tenant compte de la résistance à l'écoulement, de la photosynthèse et du bilan d'énergie au niveau de la canopée des plantes n'a été proposée. De plus, aucun outil permettant d'intégrer le calcul du bilan d'énergie au niveau de la canopée des plantes dans un logiciel de simulation énergétique du bâtiment supporté, validé, gratuit et publiquement disponible n'a été développé. D'autre part, certaines informations ayant un impact sur les résultats de la simulation de la performance énergétique des espaces d'AEC-HD, tels que les coefficients de transfert de chaleur convectifs (CHTCs) des surfaces internes utilisés dans le logiciel de simulation énergétique, ne sont pas spécifiées dans la littérature scientifique consultée. Ainsi, il existe une lacune des connaissances scientifiques au niveau de l'impact des algorithmes de calcul des CHTCs sur les résultats de simulation énergétique des espaces d'AEC-HD effectuées avec des outils de BPS.

CHAPITRE 2

MÉTHODOLOGIE

Cette section détaille la méthodologie globale utilisée pour atteindre l'objectif principal de cette thèse : développer une méthode de modélisation énergétique des espaces d'AEC basée sur l'utilisation d'outils de simulation de la performance énergétique du bâtiment (BPS) en tenant compte de l'uniformité du microclimat de production. Ainsi, la méthodologie globale est scindée en trois étapes correspondant aux sous-objectifs du projet de recherche et aux trois articles scientifiques rédigés. Ainsi, le bilan d'énergie à la feuille (voir section 1.2.3.1) est utilisé dans le modèle de dynamique des fluides numérique (CFD) (Article #1) et dans le modèle énergétique basé sur un outil de simulation énergétique du bâtiment (Article #2). Le modèle CFD ainsi bonifié est utilisé dans l'article #1 pour atteindre le premier sous-objectif soit : « Optimiser la distribution de l'air afin d'uniformiser la distribution spatiale des variables du microclimat de production ». Par la suite, l'intégration du même bilan d'énergie à la feuille dans un outil de simulation énergétique du bâtiment permet de bonifier un modèle énergétique afin d'atteindre le deuxième sous-objectif : « Intégrer le calcul du bilan d'énergie à la feuille dans un logiciel de simulation énergétique du bâtiment supporté, validé, gratuit et publiquement disponible ». Finalement, les deux modèles développés sont utilisés conjointement afin d'atteindre le troisième sous-objectif : « Évaluer la performance des algorithmes de calcul des coefficients de transfert de chaleur convectifs (CHTCs) du logiciel de simulation énergétique du bâtiment sélectionné pour la distribution de l'air optimisée ». La Figure 2.1 illustre les liens méthodologiques entre les sous-objectifs, associés aux articles. Les différents liens démontrent que les articles rédigés portent sur un même thème avec une suite logique claire tel qu'exigé pour le dépôt d'une thèse par article.

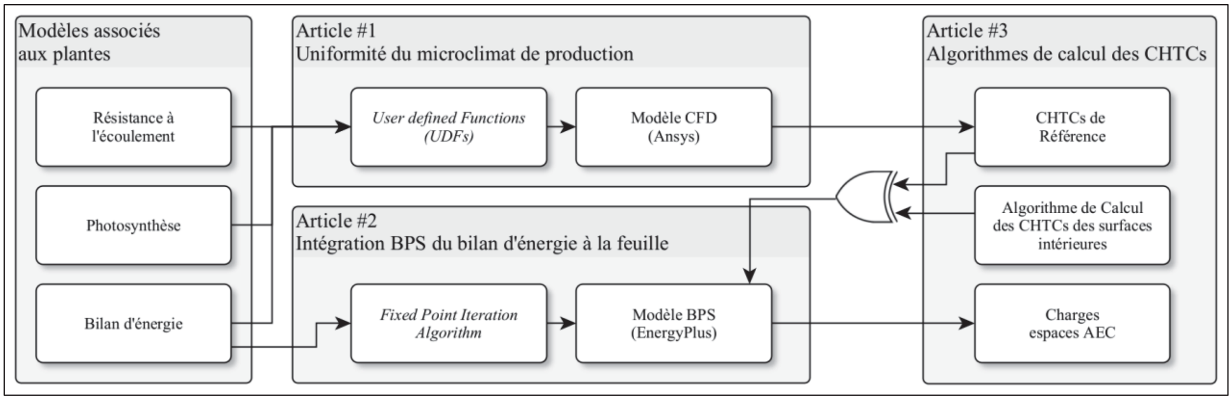

Figure 2.1 Schéma de la méthodologie globale utilisée

L'atteinte des trois sous-objectifs du projet de recherche a mené à trois contributions originales telles que détaillées au Tableau 2.1. Au moment du dépôt, l'article #1 (doi.org/10.1080) et l'article #3 (doi.org/10.1016) sont publiés. L'article #2 a été soumis dans une revue avec comité de lecture. Les trois prochaines sous-sections résument les étapes méthodologiques utilisées dans le cadre de chacun des articles afin de répondre à chacun des sous-objectifs.

Tableau 2.1 Relation entre les articles et les sous-objectifs de recherche

#	Titre de l'article	Chapitre	Sous-Objectif	Journal
1	*High-Density Controlled Environment Agriculture (CEA-HD) air distribution optimization using Computational Fluid Dynamics (CFD)*	3	#1	*Engineering Applications of Computational Fluid Mechanics*
2	*Advancing EnergyPlus: A Tool for Modeling Controlled Environment Agriculture Spaces*	4	#2	*Energy and Buildings*
3	*Comparison of EnergyPlus Inside Surfaces Convective Heat Transfer Coefficients Algorithms for Energy Modelling of High-Density Controlled Environment Agriculture*	5	#3	*Energy and Buildings*

2.1 Article #1 - Modélisation spatiale du microclimat

L'article #1, intitulé « *High-Density Controlled Environment Agriculture (CEA-HD) air distribution optimization using Computational Fluid Dynamics (CFD)* », détaille une méthode de modélisation et d'optimisation de la distribution de l'air visant l'uniformisation du microclimat de production d'un espace d'agriculture en environnement contrôlé à haute densité (AEC-HD). La méthodologie utilisée dans l'article #1 comporte deux étapes principales : (1) intégrer le bilan d'énergie au niveau de la canopée de la plante, un modèle de photosynthèse ainsi que la résistance à l'écoulement des plantes à l'outil de modélisation CFD ANSYS Fluent sous la forme de fonctions définies par l'utilisateur (UDFs) et (2) la formulation d'un problème d'optimisation utilisant un modèle simplifié (c.-à-d. 2D) du modèle CFD développé (c.-à-d. 3D) pour améliorer l'uniformité de l'espace de production tout en maximisant la vitesse de l'écoulement au niveau des plantes.

Le modèle CFD ainsi développé incorpore le bilan d'énergie au niveau de la canopée des plantes cultivées (voir section 1.2.3.1), un modèle de photosynthèse (voir section 1.2.3.2) et la résistance à l'écoulement induite par les plantes (voir section 1.2.3.3). Le modèle CFD utilise le modèle de turbulence k-ε (Launder & Spalding, 1974) (voir section 1.3) ainsi qu'un modèle de transport pour la vapeur d'eau et le dioxyde de carbone. L'optimisation de la distribution de l'air est réalisée en faisant varier la vitesse et l'angle de la sortie du diffuseur ainsi que la position et l'angle d'incidence d'une ailette incurvée positionnée près du diffuseur. Un algorithme d'optimisation génétique (NSGA-II (Deb et al., 2002)) et la fonction objectif (équation (2.1)) sont par la suite combinés afin d'identifier les valeurs optimales des variables du problème d'optimisation. La fonction objectif vise à maximiser l'uniformité du microclimat de production et la vitesse d'écoulement moyenne au niveau des plantes (équation (2.1)).

$$f(x) = \frac{\sum_1^n \mathrm{CV}(s_n)}{n_{tiers}} + \sum_1^n \mathrm{CV}(s_n) + \frac{\sum_1^n \mathrm{CV}(\omega_n)}{n_{tiers}} + \sum_1^n \mathrm{CV}(\omega_n) - \sum_1^n \mathrm{Mean}(s_n) \qquad (2.1)$$

Où : CV = coefficient de variation

s = vitesses de l'écoulement d'air ($m \cdot s^{-1}$)

n_{tiers} = nombre d'étages du système de production

ω_n = humidité absolue ($kg \cdot kg^{-1}$)

La Figure 2.2 illustre certaines des variables du problème d'optimisation de la distribution de l'air effectuée à partir du modèle CFD à géométrie simplifiée (c.-à-d. 2D). La portion magnifiée de la Figure 2.2 indique les positions possibles ainsi que la relation entre l'angle d'incidence de l'ailette incurvée, le diffuseur du système de ventilation et le système de production. Afin d'examiner les résultats obtenus à partir de l'optimisation du modèle 2D, ceux-ci sont confrontés à ceux obtenus avec un modèle 3D en tant que comparaison finale.

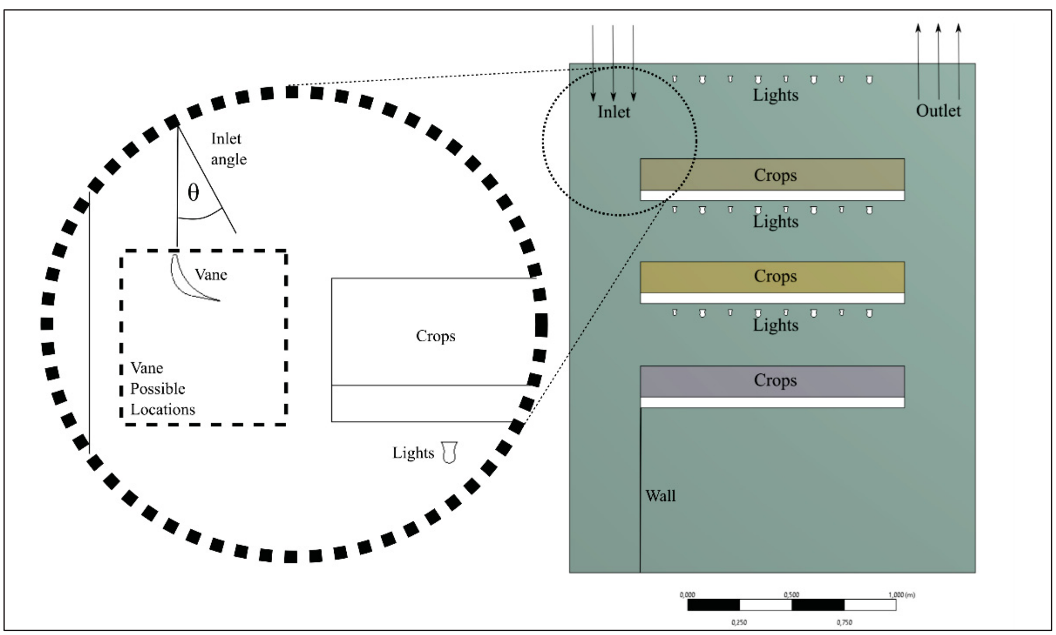

Figure 2.2 Schéma de certaines variables du problème d'optimisation de la distribution de l'air effectuée à partir du modèle CFD à géométrie simplifiée

2.2 Article #2 - Modélisation du bilan d'énergie à la feuille dans un outil de BPS

L'article #2, intitulé « *Development of a tool for modelling Controlled Environment agriculture (CEA) spaces in EnergyPlus* », propose une méthode efficiente de résolution du bilan thermique à la feuille des plantes permettant de déterminer les flux induits sensibles et latents liés à la conversion du rayonnement net. La méthodologie utilisée dans l'article #2 inclut une revue exhaustive de la littérature sur la modélisation d'espaces d'AEC utilisant des outils de BPS. La revue de littérature (section 4.1) indique clairement que dans plusieurs des articles identifiés (près de 50%), les plantes ne sont pas considérées dans la modélisation énergétique de l'espace de production effectuée avec un outil de simulation énergétique du bâtiment. Afin d'effectuer la résolution du bilan d'énergie à la feuille, un couplage externe est proposé en utilisant l'interface de programmation (API) du logiciel EnergyPlus. De plus, la performance de l'algorithme de résolution du bilan d'énergie à la feuille est drastiquement améliorée par l'utilisation d'une méthode numérique itérative. La Figure 2.3 illustre la méthode de résolution utilisée pour résoudre efficacement le bilan d'énergie à la feuille. L'approche de couplage proposée est évaluée à l'aide de deux comparaisons interlogicielles différentes. La première consiste à évaluer la température de surface des feuilles calculée et les gains/pertes calculées à l'aide du modèle développé. La seconde compare la demande de pointe et la consommation d'énergie annuelle d'une étude de cas, un espace d'agriculture en environnement contrôlé à haute densité (AEC-HD) de petite échelle.

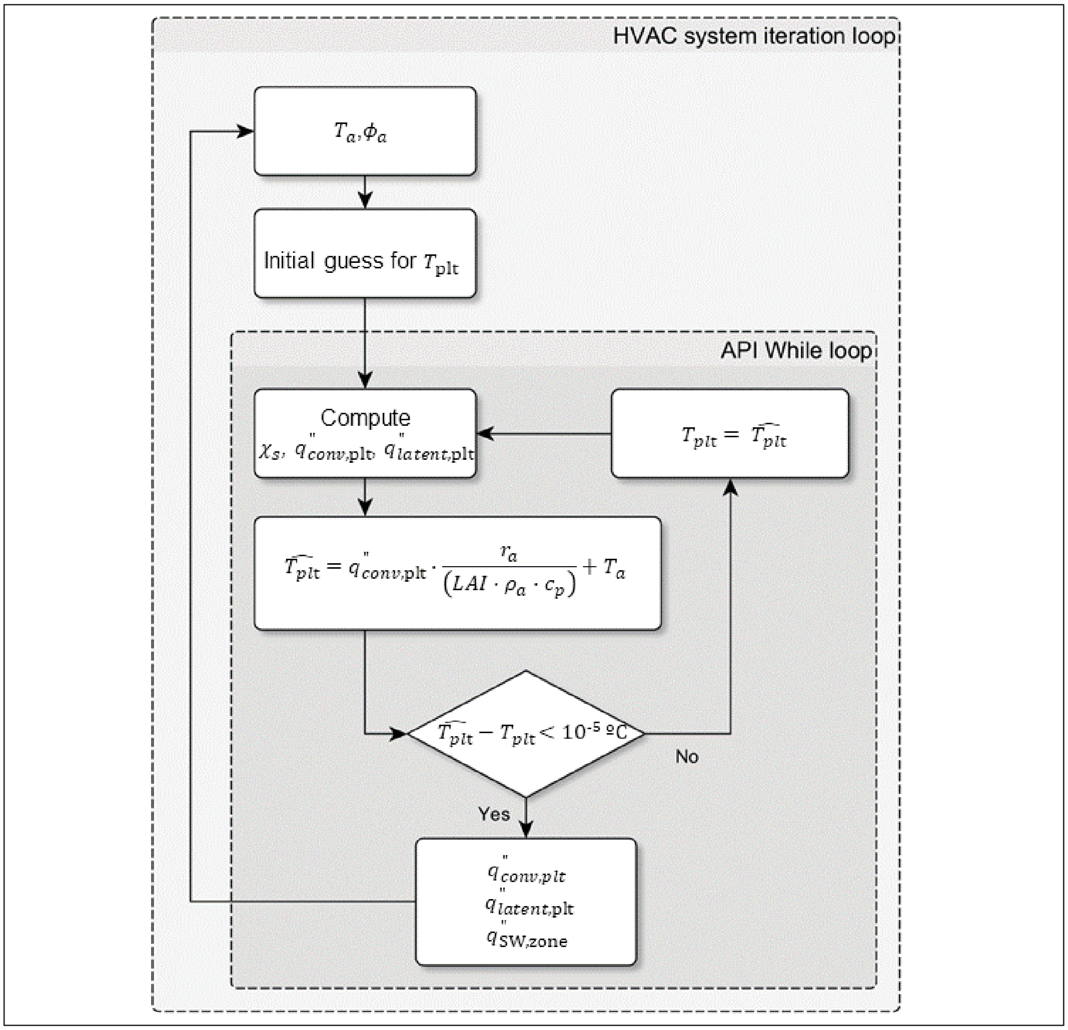

Figure 2.3 Méthodologie utilisée pour résoudre le bilan d'énergie au niveau de la canopée des plantes dans le logiciel EnergyPlus de l'article #2

2.3 Article #3 - Évaluation des algorithmes de calcul des CHTCs

L'article #3, intitulé « *Comparison of Convective Heat Transfer Coefficients Algorithms in EnergyPlus for High-Density Controlled Environment Agriculture Spaces* », estime l'impact des algorithmes de calcul des coefficients de transfert de chaleur convectifs (CHTCs) pour les surfaces internes sur les résultats de modélisation énergétique d'espaces d'agriculture en environnement contrôlé à haute densité. La méthodologie utilisée dans l'article #3 tire profit des modèles développés dans l'article #1 et l'article #2 par la comparaison des paramètres issus des algorithmes de calcul des coefficients de transfert de chaleur convectifs (CHTCs) pour les surfaces internes compris dans le logiciel EnergyPlus avec des valeurs de références calculées à partir d'une modélisation basée sur la dynamique des fluides numérique (CFD). Les valeurs de référence sont obtenues par la résolution de la couche limite sur les surfaces intérieures du modèle CFD. La Figure 2.4 illustre la méthodologie utilisée dans l'article #3 pour évaluer l'impact des CHTCs des surfaces intérieures sur les résultats de la simulation énergétique. Ces impacts sont quantifiés et comparés à partir de la consommation d'énergie, de la demande de pointe, de la température de l'air de la zone thermique, de l'humidité de l'air de la zone thermique, de la température des plantes et des échanges de chaleur sensible et latente entre les plantes et la zone thermique.

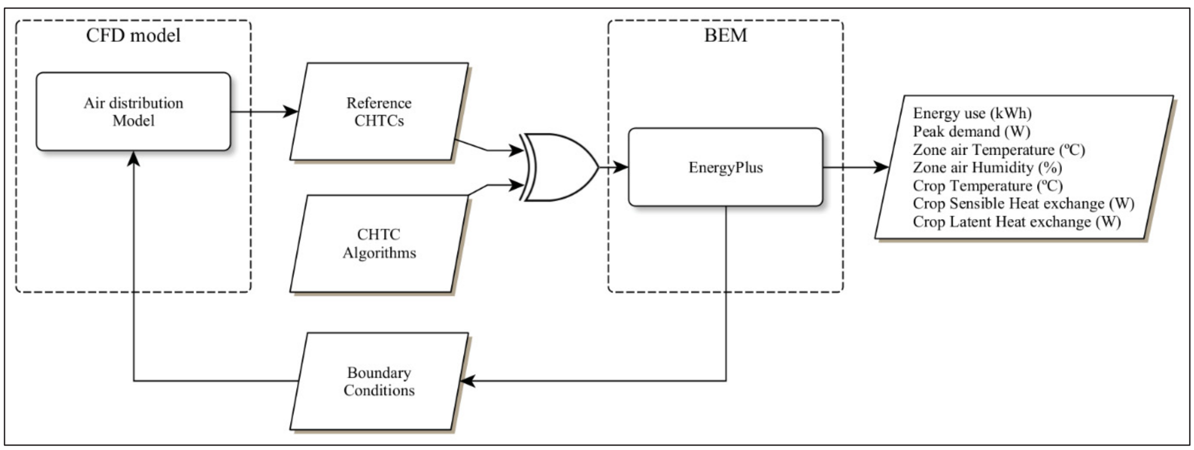

Figure 2.4 Méthodologie globale utilisée pour l'article #3

CHAPITRE 3

HIGH-DENSITY CONTROLLED ENVIRONMENT AGRICULTURE (CEA-HD) AIR DISTRIBUTION OPTIMIZATION USING COMPUTATIONAL FLUID DYNAMICS (CFD)

Gilbert Larochelle Martin[a], Danielle Monfet[a]

[a] Département de Génie de la construction, École de Technologie Supérieure,
1100 Notre-Dame Ouest, Montréal, Québec, Canada H3C 1K3

Article publié dans « Engineering Applications of Computational Fluid Mechanics »,
janvier 2024

Abstract

In this paper, the indoor environment of an experimental small-scale high-density controlled environment agriculture (CEA-HD) space was simulated using computational fluid dynamics (CFD). Spatial modelling of the indoor environment considering the influential phenomena (e.g., transpiration and photosynthesis) over the indoor temperature, relative humidity, carbon dioxide (CO2) concentration, and airflow velocity is still challenging. These indoor environment conditions were computed for a 3D model of a CEA-HD experimental space while simultaneously modelling crop airflow impingement, transpiration and photosynthesis. The crops being grown were represented in the model as porous media zones and their exchanges with the indoor air were modelled using user defined functions (UDFs). The air distribution parameters and configuration were optimized using a simplified 2D model to overcome the steep computational time, and associated cost, of 3D simulation. The objective function of the optimization problem relied on a correlation analysis of the simulation output. The optimization of the 2D model yielded an airfoil configuration that reduced the mean airflow speed and relative humidity variations between the cultivation tiers while achieving higher mean velocities (≈1.9 m·s-1) at a lower inlet speed (8 m·s-1) than reported in the literature. The proposed modelling and optimization approach, with further validation, is a small step forward towards model-based design and operation of CEA-HD production spaces.

Keywords: CEA, CEA-HD, CFD, optimization, plant factory, vertical farm

3.1 Introduction

In high-density controlled environment agriculture (CEA-HD) spaces, crops are grown indoor using multi-tiered hydroponic cultivation systems under complete artificial lighting. The crops are thus protected from meteorological variations, pests and other stress factors while growing in a precisely controlled indoor environment, promoting growth and resource use efficiency. The control of the indoor environment in CEA leads to higher yield than agriculture in fields: the mass of crops harvested in a CEA-HD can be fifteen times higher than in greenhouses and a hundred times higher than in the field (Kozai et al., 2015).

This higher yield is possible by maintaining specific indoor environmental conditions: the indoor air (1) temperature, (2) relative humidity, (3) CO_2 concentration, (4) airflow speed, and (5) the photosynthetically active radiation (PAR), all of which influence plant growth (Okayama et al., 2008b). The PAR is often provided using light emitting diode (LED) lighting with crop specific optimized spectrum and photoperiod. The other indoor environmental conditions are maintained within an optimal range using Heating, Ventilation and Air Conditioning (HVAC) equipment. The proper design and operation of the HVAC equipment in CEA-HD spaces is currently challenging as the information available is sparse since most of the knowledge is proprietary (Jonlin & Lewellen, 2017). Still, in recent years, there have been several advancements made in this field.

For example, the loads and energy consumption of a CEA-HD space using the «*perfectly stirred tank*» hypothesis was assessed by Graamans et al. (2017). This assumes that the air inside the space is perfectly mixed and that the indoor environmental conditions are homogeneous. While this assumption can be used for equipment sizing and evaluating energy consumption or the mean indoor environmental conditions, it does not support the representation of the spatial distribution of the indoor environmental conditions around the crops. Maintaining the indoor environment spatial uniformity is challenging in CEA-HD spaces (Lim & Kim, 2014; Baek et al., 2015). The number of cultivation shelves, the increased resistance to airflow by crops and the heat generated by the artificial lighting can influence the indoor environment spatial uniformity, which is essential to obtain a homogeneous crop production and prevent localized *«hot spots»* (Lim & Kim, 2014). Even with fans, local high temperature areas may exist in the cultivation zone (Jiang et al., 2018b). High local relative humidity can also lead to proliferation of fungi, causing production issues. Okayama et al. (2008b) stated that improved airflow control could lead to energy savings while maintaining the quality of crops being grown. Often, in CEA-HD, distributed or centralized fans are used to ensure adequate airflow speed over the leaves and the uniformity of the indoor environmental conditions to enhance crops growth. Currently, limited modelling tools and approaches to improve the airflow distribution of CEA facilities are available (Engler & Krarti, 2021), making it difficult to easily evaluate and enhance the uniformity of the space indoor environmental conditions.

Computational fluid dynamics (CFD) is an effective tool yielding reasonable accuracy in modelling complex phenomena in controlled environments (Zhang et al., 2016; Zhang & Kacira, 2018). Table 3.1 presents a review of 24 studies on CFD applications in greenhouses and CEA-HD spaces. CFD has been used to predict airflow characteristics in greenhouses such as ventilation rate or condensation risk, with several limitations being reported, such as model coupling issues (Bournet & Rojano, 2022). Among the reviewed studies, the air distribution in CEA-HD spaces using CFD was only modelled in 12 cases (Table 3.1). Also, Table 3.1 shows that less than 20% of the studies included a transpiration model to assess the relative humidity and less than 50% included a photosynthesis model to assess the CO_2 concentration. Hence, the spatial distribution of these two indoor environmental variables, influenced by the transpiration and photosynthesis of the crops, has been assessed sparsely. Additionally, the effect of the crops on the airflow has also been neglected in several studies. Yet, the influence of vegetation on airflow was highlighted by Koch et al. (2019) and recommended as future work by Zhang et al. (2016).

Table 3.1 Identified references concerning CFD analysis in CEA spaces after 2008

References	CEA Space Type	Geometry	Crops	Radiation	Turbulence model	Energy	Photosynthesis	Transpiration
Kim et al. (2008)	GH	3D	-	DO	k-ε	✓	-	-
Piscia et al. (2011)	GH	3D	-	-	k-ε	✓		✓
Kichah et al. (2012)	GH	2D	✓	-	k-ε	✓	-	✓
Nebbali et al. (2012)	GH	3D	✓	DO	k-ε	✓	-	✓
Roy et al. (2013)	GH	3D	-	DO	k-ε	✓	✓	✓
Piscia et al. (2013)	GH	3D	-	-	k-ε	✓	-	constant source
Farber et al. (2015)	GH	3D	✓	DO	k-ε	✓	✓	✓
Benni et al. (2016)	GH	2D	-	-	ml	✓	-	-
Farber et al. (2017)	GH	3D	✓	DO	k-ε	✓	-	✓
Boulard et al. (2017)	GH	3D	✓	DO	k-ε	✓	✓	✓
Hwang et al. (2017)	CEA-HD	3D	-	DO	k-ε	✓	-	-
Saberian and Sajadiye (2019)	GH	3D	✓	DO	k-ε	✓	-	-
Zhang et al. (2019a)	GH	3D	-	-	-	-	-	-
Niam et al. (2019a)	CEA-HD	3D	-	-	k-ε	✓	-	-
Niam et al. (2019b)	CEA-HD	2D	-	-	-	-	-	-
Fang et al. (2020)	CEA-HD	3D	✓	-	k-ε	✓	-	-
Lu et al. (2020)	CEA-HD	3D	-	-	-	-	-	-
Mohd Noh et al. (2020)	CEA-HD	3D	-	-	k-ε	✓	-	-
Zhou et al. (2020b)	CEA-HD	3D	-	-	k-ε	✓	-	-
Zhou et al. (2020a)	CEA-HD	3D	-	-	k-ε	✓	-	-
Fan et al. (2020)	CEA-HD	3D	-	-	-	✓	-	-
Naranjani et al. (2022)	CEA-HD	3D	-	-	k-ε	✓	constant source	constant source
Natarajan et al. (2022)	CEA-HD	3D	✓	-	k-ε	✓	-	-
Zhang and Kacira (2022)	CEA-HD	3D	✓	-	k-ε	✓	-	✓

GH : greenhouse, DO : discrete ordinates radiation model, ml : mixing length turbulence model

In terms of assessing the air distribution within CEA spaces, Okayama et al. (2008b) investigated three airflow control patterns over a single lettuce cultivation shelve using a simplified geometry in a commercial CFD tool. They also estimated the effect of the airflow speed on the photosynthetic rate using a relationship extracted from results obtained by Kitaya et al. (2003). Lim and Kim (2014) modelled and validated the airflow distribution inside a small-scale CEA-HD space and investigated four air distribution inlet-outlet combinations with their validated model to improve airflow distribution. Baek et al. (2016) studied different combinations of airflow equipment using CFD. They subsequently conducted growth experiments based on their CFD results and obtained improved yield. Zhang et al. (2016) investigated perforated tube air distribution system layouts inside a small CEA-HD space using CFD. The airflow uniformity in the CEA-HD space was evaluated using the coefficient of variation (CV), which is defined as the standard deviation over the mean, computed over the mesh cells at the top of the crop canopy. Zhang and Kacira (2018) also evaluated the performance of five air distribution configurations varying inlet and outlet locations using the CV.

Niam et al. (2019c) investigated the effect on the air temperature distribution for two different locations of an air conditioner installed in a shipping container plant factory. They reported high CO_2 concentration uniformity, but neglected to model the crops photosynthesis and airflow impingement. Fang et al. (2020) investigated three overhead perforated air tube designs in a CEA-HD setting. They also proposed an experimental setup to validate the LED lights as an energy source in a CFD model. Naranjani et al. (2022) modelled the crops as an exchange zone with constant rates of CO_2 consumption, O_2 production and water transpiration. They used their CFD model to study eight inlet outlet configurations in a 5-tier small CEA-HD production space. Zhang and Kacira (2022) modelled a CEA-HD space including the transpiration of the crops in five different inlet-outlet configurations. They concluded that the position of the air inlet had a major influence on the airflow and that the outlet had minimal influence.

This review highlights that none of the revised studies proposed an approach to optimize the airflow distribution within the space while simultaneously modelling crop airflow impingement, transpiration, and photosynthesis. These phenomena all directly affect the indoor growing environment, which in turn influences crop yield, quality and energy costs. Market demands require growers to produce a consistent, desirable and competitive product. Hence there is a need, at the CEA-HD level, to propose an approach to optimize the air distribution of CEA-HD spaces considering all of these phenomena. In this paper, an optimization approach to improve the airflow distribution using a CFD model of a small scale high-density controlled environment agriculture (CEA-HD) space is proposed. The model of the CEA-HD indoor environment considered the impact of crops in terms of airflow impingement, transpiration, and photosynthesis through the use of a porous media model, a heat balance algorithm at the leaf and an empirical model, respectively. The proposed approach also implements an optimization strategy that uses correlation analysis and simplified geometry modelling to maintain the simulation time acceptable while considering all of the above-mentioned phenomena. It allows optimizing the configuration of the air distribution system and of the production space to improve the uniformity of the indoor environmental conditions around the crops.

3.2 Materials and Methods

In this paper, an approach is proposed to optimize the supply air inlet conditions and the geometry of the air distribution system using computational fluid dynamics (CFD) and crop modelling. The optimization implicates geometry simplifications, objective function simplifications and a metaheuristic optimization algorithm. This approach aims to maximize the spatial uniformity of the environmental conditions of a small-scale CEA-HD space while minimizing the air inlet speed and thus the inlet air flow rate. In this section, the governing equations of CFD, the crop model and the optimization approach are detailed.

3.3 Computational Fluids Dynamics

The fundamental equations of fluid dynamics – continuity (equation (3.1)), conservation of momentum (equation (3.2)) and conservation of energy (equation (3.3)) equations – are stated below.

$$\frac{\partial \rho}{\partial t} + \nabla \cdot (\rho \cdot \boldsymbol{V}) = 0 \tag{3.1}$$

$$\frac{\partial (\rho \cdot \boldsymbol{V})}{\partial t} + \nabla \cdot (\rho \cdot \boldsymbol{V} \cdot \boldsymbol{V}) = -\nabla p + \nabla(\bar{\bar{\tau}}) + \rho \cdot \boldsymbol{g} + \boldsymbol{F} \tag{3.2}$$

$$\frac{\partial (\rho \cdot E)}{\partial t} + \nabla \cdot \big(\boldsymbol{V}(\rho \cdot E + p)\big) = \nabla \cdot \left(k_{eff} \cdot \nabla T - \sum_j h_j \cdot J_j + \big(\bar{\bar{\tau}}_{eff} \cdot \boldsymbol{V}\big) \right) + S_h \tag{3.3}$$

Where ρ is the fluid density (kg·m^{-3}), $\boldsymbol{V}$ is the velocity (m·s^{-1}), p is the pressure (Pa), $\bar{\bar{\tau}}$ is the stress tensor (Pa), $\bar{\bar{\tau}}_{eff}$ is the deviatoric stress tensor (Pa), $\boldsymbol{g}$ is the gravity vector (m·s^{-2}), $\boldsymbol{F}$ is the external forces (N), k_{eff} is the effective conductivity (W·m^{-1}·K^{-1}), T is the temperature (K), h_j the enthalpy (kJ·kg^{-1}), J_j the diffusion flux (kg·m^{-2}·s^{-1}), and S_h is the volumetric heat sources (W·m^{-3}).

As most indoor flows are turbulent in nature, the turbulence of the airflow is modelled using the k-ε turbulence model since it is the most used turbulence model as illustrated in Table 1. This model is described in equation (3.4) for the turbulence kinetic energy (k, m^2·s^{-2}) and equation (3.5) for the dissipation of the turbulence kinetic energy (ε, m^2·s^{-3}).

$$\frac{\partial (\rho \cdot k)}{\partial t} + \nabla \cdot (\rho \cdot k \cdot \boldsymbol{V}) = \nabla \cdot \left[\frac{\eta_t}{\mathrm{Pr}_k} \cdot \nabla \mathrm{k}\right] + 2\mu_t \cdot E_{ij} \cdot E_{ij} - \rho \cdot \varepsilon \tag{3.4}$$

$$\frac{\partial (\rho \cdot \varepsilon)}{\partial t} + \nabla \cdot (\rho \cdot \varepsilon \cdot \boldsymbol{V}) = \nabla \cdot \left[\frac{\eta_t}{\mathrm{Pr}_\varepsilon} \cdot \nabla \varepsilon\right] + C_{1\varepsilon} \cdot \frac{\varepsilon}{k} \cdot 2 \cdot \mu_t \cdot E_{ij} \cdot E_{ij} - C_{2\varepsilon} \cdot \rho \cdot \frac{\varepsilon^2}{k} \tag{3.5}$$

Where η_t is the turbulent viscosity (Pa·s^{-1}), Pr are the turbulent Prandtl numbers and $C_{1\varepsilon}$ and $C_{2\varepsilon}$ are constants (default values used). The water and CO_2 transport are modelled using the species transport model presented in equation (3.6).

$$\frac{\partial(\rho \cdot Y_i)}{\partial t} + \nabla \cdot (\rho \cdot \boldsymbol{V} \cdot Y_{\boldsymbol{i}}) = -\nabla \cdot (\boldsymbol{J}_i) + R_i + S_i \tag{3.6}$$

Where $Y_{\boldsymbol{i}}$ is the local mass fraction (kg·kg^{-1}), $\boldsymbol{J}_i$ the diffusive flux (kg·m^{-2}·s^{-1}), R_i the net rate of production (kg·m^{-3}·s^{-1}) and S_i the species sources (kg·m^{-3}·s^{-1}). For a turbulent flow, the diffusive flux is modelled as per equation (3.7).

$$\boldsymbol{J}_i = -\left(\rho \cdot D_{i,m} + \frac{\mu_t}{Sc_t}\right) \cdot \nabla Y_i - D_{T,i} \cdot \frac{\nabla T}{T} \tag{3.7}$$

Where Sc_t is the turbulent Schmidt number and D_T is the turbulent diffusivity (m^{-2}·s^{-1}).

Equations (3.1) to (3.7) address continuity, momentum, energy, turbulence and mass transport, but do not consider the impact of crops interaction with the air inside the CEA-HD production space. For this to be considered, a crop model is proposed, based on additional equations, that are integrated to the CFD model of the CEA-HD space.

3.3.1.1 Crop model

Crops inside a CEA space exchange momentum, heat and mass with the environment, which influence the indoor environmental conditions. Modelling of these exchanges can be crop specific but is often linked to the leaf area index (LAI) or the leaf area density (LAD, m^{-1}). The LAI is defined by the total one-sided leaf area per horizontal surface unit (Watson, 1947) and the LAD is defined as the LAI divided by the crop height (Boulard et al., 2017).

In this paper, the cop model is detailed for lettuce since it is frequently cultivated in CEA-HD space due to its short cultivation cycle and low light intensity requirements (Okayama et al., 2008b). The crop model includes equations embedded in *«User Defined Functions»* (UDFs) to consider the impact of the crops on the computed temperature, relative humidity, CO_2 concentration, and velocity. These UDFs can be adapted to most CFD codes, but are tailored to ANSYS Fluent R19.2. The crop model includes three distinct phenomena: (1) crop airflow impingement, (2) crop transpiration and (3) crop photosynthesis.

3.3.1.2 Crop airflow impingement

Modelling a plant inside a plant canopy, including the individual leaves, is very challenging (Defraeye et al., 2013). As a compromise between accuracy and computational time, the plant canopy can be modelled as a porous media zone (Boulard et al., 2002; Kichah et al., 2012; Nebbali et al., 2012; Boulard et al., 2017; Farber et al., 2017; Fang et al., 2020; Natarajan et al., 2022; Zhang & Kacira, 2022). In this paper the formulation from Boulard et al. (2017) is used to represent the effect of the crops on the momentum as detailed in equation (3.8).

$$\boldsymbol{F_{x,y}} = -\rho_a \cdot C_d \cdot LAD \cdot s \cdot u_{x,y} \tag{3.8}$$

Where ρ_a is the air density (kg·m^{-3}), C_d is the drag coefficient of the canopy, s is the airflow speed (m·s^{-1}) and $u_{x,y}$ is the corresponding cartesian velocity (m·s^{-1}).

3.3.1.3 Crop Transpiration

In enclosed hydroponic systems, the only source of water vapour is the transpiration from the crops since the evaporation of the nutritive solution can be assumed to be negligible (Monje (1998)). Multiple transpiration models have been proposed, most of which are derived from an energy balance at the leaf (Talbot & Monfet, 2020). In this paper, the model proposed by Graamans et al. (2017) is used since it has been validated experimentally under steady-state conditions as part of a study of a controlled-environment agriculture (CEA) space (equation (3.9)).

$$R_n - H - LE = 0 \tag{3.9}$$

Where R_n is the net radiation flux (W·m^{-2}), essentially the PAR, absorbed by the crops from lights. In this paper, the PAR is set to a constant value and it is supposed that it corresponds to the lighting short-wave radiation that is entirely absorbed by the cultivated crops. H is the sensible heat flux (W·m^{-2}) computed as a convective exchange flux with the indoor air and LE is the latent exchange flux (W·m^{-2}) with indoor air. The convective exchange flux is computed using equation (3.10).

$$H = LAI \cdot \frac{\rho_a \cdot c_p}{r_a} (T_{plt} - T_a) \tag{3.10}$$

Where r_a is the aerodynamic resistance (s·m^{-1}), T_{plt} is the leaf surface temperature (ºC), c_p is the air specific heat capacity (kJ·kg^{-1}) and T_a is the indoor air temperature (ºC). The heat balance equation (equation (3.9)) is solved for the leaf temperature using the secant method (Kreyszig, 1999) in each cell of the porous media zones. The latent exchange flux is estimated according to equation (3.11).

$$LE = LAI \cdot \frac{\rho \cdot c_p}{66\,(r_a + r_{sl})} \left(SP\left(T_{plt}\right) - SP(T_a) \cdot RH\right) \tag{3.11}$$

Where r_{sl} is the stomatal resistance (s·m^{-1}), SP is the saturation pressure function (ASHRAE, 2013a) and RH is the air relative humidity. The aerodynamic resistance (r_a) is modelled using equation (3.12), while the stomatal resistance (r_{sl}) is modelled using equations (3.12) to (3.15).

$$r_a = 305 \cdot \frac{0.15}{\sqrt{\|\boldsymbol{V}\| + \left(9.81 \cdot 0.0034 \cdot \left|T_{plt} - T_{air}\right|\right)^{0.5}}} \tag{3.12}$$

$$r_{sl} = 120 \cdot f_1 \cdot f_2 \tag{3.13}$$

$$f_1 = 1 + e^{0.043 \cdot (R_n - 49)^{-1}} \tag{3.14}$$

$$f_2 = 1 + e^{0.043 \cdot (T_{plt} - 0.38)} \tag{3.15}$$

3.3.1.4 Crop Photosynthesis

CO_2 is essential to the growth of crops via the Calvin cycle and photosynthesis. In a CEA-HD space, the CO_2 concentration is usually maintained around 1000 – 1200 ppm using an injection system to promote crop growth. Only one photosynthesis equation applied to the CFD analysis of the airflow in CEA-HD was found, which was proposed by Okayama et al. (2008b) based on the results of Kitaya et al. (2003). As such, equation (3.16), which specifically applies to CEA-HD production spaces and is not adapted from greenhouse production, is used to model photosynthesis.

$$P_{cell} = 1.4 \cdot (1 - e^{-12.8 \cdot s}) + 1.52 \qquad (3.16)$$

Where P_{cell} is the cell net photosynthetic rate (μmol·s^{-1}) and s is the airflow speed. Equation (3.16) is used in the model and is a simplified representation of a complex process. Still, this model implementation in a commercial CFD code is an improvement compared to a constant photosynthesis rate (Naranjani et al., 2022) or completely neglecting photosynthesis (Zhang & Kacira, 2022).

3.3.2 Air distribution optimization

An optimization algorithm is proposed to improve the spatial uniformity of the environmental conditions inside the CEA-HD space by modifying the configuration of the air distribution systems and of the production space. This is achieved by varying the inlet boundary conditions of the distribution system and the configuration of the production space. As such, the fluctuations of the indoor environmental conditions surrounding the crops inside the modelled production space are minimized, while maintaining acceptable airflow speed. The proposed air distribution optimization involves four steps: (1) simplifying the geometry, (2) analyzing the simulation outputs, (3) refining the objective function, (4) optimizing the inlet conditions and the production space configuration.

The metric used to assess the spatial uniformity is the CV (equation (3.17)), as suggested by Zhang et al. (2016).

$$\mathrm{CV} = \frac{\sigma}{\mu} \tag{3.17}$$

Where σ is the standard deviation and μ is the mean.

The optimization algorithm used is NSGA-II (Deb et al., 2002), a widely used metaheuristic genetic optimization algorithm. This non-dominated sorting genetic algorithm is designed to escape local minima and give results that are independent of the initial solution. The algorithm replaces half of the population in each generation and generates offspring through front ranking, crossover and mutation operators. Further information about evolutionary optimization algorithms is available in Rao (2019). The simulation outputs are first analyzed using the Pearson correlation coefficient (equation (3.18)) to identify potential linear correlations between the indoor environmental variables.

$$r_{X,Y} = \frac{COV(X,Y)}{\sigma_x \cdot \sigma_y} \tag{3.18}$$

Where COV is the covariance, σ_x is the standard deviation of X and σ_y is the standard deviation of Y. The X and Y represent the indoor environmental conditions such as temperature or absolute humidity (ω).

3.4 Model description

The proposed approach is applied to an experimental small-scale CEA-HD space. The studied hydroponic production system is illustrated in Figure 3.1a and the production space enclosure is illustrated in Figure 3.1b. In the production system, light emitting diodes (LEDs) lighting is used and the nutrient solution is stored in a tank positioned beneath the lower growing tier. This system uses the nutrient film technique (NFT) to circulate the nutrient solution inside three tiers of plastic gutters and is conditioned using a forced-air system (inlets and outlet shown on Figure 3.1b).

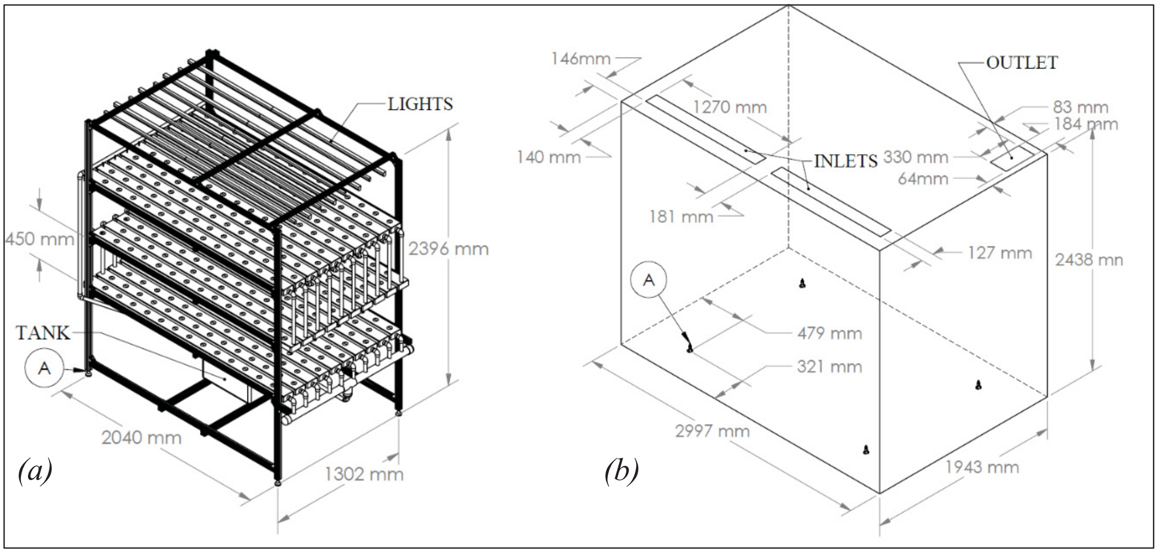

Figure 3.1 CAD models of (a) the production system and
(b) the enclosure of the small-scale CEA-HD space

The computer-aided design (CAD) model of the CEA-HD space (Figure 3.1a) is used to extract the geometry of the 3D model (Figure 3.2a) to be used as an input in the CFD software (ANSYS Fluent R19.2). A mesh of the simulation domain is subsequently generated (Figure 3.2b) to discretize the previously defined equations over both the production space and the crops. The mesh is then checked for orthogonal quality, skewness and aspect ratio.

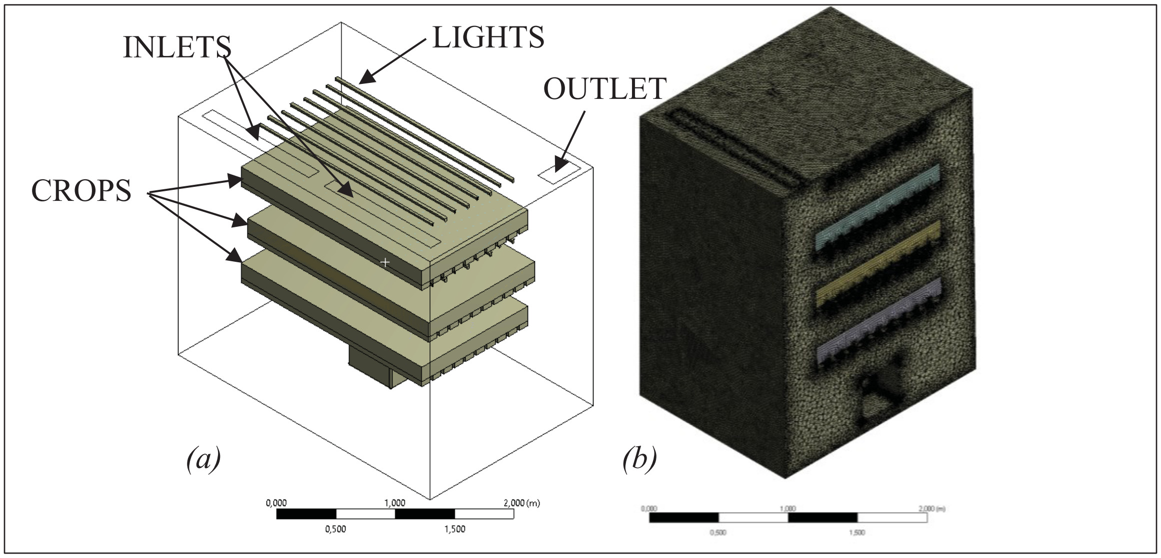

Figure 3.2 Small-scale CEA-HD space (a) 3D model geometry (left) and (b) section view of the 3D mesh generated in ANSYS (right)

The boundary conditions and the parameters used to model the effects of the crops on the airflow are listed in Table 3.2. As recommended by Zhang and Kacira (2022), only the PAR emitted by the lighting is included in the model and it is assumed to be absorbed by the cultivated crops. The lights are also modelled as having a constant surface temperature. The inlet air conditions are selected for an outdoor air system operating in cold climate conditions with dedicated outdoor air and sensible reheat. The LAD is based on a crop height of 40 cm.

Table 3.2 Inlet boundary conditions and crops modelled input parameters

Category	Parameters	Values
Inlet air	Temperature (ºC)	15
	Relative humidity (%)	20
	CO_2 concentration (ppm)	400
	Airflow speed ($m \cdot s^{-1}$)	0.5
Crops	LAI	1
	LAD	2.4
Lighting	Net radiation (R_n) - PAR ($W \cdot m^{-2}$)	120
	Surface temperature (ºC)	30

3.5 Results

The results are presented for each of the steps described in section 3.3.2. These allow a better understanding of the proposed approach as well as the potential to optimize the air distribution within a CAE-HD space.

The initial simulation results are obtained using the boundary conditions presented in Table 2. The results are presented using contour plots for the temperature (Figure 3.3a), the relative humidity (Figure 3.3b), the CO_2 concentration (Figure 3.3c), and the airflow speed (Figure 3.3d). In this paper, the relative humidity displayed in the figures is calculated using the simulation results for the absolute humidity. The temperature contour plot (Figure 3.3a) illustrates higher temperatures in the light's vicinities. Thus, the predicted sensible heat flux caused a slight increase of the temperature of the air within the vicinities of the porous media zone. The relative humidity contour plot illustrated in Figure 3.3b clearly shows (1) heterogeneity inside the three porous media zones and (2) a lower relative humidity near the lights, which is explained by the higher water vapour capacity of the air at higher temperature. Finally, in terms of CO_2 concentration (Figure 3.3c), it can be noted that there is (1) heterogeneity at the three porous media zones and (2) that the model predicts a lower concentration of a few ppm at the outlet. This is consistent with the expected behavior of the photosynthesis rate model presented in equation (3.16). Figure 3.3d clearly shows that the majority of the predicted airflow is not directed towards the cultivated crops but is diverted towards the side walls (consistent with the Coanda effect) and then passes under the cultivation rack before reaching the outlet.

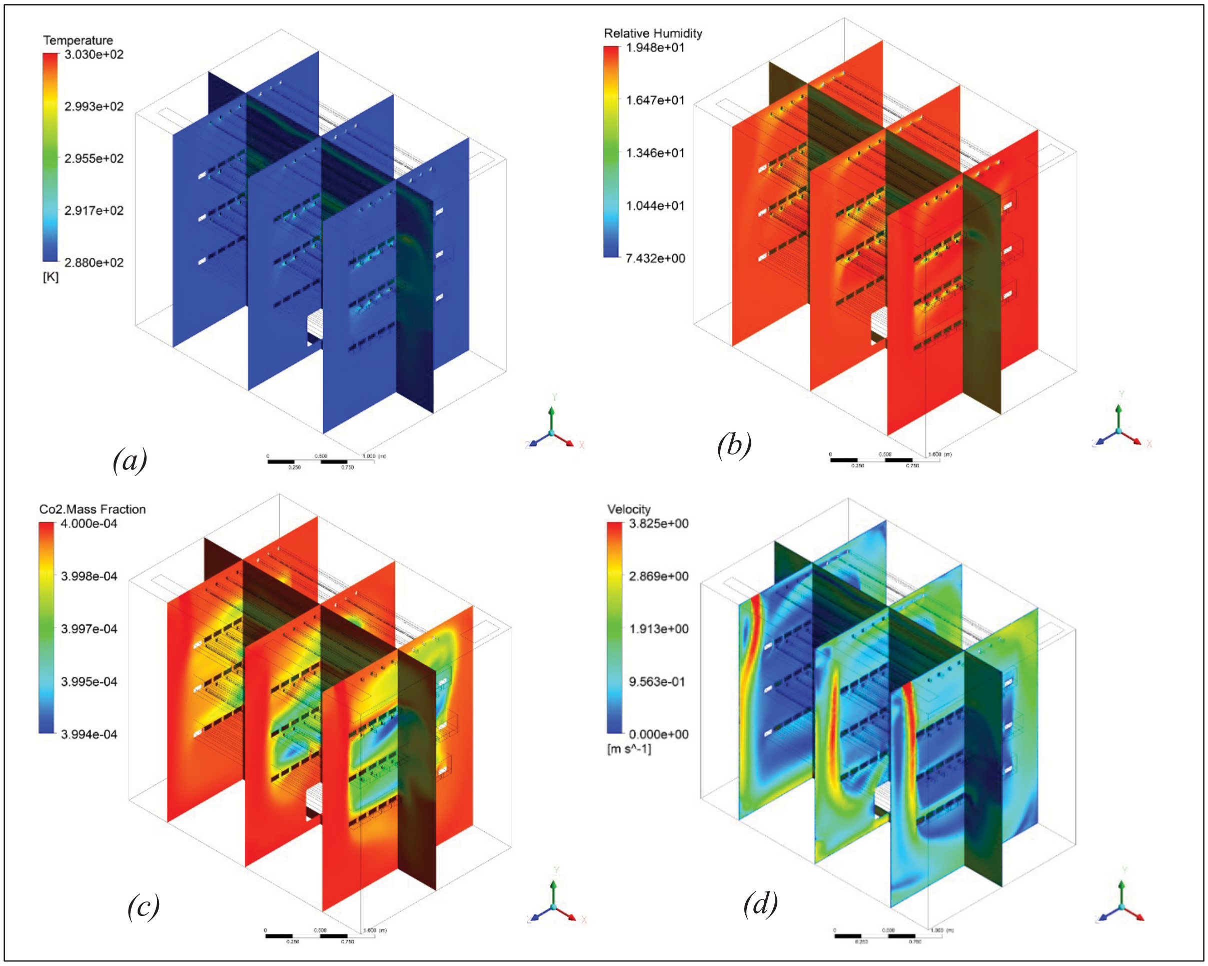

Figure 3.3 Contour plots of the modelled small-scale CEA-HD: (a) temperature, (b) relative humidity, (c) CO_2 concentration, and (d) airflow speed

3.5.1 Geometry simplification

The mesh presented in Figure 3.2 consists of approximately 17 million elements, which results in several days of simulation time to reach convergence. This prohibits the coupling with an optimization algorithm. To address this issue, the 3D geometry is simplified using a 2D projection of the model geometry. The resulting 2D geometry is illustrated with the corresponding mesh in Figure 3.4.

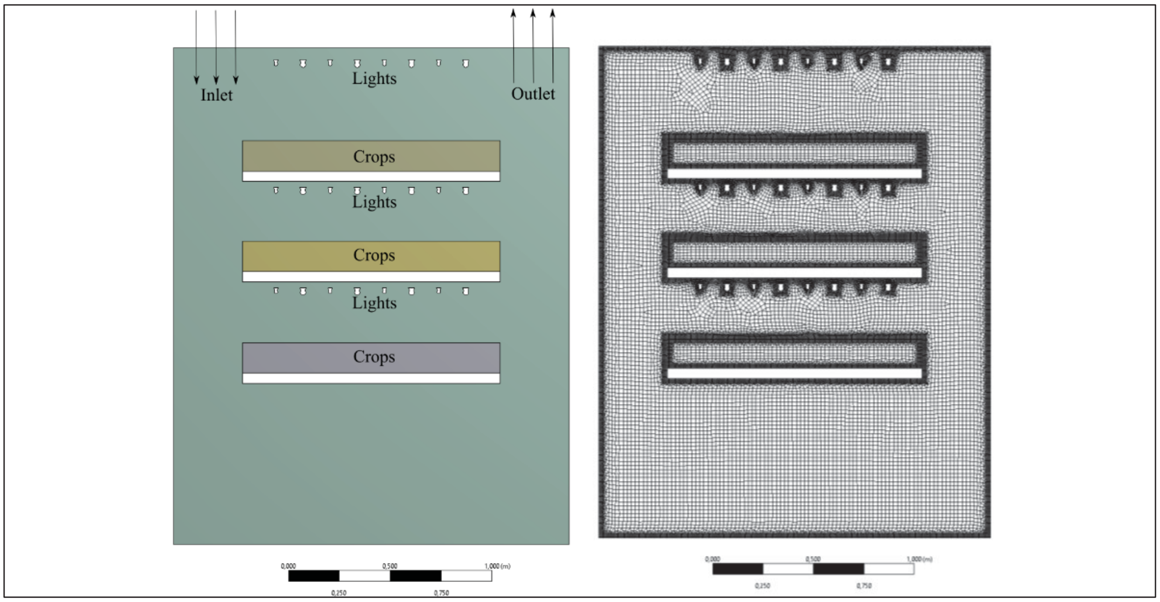

Figure 3.4 Small-scale CEA-HD space (a) 2D projection of the model geometry (left) and (b) mesh generated in ANSYS (right)

Before proceeding with the optimization approach, a grid convergence analysis, which is function of the number of mesh cells, is performed as a verification step (McHale et al., 2009). The observed output variables are the average relative humidity and average airflow speed inside the porous media zone, the crop zone, of the lower growing tier, which is one of the regions of interest of the simulation. Figure 3.5 presents the results of the grid convergence analysis and shows that beyond 50 000 cells, there is no variation of the studied output indoor environmental variables. This illustrates that the results are independent from mesh size. Additionally, manual inspection of the temperature, relative humidity, CO_2 concentration, and airflow speed contour plots exhibited the same flow characteristics. The results are presented for the finest grid size using contour plots for the temperature (Figure 3.6a), the relative humidity (Figure 3.6b), the CO_2 concentration (Figure 3.6c), and the airflow speed (Figure 3.6d).

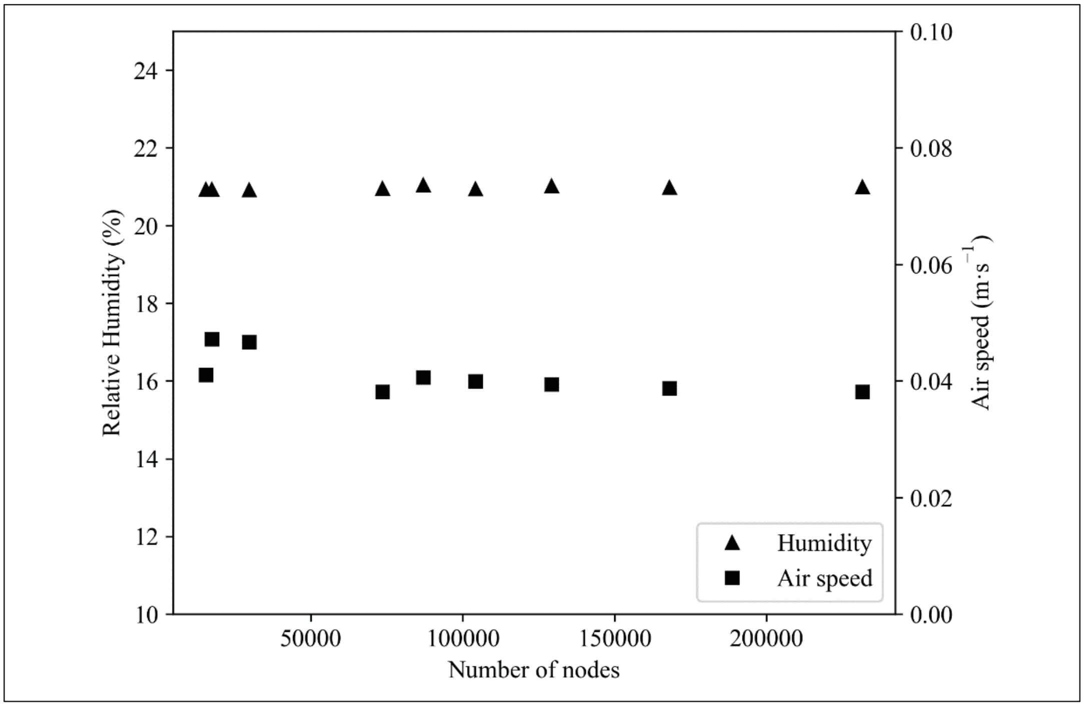

Figure 3.5 Grid convergence results for the lower growing tier porous media zone (average relative humidity and airflow speed)

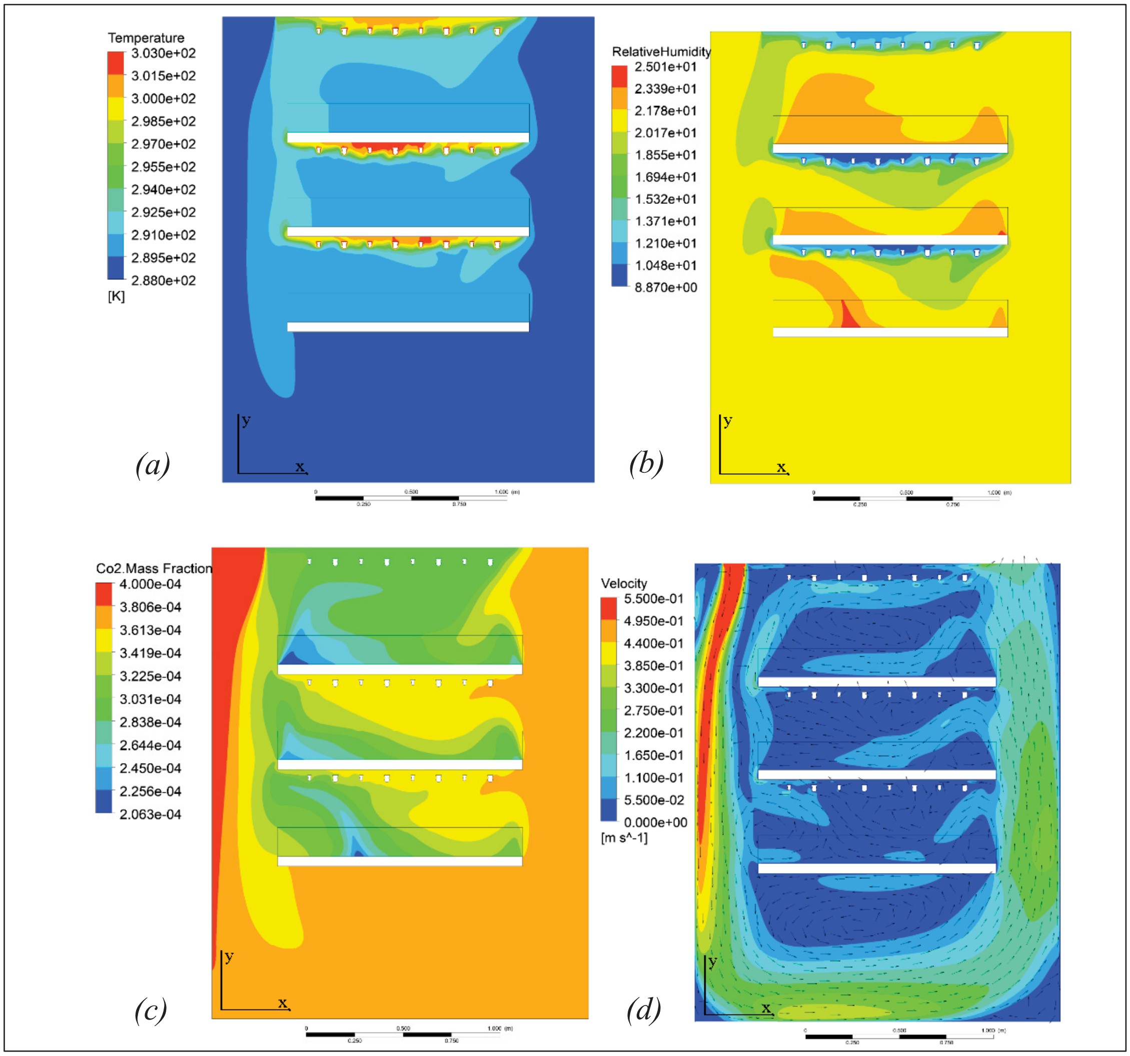

Figure 3.6 Contour plots of the modelled small-scale CEA-HD: (a) temperature, (b) relative humidity, (c) CO_2 concentration, and (d) airflow speed

As shown in Figure 3.1a, the production system has a nutrient holding tank positioned beneath the lower growing tier. The influence of the holding tank (at room temperature) is considered , as illustrated in Figure 3.7, and it is deemed to be not significant as there are only minor discrepancies in the airflow speed when Figure 3.6d and Figure 3.7 are compared.

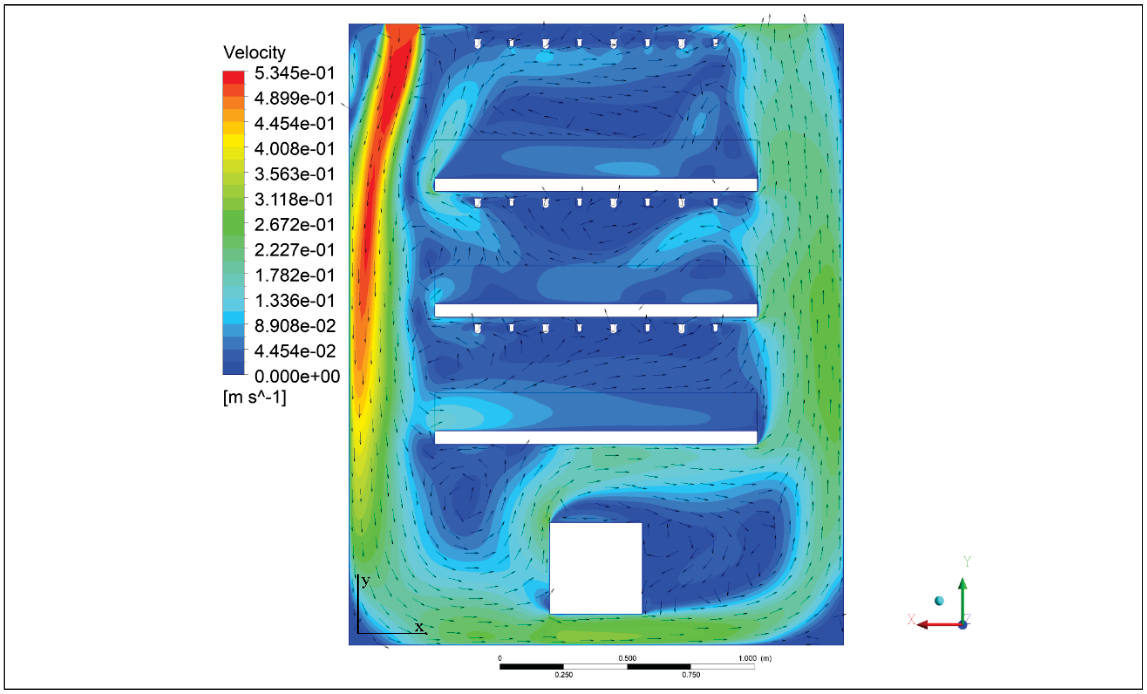

Figure 3.7 Contour plot of the airflow speed when the nutrient solution tank is modelled

3.5.2 Simulation outputs analysis

In order to reduce the optimization time, which can take up to 3 days (AMD EPYC 7351P, 64 GB of RAM) when considering all the indoor environmental variables, the Pearson correlation coefficient (equation (3.18)) is first computed. This is done to assess the linear correlation between the indoor environmental variables as observed during the review of the initial optimization results (Figure 3.8).

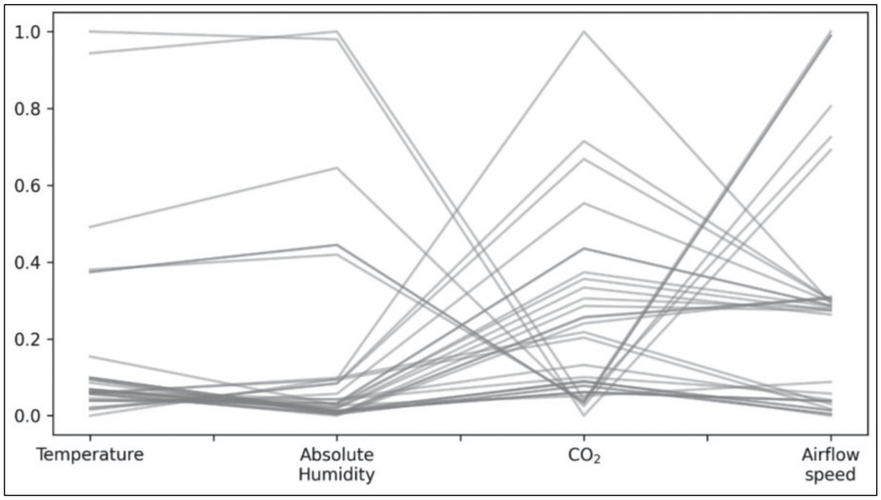

Figure 3.8 Scaled output values of the optimization runs

Figure 3.9 shows that there is a correlation between the CV of the temperature, the CO_2 concentration, and the airflow speed, while the CV of the absolute humidity does not exhibit such correlation. Hence, the CV of the temperature and CO_2 concentration can be removed from the objective function since they are adequately represented by the CV of the airflow speed.

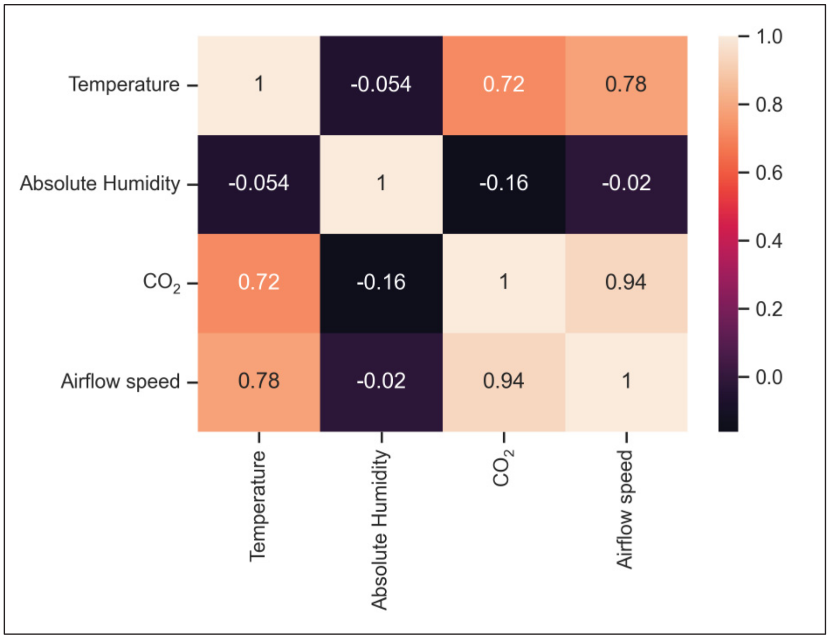

Figure 3.9 Pearson coefficient's of the computed CV
for the four indoor environmental variables

3.5.3 Objective function simplification

As a results, the objective function is formulated according to equation (3.19), which aims to minimize the coefficient of variation (CV) within the crop zone of each tier and the difference between tiers for the airflow speed and the absolute humidity while simultaneously maximizing the average airflow speed.

$$\min f(x) = \frac{\sum_1^n \mathrm{CV}(s_n)}{n_{tiers}} + \sum_1^n \mathrm{CV}(s_n) + \frac{\sum_1^n \mathrm{CV}(\omega_n)}{n_{tiers}} + \sum_1^n \mathrm{CV}(\omega_n) - \sum_1^n \mathrm{Mean}(s_n) \tag{3.19}$$

Where the coefficient of variation of the mean airflow speed (s, $m \cdot s^{-1}$) and the absolute humidity (ω, $kg \cdot kg^{-1}$) is computed for each tier (n is the number of tiers).

3.5.4 Inlet conditions and production space configuration optimization

Improving the spatial uniformity within the space can be achieved using different air distribution strategies. The first optimization run (optimization 1) varies the inlet speed and the inlet angle, while the second (optimization 2) included two additional modifications. One modification consists of implementing a wall boundary conditions at the inlet edge to block the lower part of the cultivation growing tier system since the airflow tends to circulate below the lowest cultivation tier. This can be easily implemented by inserting a thin plastic film, similar to blanking panels used in data centers, into the existing system. The second is used to alter the airflow direction by placing a single aerodynamic device near the inlet. This is modelled after a duct elbow turning vane commonly used in HVAC systems. The location of the device and pitch are included as inputs to the multi-objective second optimization run. Figure 3.10 illustrates the vane profile and the other optimization inputs, while Table 3.3 presents the inputs lower and upper bounds for the optimization algorithm for both optimization runs.

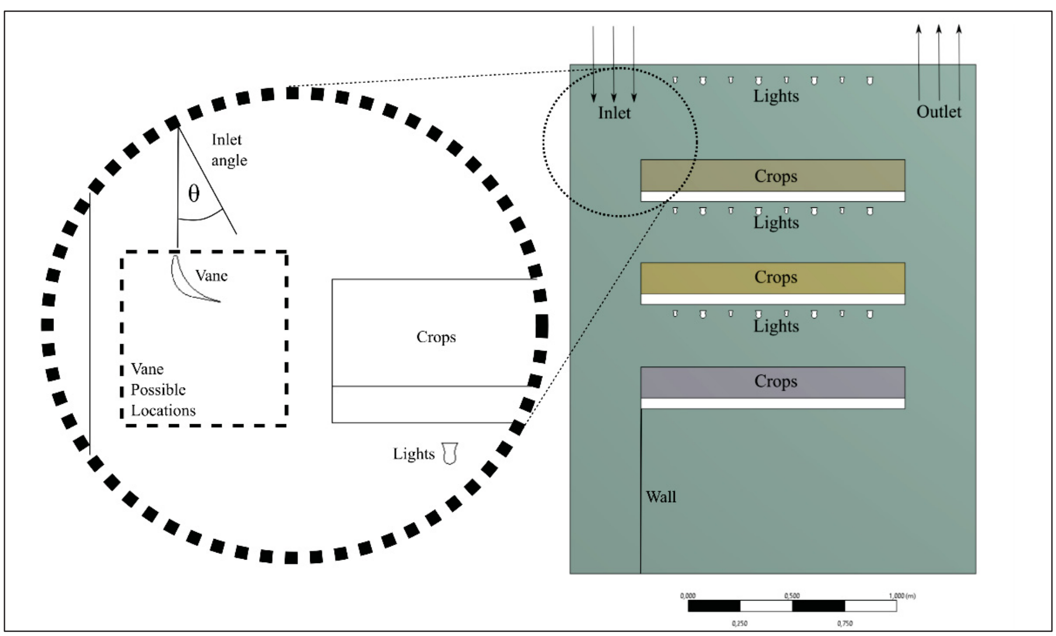

Figure 3.10 Illustration of the optimization variables

Table 3.3 Objective functions and lower and upper bounds for the optimization runs

Inputs	**Optimization 1**		**Optimization 2**	
	Lower Bound	Upper Bound	Lower Bound	Upper Bound
Inlet speed ($m \cdot s^{-1}$)	3.5	8.5	0.1	8.5
Inlet angle (rad)	0.0	0.7	-0.2	0.4
Vane angle (^{o})	-		-105	-75
Vane X position (m)	-		1.15	1.35
Vane Y position (m)	-		-0.7	-0.45

The CFD simulation, for the optimized inlet boundary conditions of 5.5 $m \cdot s^{-1}$ inlet airflow speed and 0.25 rad angle from the vertical towards the production system, are presented in Figure 3.11. The results for this optimization (optimization 1) are presented in Table 3.4.

Table 3.4 Objective function results for optimization 1

Output	**Lower Tier**	**Middle Tier**	**Upper Tier**
CV (ω), absolute humidity	2.0 %	1.2 %	1.3 %
CV (s), airflow speed	60.3 %	31.9 %	42.4 %
Mean airflow speed ($m \cdot s^{-1}$)	0.288	0.351	0.361

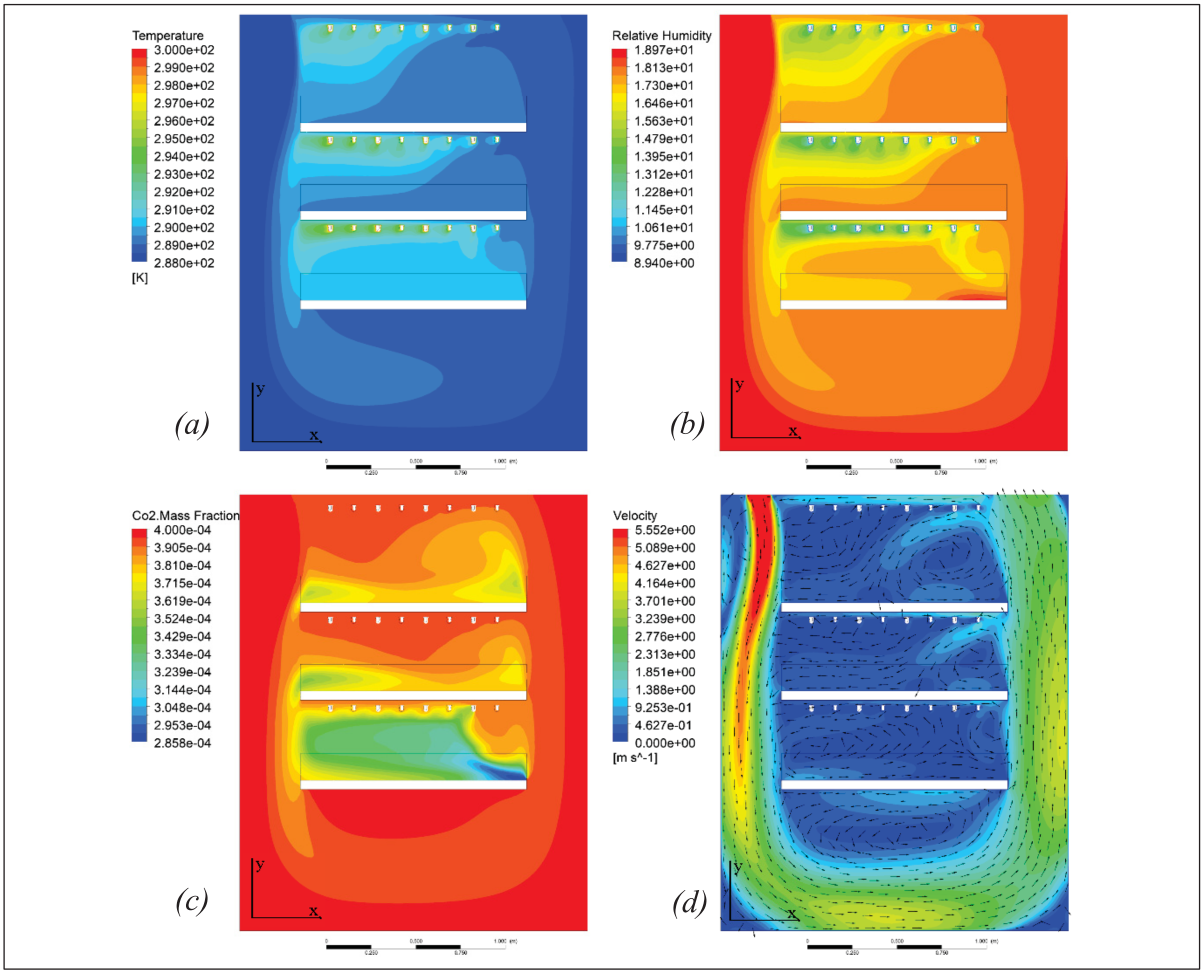

Figure 3.11 Contour plots of the modelled small-scale CEA-HD for optimization 1, with optimized inlet boundary conditions: (a) temperature, (b) relative humidity, (c) CO_2 concentration, and (d) airflow speed with velocity overlay

In Figure 3.11c, it can be observed that the airflow speed at the lowest tier is lower, which coincided with a drop-in CO_2 concentration at the outlet edge. Figure 3.11d displays the velocity overlay, indicating that the airflow is directed towards the centre of the top and middle cultivation tiers from the outlet side of the production space. Still, the majority of the airflow goes around the production system.

Figure 3.12 presents the results of the optimized inlet and aerodynamic airfoil profile parameters. The optimal input values and the results from the last optimization (optimization 2) are presented respectively in Table 3.5 and in Table 3.6.

Table 3.5 Optimization 2 optimal values

Inputs	Optimal Value
Inlet speed ($m \cdot s^{-1}$)	8
Inlet angle (rad)	-0.05
Vane angle (º)	-101
Vane X position (m)	1.23
Vane Y position (m)	-0.55

Table 3.6 Optimization 2 objective function terms results

Output	Lower Tier	Middle Tier	Upper Tier
CV (ω), absolute humidity	0.3 %	1.4 %	1.9 %
CV (s), airflow speed	34.6 %	43.5 %	54.1 %
Mean airflow speed ($m \cdot s^{-1}$)	1.813	1.904	1.976

The proposed modifications implemented in this last optimization run successfully reduce the maximum difference of the coefficient of variation of the mean airflow speed between tiers from 28.4 % to 19.5 %. However, this improvement came at the expense of increased CV variations in absolute humidity between tiers. In Figure 3.12c, a clear CO_2 concentration gradient is noted from the inlet side of the production system to the outlet side, as expected based on the simplified mass source modelled defined by equation (3.16). The effect of the airfoil device in splitting the flow is clearly demonstrated in Figure 3.12d.

The air distribution parameters and configuration results obtained from optimization 2 are then used in a final 3D simulation of the CEA-HD space, as shown in Figure 3.13. These results highlight significant improvements compared to the initial simulation results of Figure 3.3. The flow characteristics observed in Figure 3.13 align with those obtained from the 2D model results illustrated in Figure 3.12. Furthermore, Table 3.7 presents the comparison between the mean CV (equation (3.17)) over the three production tiers of the initial 3D model and the optimized 3D model for the four computed indoor environment variables. The results clearly demonstrate that the proposed 2D optimization approach yields improvements of the 3D model results across all indoor environment conditions, with the most significant improvement observed in the reduction of the mean velocity CV.

Table 3.7 Initial and Optimized 3D model mean CV of the indoor environment variables

Variable	**Initial 3D model mean CV**	**Optimized 3D model mean CV**
Velocity	87.4 %	17.7 %
Temperature	0.11 %	0.06 %
Humidity	1.84 %	0.99 %
CO_2	0.08 %	0.03 %

This suggests that a 2D model optimization can be used for practical design air distribution systems in 3D CEA-HD spaces. This enables designers to use optimization algorithms that would not be possible if a 3D model was required. This also allows the evaluation and optimization of multiple space configurations as demonstrated in this paper. All of these significant practical aspects are attainable with the proposed approach while still accounting for crop airflow impingement, crop transpiration and crop photosynthesis. Further, the proposed model can be extended for other practical applications, such as estimating the peak demand and energy required for ventilation, developing advanced cooling lighting system, proposing thermal storage solutions, etc.

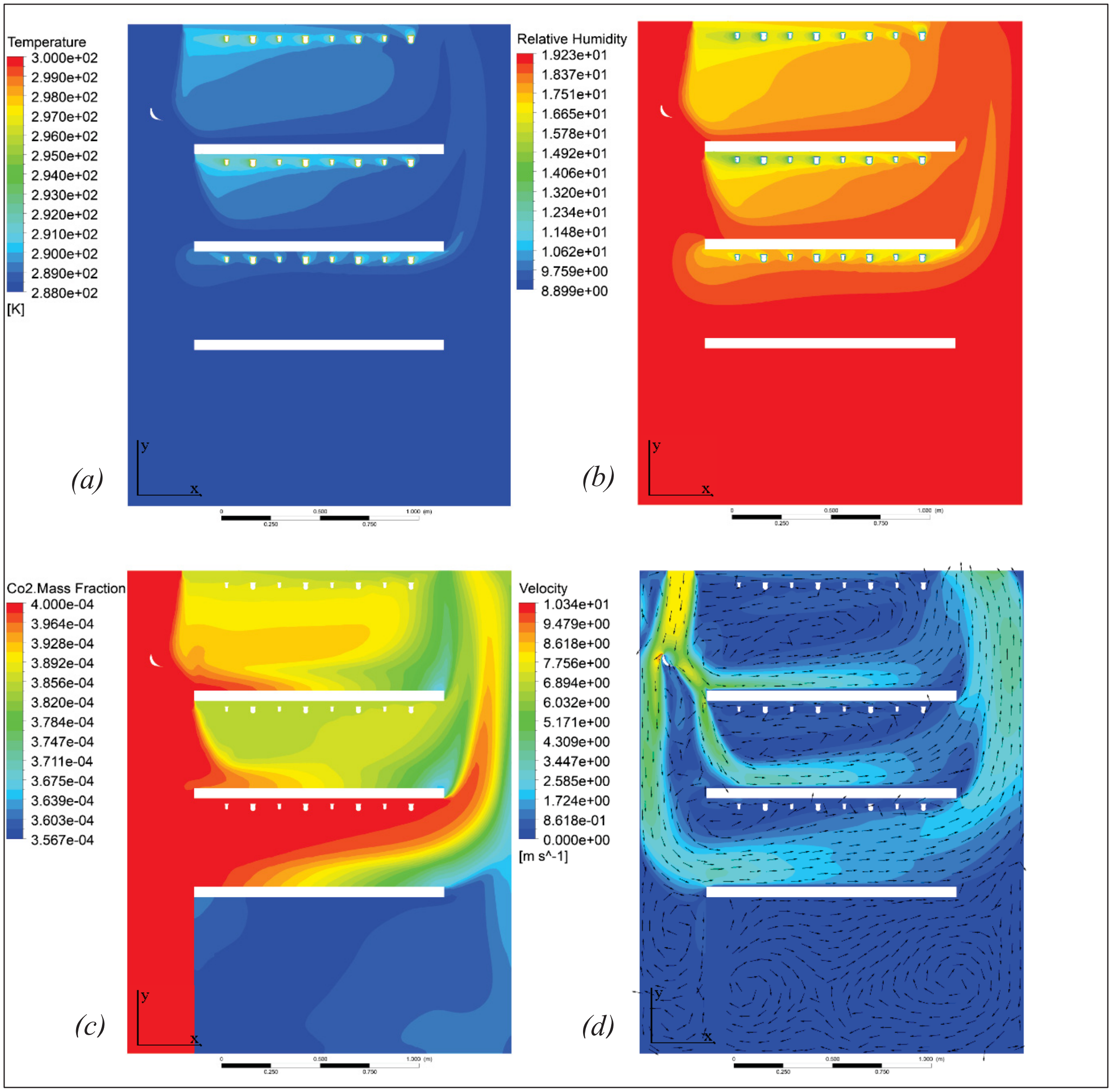

Figure 3.12 Contour plots of the modelled small-scale CEA-HD for optimization 2, with optimized inlet boundary conditions and modified production space configuration: (a) temperature, (b) relative humidity, (c) CO2 concentration, and (d) airflow speed with velocity overlay

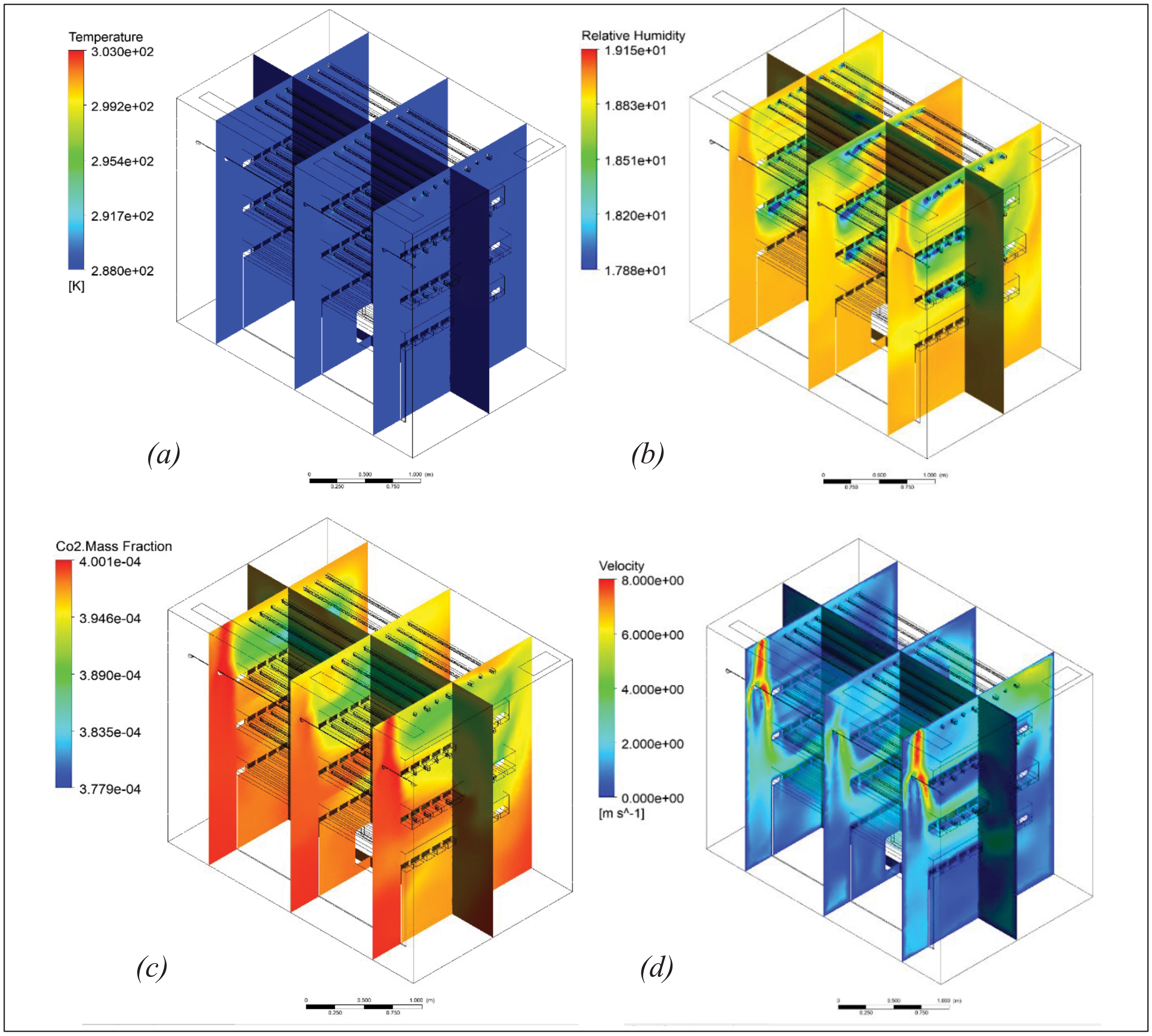

Figure 3.13 Contour plots of the 3D modelled small-scale CEA-HD with and optimized inlet boundary conditions and modified production space configuration: (a) temperature, (b) relative humidity, (c) CO_2 concentration, and (d) airflow speed

3.6 Discussion

The results presented in this paper indicate that the air distribution system of an experimental small-scale CEA-HD can be improved using the proposed optimization approach. Still, more advanced air distribution concepts or cultivation apparatus designed with efficient airflow requirements might be necessary to achieve uniform environmental conditions inside the CEA-HD space such as distributed fans or hot and cold aisles with a raised floor. The CV values obtained in this paper are on the same order of magnitude as the lowest value of 39.5 % reported by Zhang and Kacira (2018) and Zhang and Kacira (2022). However, the mean velocities obtained through optimal inlet configuration (≈1.9 $m \cdot s^{-1}$) are much higher than reported by the previous authors (≈0.4 $m \cdot s^{-1}$) while using a lower inlet velocity (8 $m \cdot s^{-1}$ vs. 10.2 $m \cdot s^{-1}$). This can be explained by the possibility to explore a larger domain using an optimization algorithm as proposed in this paper. Consequently, it resulted in a more efficient ventilation distribution for the modelled small-scale experimental CEA-HD space. The results highlight the need for establishing metrics, such as the zone air distribution effectiveness, a measure of the effectiveness of supply air distribution to the breathing zone (ASHRAE, 2013b), to improve the comparison of air distribution concepts.

Direct optimization with the 3D model of the CEA-HD would be ideal but is impractical even with current high-performance computing clusters. One disadvantage associated with computing the energy balance of the crop model for every cell is the increased calculation time that occurs with mesh refinement of the porous media zones. Thus, a compromise between accuracy and computing requirements is necessary in order to keep simulation and optimization time acceptable. Indeed, even with a two-dimensional model, the iterative solution coupled with the species transport model yielded a convergence time in the order of hours. However, as illustrated by the results shown on Figure 3.13 and the CV tabulated in Table 3.7, the optimization of the 2D model yielded improved 3D simulation results compared to the initial results displayed in Figure 3.3.

Furthermore, the objective function used (equation (3.19)) may feature dominant terms over others. The sensitivity analysis of the different terms of the objective function might yield a formulation with a faster convergence time which is important in practical design. This additional step would complement the proposed simulation output analysis shown in Figure 3.9. Still, as for the direct optimization with a 3D model, this would require computing power that is not available at the time of publication.

The short-wave radiation flux (PAR) absorbed by the crops is currently modelled as a constant for all the porous media zones. An irradiation extinction model (such as Beer law) could be added to further investigate the crop zone and obtain an irradiation profile over the depth of the crop. In the proposed CFD model, the influence of the growing tier and the nutrient holding tank on the airflow was partially verified. The hypothesis is that they do not influence the main flow characteristics inside the CEA-HD. Further evaluation of the effect of the growing tier and the nutrient tank might provide insights on how to better design these to promote airflow to the crops.

The results obtained in this study have only been verified for a small-scale CEA-HD space. The scale of the CEA-HD space used in the experiments might be too small to adequately assess stratification phenomena. In-situ characterization of the spatial distribution of indoor environmental conditions might provide more insight at the commercial scale. More extensive validation of the airflow parameters' bounds and applicability range might be uncovered by applying the proposed approach to a commercial scale CEA-HD space.

Further investigation into the models used for the stomatal resistance, aerodynamic resistance and CO_2 generation should be performed to assess the variability of the CFD predicted spatial distribution of the indoor environment variables given different input models. This analysis could provide an idea of the variability of the high concentration areas given different model assumptions prior to validation experiments. Typical air distribution configurations should be identified prior to computing the optimal parameters and using other performance metrics such as the air distribution index (Karimipanah et al., 2008) and the air residence time (Fontanini et al., 2016).

In future work, validation of the model predicted velocity could be performed with a particle image velocimetry (PIV) measurement system. This could be informative to assess the precision of the current model albeit at the expense of complex measurements. Also, the proposed model is applied to a small-scale CEA-HD space with a relatively simple air distribution system. Still, the same approach could be used to evaluate the performance of more advanced air distribution and to design novel CEA-HD space growing configurations. Integration of the local heat and mass exchanges should provide a theoretical estimate of simpler surface coefficients. These coefficients may prove useful to future HVAC system designers by providing a more accurate calculation of hygrothermal loads.

3.7 Conclusions

In this study, an approach to optimize the air distribution of CEA-HD spaces using a CFD modelling approach that considered the impact of the crops on the distributed indoor environment was proposed. It included modelling the crop impingement on airflow as well as the transpiration and photosynthesis processes. The results from the 3D model showed heterogeneity of the temperature, relative humidity, CO_2 concentration, and airflow speed. To improve the uniformity, it was proposed to optimize the air distribution parameters and configuration using a simplified 2D model to minimize the coefficient of variation of the mean airflow speed and the absolute humidity in the crop domain, modelled as porous media zones, while maximizing the average airflow speed. The optimization explored different inlet conditions and configurations that yielded lower CV and higher mean velocities ($\approx$1.9 $m \cdot s^{-1}$) at a lower inlet speed (8 $m \cdot s^{-1}$) than reported in the literature. Although the proposed approach displayed potential, it is important to note that experimental validation is still required. However, this is both challenging and costly.

As more commercial scale CEA-HD spaces emerge, engineers will be asked to answer practical operation questions about these types of growing spaces. Future research work should leverage the proposed approach to recommend air distribution parameters for typical CEA-HD production system configurations, focusing on the development of guidelines that address energy performances and crop abiotic stress. This paper aims to provide them with a step forward in terms of CEA-HD space air distribution modelling so that innovative growing room designs can be evaluated with commercial CFD software with the transpiration and photosynthesis processes included.

3.8 Conflict of Interest

The authors have no conflicting financial or other interests.

CHAPITRE 4

ADVANCING ENERGYPLUS: A TOOL FOR MODELING CONTROLLED ENVIRONMENT AGRICULTURE SPACES

Gilbert Larochelle Martin[a], Danielle Monfet[a]

[a] Département de Génie de la construction, École de Technologie Supérieure,
1100 Notre-Dame Ouest, Montréal, Québec, Canada H3C 1K3

Article soumis pour publication dans « Energy & Buildings », août 2024

Abstract

This paper proposes a tool for building performance simulation (BPS) modelling of controlled environment agriculture (CEA) spaces. A comprehensive review of the recent literature on CEA energy modelling using building performance simulation (BPS) software highlighted the need for the proposed tool. Developed using the EnergyPlus Python application programming interface (API), the tool estimates the hygrothermal (sensible and latent) CEA space loads by applying a fixed-point iteration root-finding algorithm solver based on the energy balance of the crop at the leaf level. The implementation was verified using data from the literature. A graphical user interface (GUI) has been developed to assist BPS modellers in creating models. This tool and the GUI will streamline the modelling of CEA spaces in the future.

Keywords: CEA, CEA-HD, BEM, BPS, EnergyPlus, TRNSYS

4.1 Introduction

Controlled environment agriculture (CEA) is sparking new interest in commercial endeavours and the scientific community to maintain food sovereignty and mitigate the risks of globalised food supply chains. CEA is a crop production system isolated from the weather by some enclosure where the growing environment conditions (light, temperature, humidity, airflow speed and CO_2) are controlled to enhance crop yield. This is accomplished through active energy systems, which add or remove heat from the production space using a predefined control strategy.

CEA production space types span multiple configurations, such as greenhouses, building-integrated controlled environment agriculture (BI-CEA), and high-density controlled environment agriculture (CEA-HD) spaces, sometimes referred to as vertical or interior farms, container farms, plant factories or indoor plant environments as illustrated in Figure 4.1.

Figure 4.1 Different types of CEA spaces: (a) greenhouse, (b) BI-CEA and (c) CEA-HD

Greenhouses have been studied extensively in the literature (Kimball, 1973; Deltour et al., 1985; Boulard et al., 2017), while the research on BI-CEA spaces is gaining momentum (Appolloni et al., 2021). BI-CEA spaces are generally more expensive and complex, but they offer energy efficiency potential due to the synergies possible between different types of spaces within the building (Muñoz-Liesa et al., 2022). CEA-HD can be defined as spaces where crops are stacked vertically, making it suitable for local production in any climate and dense urban areas. Industrial applications have been reported to require 6 to 8 MW of peak demand with annual consumption of up to 70 000 MWh, with even larger installations in the planning stages (EPRI, 2018). The electricity costs can represent 20 % (Kozai et al., 2019) to 40 % (Avgoustaki & Xydis, 2021) of the operating expenses of CEA-HD production spaces. In these installations, electric lighting can represent 55 % (Agritecture, 2021) to 80 % (Avgoustaki & Xydis, 2021) of the total electricity consumption. Thus, CEA-HD spaces are typically exothermal spaces with significant cooling and dehumidifying loads.

One way to assess energy-related expenditures and energy efficiency potential is through modelling. The level of complexity when modelling CEA spaces can vary significantly, from simple energy balances (Graamans et al., 2017) and 1D dynamic models to 3D computational fluid dynamics models (Boulard et al., 2017). Furthermore, a few interfaces have been proposed to assist greenhouses analysis, such as virtual grower (Frantz et al., 2010) and SimulSerre (Gary et al., 1998). The proposed greenhouse models and interfaces in the literature cannot be easily used or adapted to analyse other CEA or non-CEA spaces (e.g., office, retail store) for BI-CEA applications. These tools also offer limited modelling options for heating, ventilation and air conditioning (HVAC) systems, which restricts their applicability for the design and energy analysis of the HVAC systems in CEA spaces.

Conventional buildings exhibit significant variations in geometry, envelope, vocation, occupancy, HVAC systems, etc. Nevertheless, several software tools have been developed to assess their energy performance. For decades now, building performance simulation (BPS) or building energy modelling (BEM) tools (University of Wisconsin--Madison. Solar Energy, 1975; Herron et al., 1981; Birdsall et al., 1990; Crawley et al., 2001; Strachan et al., 2008) have been used to model building thermal loads, assess the energy performance of designs, promote the implementation of energy-efficient HVAC systems, and quantify demand response control sequences, etc. More than 200 tools are listed in the Building Energy Software Tools directory (Crawley, 1997). These tools have been leveraged since at least 2012 to assess CEA spaces' thermal and energy performances. Still, a crucial component of the energy and mass balances of CEA spaces – the energy balance at the crop leaf level – is not often inherently modelled in these tools.

Between 2012 and 2023, 94 papers related to energy modelling of CEA production space (greenhouses, plant factories, vertical farms, etc.) using BPS software tools (EnergyPlus, TRNSYS, etc.) were reviewed from the Scopus and Compendex databases (Table 4.1 and Table 4.2). Yet, among the reviewed papers that used a BPS software tool, 50 did not include crop transpiration as part of the CEA space model (Table 4.1). When a crop model was included, ten introduced a constant humidity gain with a fixed value regardless of the indoor conditions (Table 4.2). This is concerning because the crop energy balance significantly influences the space peak loads, and failing to model crops could result in improperly sized HVAC equipment, especially for CEA-HD spaces (Talbot & Monfet, 2020; Chahidi et al., 2021). Out of the reviewed papers, 41 of them incorporated some crop modelling, which included the use of empirical data (Labihi et al.; Yeo et al., 2022), the TRNSYS pool model, and user-specific models such as those proposed by Bonachela et al. (2006), Frankenstein and Koenig (2004), Ishigami et al. (2013) and Pieters and Deltour (1997) as shown on Table 4.2. However, few considered the influence indoor air conditions have on the crop energy balance. As such, it was recommended to add vapour pressure deficit (VPD) calculation capabilities to BPS software tools (Akpenpuun et al., 2022).

Thus, coupling of BPS software tools with CEA-related sub-models has been investigated for over a decade (Lee et al., 2012). The capabilities of these tools have been described extensively (University of Wisconsin--Madison. Solar Energy, 1975; Crawley et al., 2001; Crawley et al., 2008). In a nutshell, TRNSYS is a more research-oriented, relatively expensive simulation tool where one can write and customise code relatively easily and leverage the solver for specific research needs. EnergyPlus is free software, but modifying or tailoring it to a particular modelling need can be more challenging. Basic routines can be added through an Energy Management System (EMS) routine using the EnergyPlus Runtime Language (ERL) language, and a Python API has been recently introduced. Among the reviewed papers, 37% used EnergyPlus, 54% used TRNSYS, and 3% used other tools (Table 4.1 and Table 4.2). A crop model was included in about 45% of the cases for both tools (EnergyPlus and TRNSYS). Modelling of CEA-HD represents about 10% of the reviewed papers. However, none of the modelled CEA-HD spaces in EnergyPlus included a fully integrated crop model that could be used under different growing conditions.

Table 4.1 Examples of CEA spaces models in BPS software with no crop models

References	BPS tool	Space type	Number of papers
Fabrizio (2012)	EnergyPlus	GH	20
Alvarez-Sánchez et al. (2014)	EnergyPlus	GH	
Treethidtaphat et al. (2015)	EnergyPlus	GH	
Zhang et al. (2015)	EnergyPlus	GH	
Lee et al. (2016)	EnergyPlus	GH	
Denzer et al. (2017)	EnergyPlus	GH	
Gao et al. (2017)	EnergyPlus	GH	
Thomas et al. (2017)	EnergyPlus	GH	
Chen et al. (2018)	EnergyPlus	GH	
Dahlan et al. (2018b)	EnergyPlus	GH	
Léveillé-Guillemette and Monfet (2018)	EnergyPlus	GH	
Chen et al. (2019)	EnergyPlus	GH	
Molina et al. (2019)	EnergyPlus	GH	
Mohsenipour et al. (2020)	EnergyPlus	GH	
Lebre et al. (2021)	EnergyPlus	GH	
Jahangir et al. (2022)	EnergyPlus	GH	
Kaliakatsos et al. (2022)	EnergyPlus	GH	
Ma et al. (2022)	EnergyPlus	GH	
Pakari and Ghani (2022)	EnergyPlus	GH	
Tian et al. (2022)	EnergyPlus	GH	
Attar et al. (2013)	TRNSYS	GH	29
Attar and Farhat (2015)	TRNSYS	GH	
Awani et al. (2015)	TRNSYS	GH	
Ha et al. (2015)	TRNSYS	GH	
Ataei (2016)	TRNSYS	GH	
Vadiee et al. (2016)	TRNSYS	GH	
Awani et al. (2017)	TRNSYS	GH	
Henshaw (2017)	TRNSYS	GH	
Jin et al. (2017)	TRNSYS	GH	
Rasheed et al. (2017)	TRNSYS	GH	
Yildirim and Bilir (2017)	TRNSYS	GH	
Rasheed et al. (2018)	TRNSYS	GH	
Asa'd et al. (2019)	TRNSYS	GH	
Rasheed et al. (2019)	TRNSYS	GH	
Pineda et al. (2020)	TRNSYS	GH	
Rasheed et al. (2020b)	TRNSYS	GH	
Rasheed et al. (2020a)	TRNSYS	GH	
Sayyah et al. (2020)	TRNSYS	GH	
Torres Pineda et al. (2020)	TRNSYS	GH	
Wang et al. (2020)	TRNSYS	GH	
Yang et al. (2020)	TRNSYS	GH	
Agrebi et al. (2021)	TRNSYS	GH	
Chahidi and Mechaqrane (2021)	TRNSYS	GH	
Mohammadi et al. (2021)	TRNSYS	GH	
Rasheed et al. (2021)	TRNSYS	GH	
Lee et al. (2022)	TRNSYS	GH	
Ogunlowo et al. (2022)	TRNSYS	GH	
Rabiu et al. (2022)	TRNSYS	GH	
Rasheed et al. (2022)	TRNSYS	GH	
Yang et al. (2021)	TRNSYS	CEA-HD	1

Table 4.2 Examples of CEA spaces models in BPS software with crop models

Crop Models	References	BPS tool	Space type	Number of papers
Constant humidity gain	Harbick and Albright (2016)	EnergyPlus	GH	3
	Dahlan et al. (2018a)	EnergyPlus	GH	
	Fuller et al. (2009)	EnergyPlus	GH & CEA-HD	
	Candy et al. (2012)	TRNSYS	GH	7
	Semple et al. (2018)	TRNSYS	GH	
	Semple et al. (2017b)	TRNSYS	GH	
	Semple et al. (2017a)	TRNSYS	GH	
	Vadiee and Martin (2013)	TRNSYS	GH	
	Ahamed et al. (2020)	TRNSYS	GH	
	Adesanya et al. (2022)	TRNSYS	GH	
FAO - Penman (1948)	Alinejad et al. (2020)	EnergyPlus	GH	2
	Liebman-Pelaez et al. (2021)	EnergyPlus	GH & CEA-HD	
	Baglivo et al. (2020)	TRNSYS	GH	4
	Mazzeo et al. (2021)	TRNSYS	GH	
	Bonuso et al. (2020)	TRNSYS	GH	
	Zhang and Kacira (2020)	TRNSYS	GH & CEA-HD	
Stanghellini (1987)	Benis et al. (2017)	EnergyPlus	GH	2
	Ledesma et al. (2022)	EnergyPlus	iRTG	
	Choab et al. (2020)	TRNSYS	GH	3
	Lee et al. (2021)	TRNSYS	GH	
	Banakar et al. (2021)	TRNSYS	GH	
	Ward et al. (2015)	Other	GH	2
	Altes-Buch et al. (2022)	Other	GH	
Graamans et al. (2017)	Jans-Singh et al. (2021)	EnergyPlus	GH	6
	Graamans et al. (2018)	EnergyPlus	GH & CEA-HD	
	Graamans et al. (2020)	EnergyPlus	GH & CEA-HD	
	Eaton et al. (2023)	EnergyPlus	CEA-HD	
	Lalonde et al. (2019)	TRNSYS	CEA-HD	2
	Talbot and Monfet (2020)	TRNSYS	CEA-HD	
Other	Chahidi et al. (2021)	EnergyPlus	GH	4
	Ouazzani Chahidi and Mechaqrane (2022)	EnergyPlus	GH	
	Nadal et al. (2017)	EnergyPlus	iRTG	
	Muñoz-Liesa et al. (2022)	EnergyPlus	iRTG	
	Mashonjowa et al. (2013)	TRNSY	GH	6
	Amin and Kissock (2016)	TRNSYS	GH	
	Goto et al. (2017)	TRNSYS	GH	
	Liu et al. (2021)	TRNSYS	GH	
	Yeo et al. (2022)	TRNSYS	GH	
	Labihi et al.	TRNSYS	GH	
Unspecified	Bambara and Athienitis (2018)	TRNSYS	GH	2
	Bambara et al. (2021)	TRNSYS	GH	
	Lee et al. (2013)	Other	GH	1

The reviewed literature emphasises the need for a tool to efficiently model various types of CEA spaces. This can be achieved by coupling multiple tools to model and simulate specific systems and building concepts (Beausoleil-Morrison et al., 2014). An alternate approach is to integrate all the elements within the same tool as proposed in this paper. As such, a tool to assist BPS users in modelling controlled environment agriculture (CEA) spaces is proposed. This tool integrates a crop model into the EnergyPlus building simulation software (Crawley et al., 2001) via external coupling through a Python API. The integration of the crop model into EnergyPlus is verified using data available in the literature. Additionally, a graphic user interface (GUI) is proposed to support easy modelling of the CEA space, assisting dissemination and future research efforts. The following sections will describe the proposed modelling method (section 4.2), the obtained results following the implementation of the crop sub-model (section 4.3), the proposed GUI (section 4.4), and end with a discussion (section 4.5) and conclusion (section 4.6).

4.2 Method: crop modelling in EnergyPlus

The reviewed literature highlighted the insufficient detail to accurately replicate and implement the fundamental energy balance at the crop level in modelling CEA spaces within BPS software. This section details the modelling method used to compute the sensible and latent heat gain/loss induced by crops in the EnergyPlus software. This consists of two parts: (1) the algorithm used to solve the energy balance at the crop level and (2) the implementation in EnergyPlus using the Python API.

4.2.1 Crop energy balance model

Crops can be modelled using a simple energy balance at the leaf level (Penman, 1948) or with highly detailed growth models (Jones et al., 1991; Brisson et al., 2003). The implemented model is based on the simplified lettuce model proposed by Graamans et al. (2017), which has been validated experimentally under steady-state conditions as part of a study of a controlled-environment agriculture (CEA) space. This crop model has also been implemented in TRNSYS, with the system of equations solved using the superlinear secant method (Talbot and Monfet (2020). Thus, it is this steady-state lettuce crop model that is implemented in EnergyPlus because it enables the estimation of the heat gain/loss induced by crops under varying indoor conditions (lighting intensity, temperature and humidity setpoints, etc.).The energy balance is illustrated in Figure 4.2 and defined by equation (4.1), where the net radiation ($q"_{SW,plt}$), the latent ($q"_{latent,plt}$) and the convective ($q"_{plt,conv}$), also referred to as the sensible gain/loss, from crops are defined by equations (4.2) to (4.4). The impact of longwave radiation ($q"_{LWX,plt}$) and the thermal storage in the leaf and stems are considered negligible (Stanghellini, 1987).

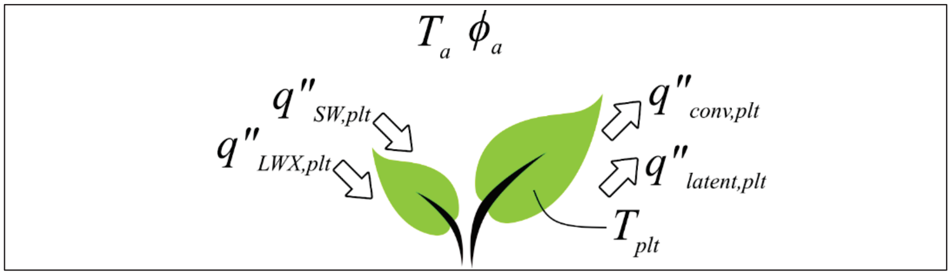

Figure 4.2 Energy balance at the leaf level
Adapted from Talbot and Monfet (2020)

$$q''_{SW,plt} - q''_{conv,plt} - q''_{latent,plt} = 0 \tag{4.1}$$

$$q''_{SW,plt} = (1 - \rho_r) \cdot P_{el} \cdot f_v \cdot \mathrm{CAC} \tag{4.2}$$

$$q''_{latent,plt} = LAI \cdot \lambda \frac{\chi_s - \chi_a}{r_s + r_a} \tag{4.3}$$

$$q''_{conv,plt} = LAI \cdot \rho_a \cdot c_{p_a} \frac{T_{plt} - T_a}{r_a} \tag{4.4}$$

Where ρ_r is the reflection coefficient of the crop (-), P_{el} is the installed electric lighting power density (W·m^{-2}), f_v is the fraction visible (-), CAC is the cultivation area cover (-), LAI is the leaf area index (-), the total one-sided leaf area per horizontal surface unit (Watson, 1947), λ is the latent heat of vaporisation (kJ·kg^{-1}), χ_s and χ_a are the vapour concentration at the leaf surface and of the indoor air (g·m^{-3}), r_s and r_a are the stomatal and aerodynamic resistances (s·m^{-1}) as defined by equations (4.5) and (4.6) respectively, ρ_a is the indoor air density (kg·m^{-3}), c_{p_a} is the indoor air specific heat at constant pressure (kJ·kg^{-1}), T_{plt} is the leaf temperature (°C), T_a is the indoor air temperature (°C), and ϕ_a is the relative humidity (%).

$$r_a = 100 \tag{4.5}$$

$$r_s = 60 \cdot \frac{(1500 + \mathrm{PPFD})}{(200 + \mathrm{PPFD})} \tag{4.6}$$

Where PPFD is the photosynthetic photon flux density (μmol·s^{-1}·m^{-2}) and represents the number of photons in the 400 to 700 nm waveband incident per unit time on a unit surface.

The 400-700 nm waveband is known as the photosynthetically active radiation (PAR) linked to the photosynthesis chemical process in the produced crops. The PPFD is computed using the installed electric lighting power per unit area (P_{el}, W·m^{-2}) and the photosynthetic photon efficiency (PPE, μmol·J^{-1}) as described in equation (4.7). The proposed formulation implies that all of the PAR emitted by the lighting fixtures is intercepted by the crops.

$$\text{PPFD} = P_{el} \cdot \text{PPE} \tag{4.7}$$

The proposed model is programmed to be solved using a fixed-point iteration algorithm rather than the superlinear secant method, as implemented in the TRNSYS version of the model (Talbot and Monfet (2020), for which convergence was not guaranteed. This modification improves code performance. Using fixed-point iteration implies writing the energy balance equation in the form described by equation (4.8), which has been shown to converge for $|g'(x)| < 1$ and where the rate of convergence is at least quadratic if $g'(r) = 0$, where r is the root.

$$x = g(x) \tag{4.8}$$

As illustrated in Figure 4.3, the algorithm is solved by first calculating the vapour concentration at the leaf surface (χ_s, g·m^{-3}) according to equation (4.9) for an initial leaf surface temperature (T_{plt}, ºC) guess and indoor air conditions retrieved from the BPS software. The indoor air conditions are determined according to the indoor air temperature (T_a, ºC), indoor air saturated vapour concentration (χ_a^*, g·m^{-3}), air density (ρ_a, kg·m^{-3}), air specific heat at constant pressure (c_p, kJ·kg^{-1}), the latent heat of vaporisation (λ, kJ·kg^{-1}), and the slope of the saturation function curve (ε, -). It is essential to mention that the indoor air saturated vapour concentration and the indoor air vapour concentration are not dependent on the leaf surface temperature.

$$\chi_s = \chi_a^* + \frac{\rho_a \cdot c_p \cdot \varepsilon}{\lambda} \cdot \left(T_{plt} - T_a\right) \tag{4.9}$$

Once the algorithm has solved for the vapour concentration at the leaf surface, the latent heat gain per surface area ($q^{"}_{latent,plt}$, W·m^{-2}) is computed according to equation (4.3). Then, the convective (sensible) heat gain per surface area ($q^{"}_{conv,plt}$, W·m^{-2}) is computed according to equation (4.4), using the net radiation, often referred to as R_{net} in the literature, which is equivalent to the short-wave radiation by electric lighting ($q"_{SW,plt}$, W·m^{-2}) presented in equation (4.2). A new leaf surface temperature is then estimated using equation (4.10).

$$\widehat{T_{plt}} = q^{"}_{conv,plt} \cdot \frac{r_a}{\left(LAI \cdot \rho_a \cdot c_p\right)} + T_a \tag{4.10}$$

The residual (res, ºC) is computed using equation (4.11). On the next iteration, the leaf surface temperature (T_{pl}, ºC) is replaced by the estimated leaf surface temperature ($\widehat{T_{pl}}$, ºC) at the previous iteration and the algorithm is run again until the convergence criterion of 10^{-5} ºC is met. During an annual simulation, the algorithm converged in 6 iterations for most of the timesteps (10 minutes).

$$res = \widehat{T_{plt}} - T_{plt} \tag{4.11}$$

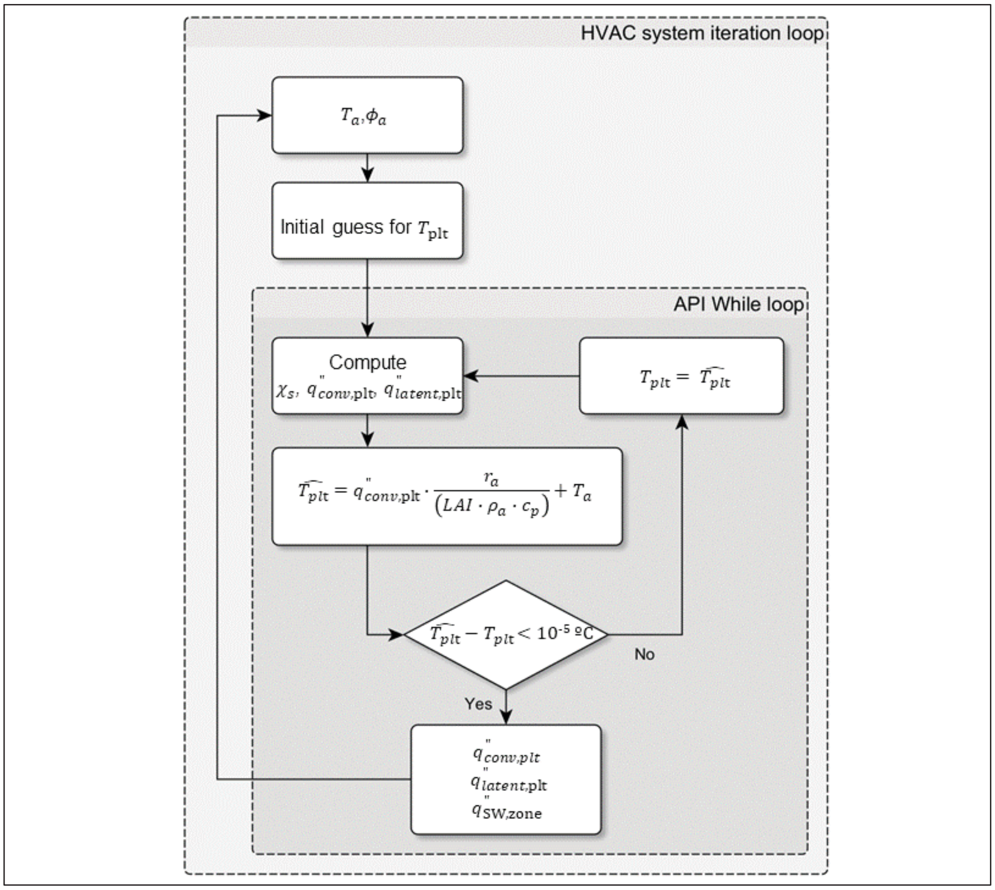

Figure 4.3 Flowchart of the proposed fixed point iteration algorithm developed to solve the leaf level energy balance

4.2.2 Implementation in EnergyPlus using an API

The EnergyPlus Python API is used to manage the data exchange between the crop energy balance and the thermal zone during the simulation run period using the «*on_begin_new_environment*» and the «*on_inside_hvac_system_iteration_loop*» EnergyPlus simulation calling points. The «*on_begin_new_environment*» is called only once during the simulation run time, and the «*on_inside_hvac_system_iteration_loop*» is called at least once every simulation timestep. Figure 4.4 illustrates the proposed simulation process leveraging the EnergyPlus Python API and the energy balance at the crop level (Graamans et al., 2017; Talbot & Monfet, 2020).

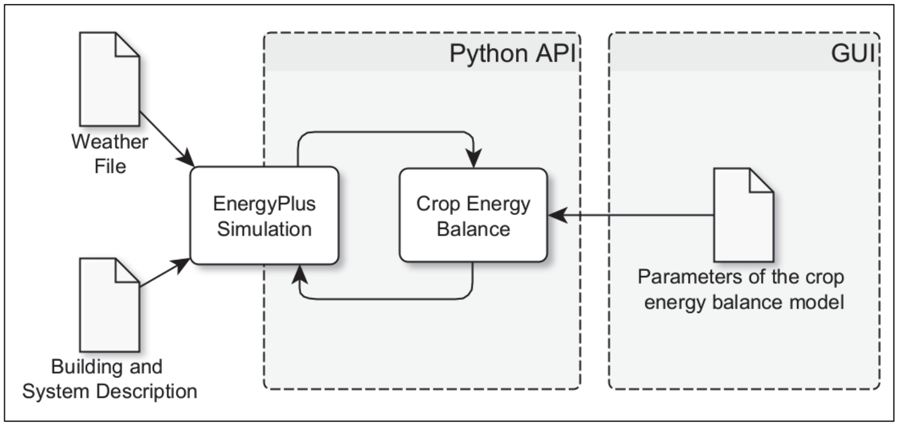

Figure 4.4 Overview of the data exchange between EnergyPlus,
the API and the crop energy balance model

The weather file and building description represent the typical information needed to create a building energy model with building performance simulation (BPS) software. The parameters of the crop energy balance model, presented in Table 4.3, are stored in a separate file that is read before starting the simulation. The cultivated area cover (CAC), estimated as being equal to 30.74×LAI for LAI≤2.45 (Tei et al., 1996) and cultivated density (CD), defined as the sum of all the growing bed areas over the CEA space floor area, are derived from these inputs. The fraction visible (f_v) is the percentage of energy converted into shortwave radiation, the fraction radiant (f_{LW}) is the longwave radiation to the zone, and the balance is considered a convective gain.

Table 4.3 Parameters of the crop energy balance model used by the API

Software	Parameters	units
GUI	Leaf area index (LAI)	dimensionless
	Cultivated Area	m^2
	Electric lighting power density (P_{el})	$W \cdot m^{-2}$
	Fraction Radiant (f_{LW})	dimensionless
	Fraction Visible (f_v)	dimensionless
	Photosynthetic photon efficiency (PPE)	$\mu mol \cdot J^{-1}$
	Reflection coefficient of the crop (ρ_r)	dimensionless
	Thermal Zone name	-
EnergyPlus	Lighting Level	W
	Photoperiod Schedule	boolean

The EnergyPlus simulation inputs, convective (sensible), and latent and radiative gains or losses, as illustrated in Figure 4.4, are added to the thermal zone of the building model through the «*OtherEquipment*» objects and the specific Python plugin objects. The code used to solve the crop energy balance is programmed in Python, is publicly available and has been verified through inter-software comparison and a case study, as shown in the results section (section 4.3).

4.3 Results

The proposed coupling approach is assessed using data available in the literature. As such, two comparisons are completed. The first involves evaluating the computed leaf surface temperature and the gains/losses calculated using the developed model. The second compares a case study's peak demand and annual energy consumption, specifically in a small-scale, high-density controlled environment agriculture (CEA-HD) space.

4.3.1 Leaf surface temperature and heat gains/losses

The first comparison focuses on the computed leaf surface temperature, where only the outputs of the crop model are investigated. This is done by comparing the results generated using the open-access TRNSYS type crop model with those obtained from a simple box model using the

EnergyPlus ideal load option. Both simulations use the same weather file and crop energy balance equations.

The residuals between the leaf temperature simulated in TRNSYS and EnergyPlus are computed once steady-state conditions are reached in TRNSYS, i.e., the temperatures calculated over the first 20 first-time steps (200 minutes) are excluded. The maximum absolute difference (MAD) and the root mean square error (RMSE), defined according to equations (4.12) and (4.13), are respectively 0.14 ºC and 0.038 ºC.

$$\text{MAD} = max(|y_i - \hat{y}_i|),\ \ i = 1 \dots n \tag{4.12}$$

$$\text{RMSE} = \left[\frac{\sum_{i=1}^{n}(y_i - \hat{y}_i)^2}{n}\right]^{1/2} \tag{4.13}$$

Where y_i is the TRNSYS reference value, $\hat{y}_i$ is the EnergyPlus estimated output value, and n the number of reference values.

Following this first comparison, the convective (sensible) and latent heat gains/losses induced by the crops are computed as presented in Table 4.4. The normalised mean bias error (NMBE) and the coefficient of variation of the root mean square error (CV-RMSE) between the TRNSYS and EnergyPlus are used to complete the comparison. These two standard metrics are used in building energy simulation to calculate energy, demand and water savings (ASHRAE, 2014) according to equations (4.14) and (4.15). The radiative gain was precisely the same for the two models. The results are considered satisfactory for the intended purpose of model verification with such low statistics values.

$$\text{CV-RMSE} = \left[\frac{\sum_{i=1}^{n}(y_i - \hat{y}_i)^2}{(n-p)}\right]^{1/2} \Big/ \bar{y} \times 100 \tag{4.14}$$

$$\text{NMBE} = \frac{\sum_{i=1}^{n}(y_i - \hat{y}_i)}{(n-p) \times \bar{y}} \times 100 \tag{4.15}$$

Table 4.4 Computed heat gain/loss from crop energy balance model in TRNSYS versus EnergyPlus

Crop Model Output	TRNSYS		EnergyPlus		NMBE (%)	CV-RMSE (%)
	Lights off	Lights on	Lights off	Lights on		
Convective heat gain/loss (W)	-84.5	72.3	-84.9	72.4	0.04	0.7
Latent heat gain (W)	84.5	275.7	84.6	275.8	0.06	1.0

4.3.2 Case Study

As a second verification step, the peak demand and the energy consumption of a small-scale experimental high-density controlled environment agriculture (CEA-HD) space are computed using ideal loads. The production system is a three-tier hydroponic nutrient film technique (NFT) system with a nutrient holding tank below and a light-emitting diode (LED) lighting system, as illustrated in Figure 4.5. The production space has an envelope with a thermal conductance of 0.12 $W \cdot (^oK \cdot m^2)^{-1}$, a thermal capacity of 100 $J \cdot (kg \cdot ^oK)^{-1}$ and a density of 113.17 $kg \cdot m^{-3}$. During the photoperiod, which lasts for 16 hours from 4:00 to 20:00, the space is maintained at a temperature of 21°C and relative humidity of 70%. In comparison, being held at 18°C with a 74% relative humidity during the dark period (20:00 to 4:00). The installed electric lighting density is 144 $W \cdot m^{-2}$ of cultivated area with a photosynthetic photon flux density (PPFD) of 288.5 $\mu mol \cdot s^{-1} \cdot m^{-2}$ (PPE of 2), a fraction visible (f_v) of 0.4 and a fraction radiant (f_{LW}) of 0.17. The LAI is estimated at 2.1, with a cultivated-to-footprint area ratio of 1.67.

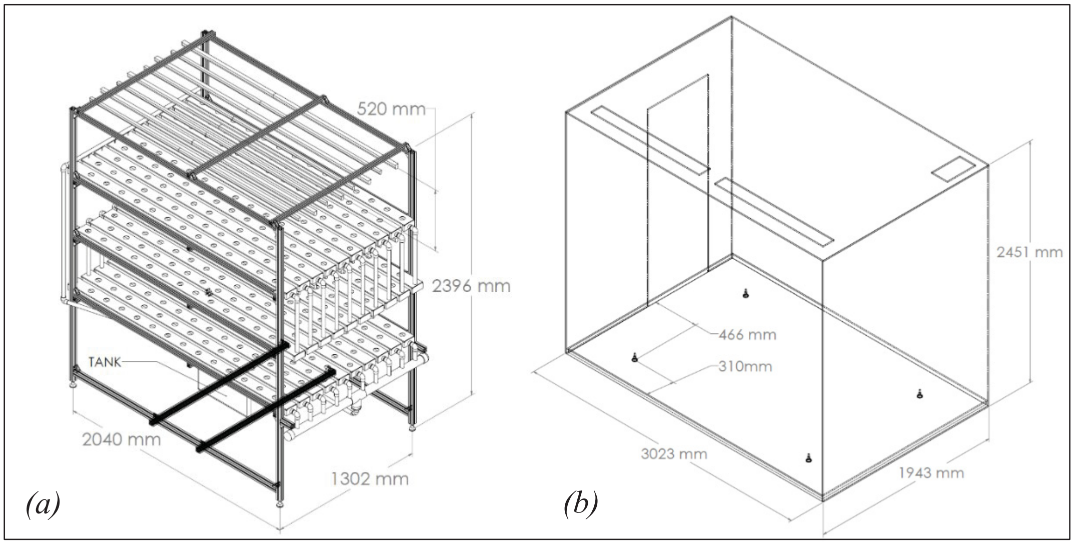

Figure 4.5 Schematics of (a) the production system and (b) the enclosure

The results obtained using the proposed modelling method in EnergyPlus described in section 4.2 are compared with results published for an equivalent TRNSYS model (Talbot et al., 2021). Table 4.5 presents the yearly dehumidification, cooling, and heating peak demand and energy consumption estimates using the TRNSYS and proposed EnergyPlus models. For both models, humidification is negligible. The results show the same order of magnitude for both models, with minor discrepancies noted. As such, it is pointed out that the TRNSYS model used at the time of publication did not consider the crop-reflected shortwave radiation (w/o radiation in Table 4.5) as an additional radiative heat gain to the space, which was adjusted in a subsequent release of the crop model (Talbot & Monfet, 2020). The last column of Table 4.5 presents the results obtained with the proposed model and shows values similar to those of the previously published data (Talbot et al., 2021).

Table 4.5 TRNSYS and EnergyPlus "ideal" peak demand and energy consumption for a CEA-HD space

		TRNSYS	EnergyPlus		
		w/o radiation	w/o radiation	R.E. (%)	proposed model
Dehumidification	Peak demand (W)	725	778	7.3	778
	Consumption (kWh)	4323	4371	1.1	4371
Cooling	Peak demand (W)	932	934	0.2	1042
	Consumption (kWh)	5415	5419	0.1	6045
Heating	Peak demand (W)	247	250	1.2	250
	Consumption (kWh)	693	698	0.7	696

Minor differences between the two software are expected as they include different modelling assumptions such as, for example, the radiative model or application of adiabatic boundary conditions (see Magni et al. (2021)). The results far exceed the latest BESTEST results (Neymark et al., 2020) of about 15% in annual cooling energy and 20% in peak cooling demand. Visual inspection of the heat exchange rates of the model, room air temperature, relative humidity and leaf temperature of the crop yielded identical profiles.

4.4 Graphical user interface

Modelling the crop energy balance is not trivial for most building performance simulation practitioners. This paper also proposes a simple graphic user interface (GUI) to assist them. The developed tool generates all the files and parameters needed to include a CEA production space model to a thermal zone of an existing EnergyPlus simulation file (.idf). Figure 4.6 illustrates the proposed interface design intended for a broader modelling audience. The GUI generates the crop model parameters in Table 4.3 and all the necessary files before simulation. The open-access proposed tool is available on GitHub.

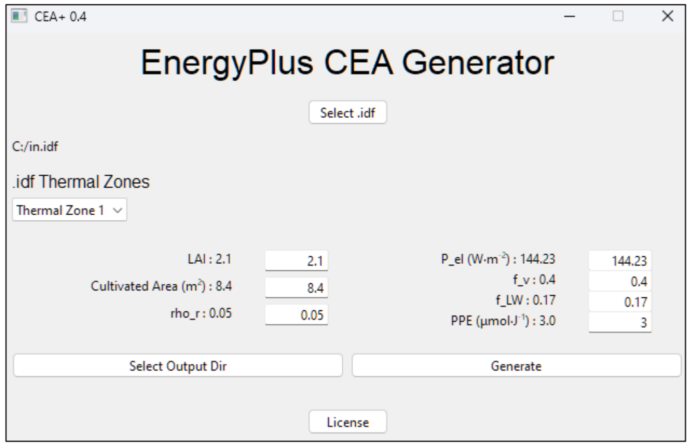

Figure 4.6 Graphical user interface of the proposed EnergyPlus CEA file generation tool

4.5 Discussion

The proposed tool addresses a gap in the literature by providing sufficient detail for the implementation of the EnergyPlus API, allowing for effective replication. Combined with the proposed GUI, a detailed, referenced and available process to properly model CEA spaces, including crops, in a free, supported, publicly available and validated BPS tool, EnergyPlus, is proposed. Even though the tool has been verified, further validation is needed. Data from real-world use cases will offer valuable feedback for other tool developments and crop modelling refinements. The proposed GUI is a basic version of a laboratory research tool designed to adapt and evolve based on users' needs and feedback. The implemented crop model also has several limitations and hypotheses related to the lighting systems, crop growth not being included, cultivar selection, abiotic stress metrics, etc. This incremental advancement represents a small step towards achieving a more comprehensive modelling of CEA spaces by leveraging decades of energy-related research embedded within BPS software. As such, it could easily be adapted to model other CEA spaces like greenhouses.

4.6 Conclusion

The literature review highlighted the limitations of modelling the crop energy balance in BPS software. This paper proposed a publicly available approach, including a simple GUI to generate the input files, to support a broader audience modelling CEA spaces. The proposed EnergyPlus Python application programming interface (API) implementation of the energy balance at the crop level using a fixed-point iteration root finding algorithm was verified using an equivalent published TRNSYS model and a case study. Hopefully, the proposed simple GUI will immediately impact the building performance simulation community by adding simulation capabilities to an extensively used and validated building energy modelling tool. This paper will assist in adequately designing, operating, and optimising future BPS-modelled CEA-related research and HVAC system design.

4.7 Disclosure statement

The authors report there are no competing interests to declare.

CHAPITRE 5

COMPARISON OF ENERGYPLUS INSIDE SURFACES CONVECTIVE HEAT TRANSFER COEFFICIENTS ALGORITHMS FOR ENERGY MODELLING OF HIGH-DENSITY CONTROLLED ENVIRONMENT AGRICULTURE

Gilbert Larochelle Martin[a], Danielle Monfet[a]

[a] Département de Génie de la construction, École de Technologie Supérieure,
1100 Notre-Dame Ouest, Montréal, Québec, Canada H3C 1K3

Article publié dans « Energy & Buildings », juillet 2024

Abstract

Energy modelling of high-density controlled environment agriculture (CEA-HD) spaces using a building performance simulation (BPS) tool and a crop energy balance model is emerging as a method to conduct load calculation and energy analysis. However, the modelling hypotheses used in BPS tools have yet to be tailored for CEA-HD spaces and might not be suitable for this specific application. This paper investigates the convective heat transfer coefficient (CHTC) algorithms for inside surfaces included in EnergyPlus to examine their applicability to CEA-HD spaces. The influence of these inside surfaces CHTC algorithms on relevant variables are quantified, with computational fluid dynamics (CFD) computed CHTCs as a reference. The results revealed that certain algorithms (Simple, TARP, and ASTMC1340) are ill-suited to model CEA-HD production spaces compared to CFD-computed reference values. Furthermore, due to the modelled flow rate, the Adaptive Convection algorithm resulted in an aberrant value for the ceiling CHTC. This paper highlights the importance of exercising caution when using BPS tools for energy modelling of CEA-HD spaces.

Keywords: CEA, CEA-HD, BEM, BPS, EnergyPlus, TRNSYS

5.1 Introduction

Controlled environment agriculture (CEA) involves decoupling crop production from weather variations using an enclosure and an active energy system to optimally control the indoor environment. CEA spaces, including greenhouses, have been extensively studied regarding their thermal modelling (Pieters & Deltour, 1999; Roy et al., 2002; Katzin et al., 2022), microclimate spatial variations (Boulard et al., 2002; Boulard et al., 2017), energy systems (Vadiee & Martin, 2012; Engler & Krarti, 2021), etc. However, since the 2010s, a new type of CEA production system has been rising: high-density controlled environment agriculture (CEA-HD). CEA-HD, sometimes referred to as vertical farms (Despommier, 2010) or plant factories (Kozai et al., 2019), densifies crop production by using multi-tiered hydroponic or aeroponic systems with solely artificial lightning in a low-footprint, highly insulated enclosure. CEA-HD spaces produce high-quality crops, such as leafy greens, lettuce, strawberries, and others, while keeping the produce exempt from pesticides, fungi, or insects at the expense of high energy consumption associated with maintaining optimal indoor conditions (Kozai et al., 2019). CEA-HD production systems can vary from one another, but Figure 5.1 provides an example of an industrial-scale CEA-HD production space.

Figure 5.1 Example of an industrial-scale
CEA-HD production space
Taken from AeroFarms (2024)

The indoor conditions within these production spaces vary from one crop to another and may not remain constant throughout the production cycle. Adjustments are implemented to promote crop growth and control diseases according to the growing stage and other influential factors. The indoor conditions of a CEA-HD space can be described using the airflow speed, the vapour pressure deficit (VPD), the carbon dioxide concentration and the photosynthetically active radiation (PAR) levels. The VPD represents the potential for evaporation at the leaf level and is computed by combining the indoor air temperature and humidity content (Fricke, 2017). The PAR is the electromagnetic radiation between 400 and 700 nm (McCree, 1971) necessary for the crop's photosynthesis. Indoor conditions setpoints and control strategies directly impact the energy use and peak demand of CEA-HD spaces, which are closely related to their financial viability. Still, little is published on those production spaces' best design and operating practices, as most of the knowledge is proprietary (Jonlin & Lewellen, 2017). Furthermore, the various aspects of CEA-HD (Al-Kodmany, 2018; Kalantari et al., 2018; Engler & Krarti, 2021) represent an ongoing area of research, given the current need for growers, engineers, utilities and policymakers to assess them.

To tackle this issue, CEA-HD energy models have been proposed in the literature (Graamans et al., 2017; Weidner et al., 2021). These models are often problem-specific, not flexible enough for broad usage and not necessarily publicly available. As such, developing CEA-HD models using more holistic modelling tools is essential. Building performance simulation (BPS) modelling tools can help analyse the thermal exchanges through the enclosure, energy systems, and associated controls. Recently, the heat balance at the crop leaf level has been integrated into a publicly available building performance simulation (BPS) tool ("Development of a tool for modelling Controlled Environment agriculture (CEA) spaces in EnergyPlus," 2024), specifically EnergyPlus. This integration is leveraging substantial ongoing research from the building performance simulation (BPS) field. BPS tools (University of Wisconsin--Madison. Solar Energy, 1975; Herron et al., 1981; Birdsall et al., 1990; Crawley et al., 2001; Strachan et al., 2008) have been used for decades to inform architects and engineers on multiple aspects of building design, optimisation and operation. Indeed, these tools can be used to perform several types of analysis, such as predicting buildings' thermal loads and assessing energy performance, energy efficiency, demand response measures, etc. (Clarke & Hensen, 2015). Furthermore, they have been designed to consider multiple building configurations and buildings' energy exchange processes. Using BPS tools to model CEA-HD production spaces could address most of the shortcomings of the previously published CEA-HD models.

In BPS tools, the energy exchanges are often modelled using the heat balance approach (Crawley et al., 2008). Figure 5.2 illustrates the different energy exchanges considered in the heat balance algorithm of EnergyPlus (Crawley et al., 2001). The air heat balance within the thermal zone is determined using the convection heat transfer between the internal surfaces and the zone air. The modelled heating, ventilation and air conditioning (HVAC) system subsequently adds or removes energy from the thermal zone to meet its specified setpoint, i.e., the specified indoor air conditions to be maintained.

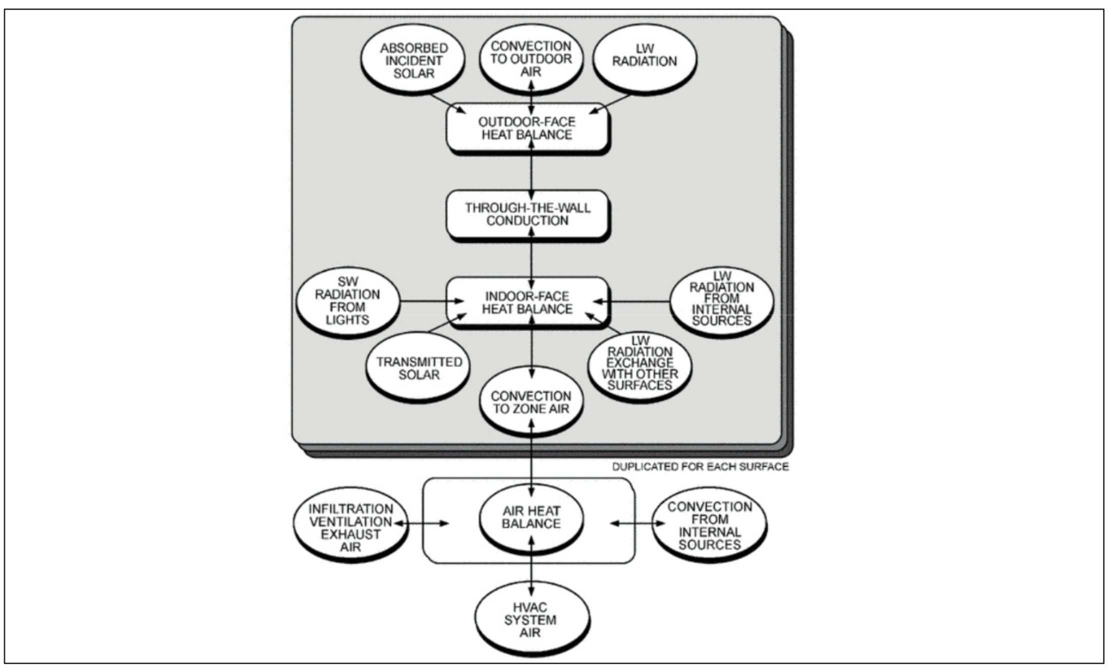

Figure 5.2 Schematic of the EnergyPlus heat balance method on a thermal zone
Taken from American Society of Heating and Air-Conditioning Engineers (2021)

The convection heat transfer to the zone air (q_{conv}) is defined according to equation (5.1), where the convective heat transfer coefficient (CHTC) for each surface (h_{ci}) can be modelled according to different approaches. The convection heat transfer to the zone air is computed using the surface area (A_i), the interior surface temperature (T_{si_i}) and the zone air temperature (T_a).

$$q_{conv} = \sum_{i=1}^{n} A_i \cdot h_{ci} \cdot \left(T_{si_i} - T_a\right) \tag{5.1}$$

In CEA-HD spaces, the inside surface boundary conditions are not representative of typical building space since the internal sensible and latent heat gains associated with crop transpiration are high (Talbot & Monfet, 2020). Thus, HVAC systems used in these production spaces are set to higher airflow rates to promote indoor environment uniformity and crop transpiration. Hence, the CHTC for each inside surface differs from conventional building spaces and the CHTC algorithms used in BPS tools might not be suitable for CEA-HD modelling.

In EnergyPlus, five options are available for calculating the CHTC for inside surfaces: Simple, TARP, Ceiling Diffuser, Adaptive Convection and ASTMC1340 algorithms. The Simple algorithm specifies a fixed CHTC value associated with natural convection for each room surface. The TARP algorithm, the default choice in EnergyPlus, is a natural convection model that correlates the CHTC to the surface orientation and the temperature difference between the zone air and the selected surface. These correlations are no longer available in the American Society of Heating and Air-Conditioning Engineers (ASHRAE) Handbook of Fundamentals (American Society of Heating & Air-Conditioning Engineers, 2021). Both the Simple and TARP algorithms are based on the work of Walton (1983). The Ceiling Diffuser algorithm, based on the experiments of Fisher and Pedersen (1997), uses correlation based on the air change per hour (ACH) to predict the CHTC of the inside surfaces. The Adaptive Convection algorithm, developed by Beausoleil-Morrison (2002), is a more general algorithm that selects specific correlations based on the flow regime and the room configuration. It leverages the work of Alamdari and Hammond (1983), Khalifa (1989), Awbi and Hatton (1999) and Fisher (1995), supplemented by mixed convection correlations obtained with blending techniques.

The ASTMC1340 algorithm, developed for attic energy models, is based on the technical document of the same name (*Standard Practice for Estimation of Heat Gain or Loss Through Ceilings Under Attics Containing Radiant Barriers by Use of a Computer Program*) and was implemented in EnergyPlus by Fontanini et al. (2018). A recent review by Camci et al. (2021) summarised the correlations for different flow types (i.e., natural convection, forced convection, mixed convection) developed for indoor applications. An overview of the variables used by the EnergyPlus inside surfaces CHTCs algorithms is presented in Table 5.1, where ΔT is the temperature difference between the interior surface and the thermal zone air temperature, θ is the surface tilt angle, ACH is the zone air changes per hour, D_h is the hydraulic diameter, H is the characteristic height, L is the characteristic length, T_{si} is the surface temperature, T_{SA} is the supply air temperature, Ra is the Rayleigh number, k is the air thermal conductivity, Gr is the Grashof number, Pr is the Prandtl number, and Re is the Reynolds number.

Table 5.1 Variables used by the EnergyPlus CHTCs algorithms

Algorithm	Variables
Simple	Constant
TARP	$f(\Delta T, \theta)$
Ceiling Diffuser	$f(\text{ACH})$
Adaptive Convection	$f(\Delta T, \theta, \text{ACH}, D_h, H, T_{si}, T_{SA}, Ra, k, \dot{V}, L)$
ASTMC1340	$f(Gr, Pr, Ra, Re, \theta, k, L)$

The choice of CHTC to be used is not trivial (Beausoleil-Morrison & Strachan, 1999). Indeed, choosing a specific type of correlation over another can impact the building's peak heating demand by up to 30.5% and peak cooling demand by up to 55.2% (Obyn & van Moeseke, 2015). Differences also exist between correlations obtained from comparable experiments as they are derived from a single geometry (Peeters et al., 2011). To the authors' knowledge, the algorithm or values used for computing the CHTC for inside surfaces in CEA-HD spaces using BPS tools are often not specified.

Hence, this paper aims to identify which internal surface CHTC algorithm available in the BPS tool EnergyPlus is more appropriate to model CEA-HD spaces. It also seeks to provide reference values based on computational fluid dynamics (CFD). The impact of selecting an inappropriate algorithm is also quantified using a small-scale CEA-HD production space case study.

5.2 Methodology

The proposed method compares different inside surfaces CHTC algorithms available in EnergyPlus with reference CHTC values computed using CFD. The five options available in EnergyPlus (Simple, TARP, Ceiling Diffuser, Adaptive Convection and ASTMC1340) are used in a case study to assess their influence on energy use and peak demand, as well as air conditions and critical aspects of crop modelling. The case study leverages two previously published models: (1) a computational fluid dynamics (CFD) model and (2) a building energy model (BEM), as illustrated in Figure 5.3. The small-scale CEA-HD production space, the CFD model and the BEM are described in the following sections.

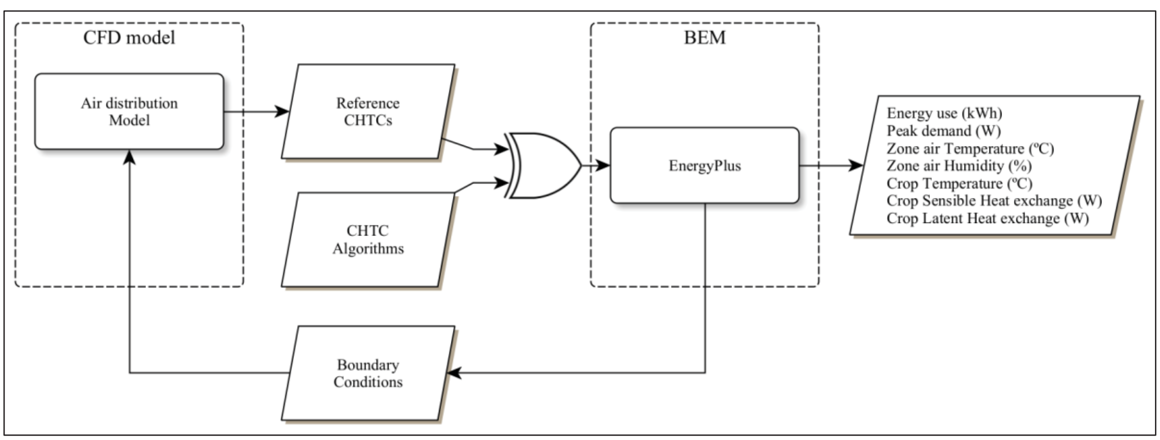

Figure 5.3 Overview of the proposed methodology

The CHTC reference values are obtained through CFD modelling of the space, including the impact of crops. Indeed, CFD has already been used to develop natural convection Nusselt number correlations for building rooms (Altmayer et al., 1983; Rincón-Casado et al., 2017). This provides a Navier-Stokes based reference tailored to the specific configuration of the small-scale CEA-HD space since in forced convection applications, the correlation used should account for the airflow rate and the locations of the inlet/outlet (Camci et al., 2021). The influence of the different CHTC values and algorithms on the energy use and peak demand and the thermal zone air temperature, air humidity, crop temperature, and crop sensible and latent heat exchanges between the crops and the zone are also quantified and compared.

5.3 Small-scale CEA-HD production space

The CEA-HD production space used as a case study is a small-scale hydroponic production system, as illustrated in Figure 5.4. The production space enclosure walls have a thermal conductance value of 0.12 $W\cdot(K\cdot m^2)^{-1}$, a thermal capacity of 100 $J\cdot(kg\cdot K)^{-1}$, and a density of 113.17 $kg\cdot m^{-3}$. The temperature and relative humidity setpoints are 21ºC/70% during the photoperiod, from 4h00 to 22h00 (18 hours), and 18ºC/74% during the dark period. The light emitting diode (LED) lamps are designed with a power density of 144.23 $W\cdot m^{-2}$ of cultivated area and a photosynthetic photon flux density (PPFD) of 288.5 $\mu mol\cdot s^{-1}\cdot m^{-2}$ and a visible fraction of 0.52. The same lighting power density was used in the CFD and energy model. The LAI, defined by the total one-sided leaf area per horizontal surface unit (Watson, 1947), is specified as 1 and the crop reflectivity as 5% for both models. The production enclosure is located in a conditioned research laboratory with controlled temperature and humidity. The location of the air distribution system inlets and outlet are shown in Figure 5.4, including the production space and system dimensions.

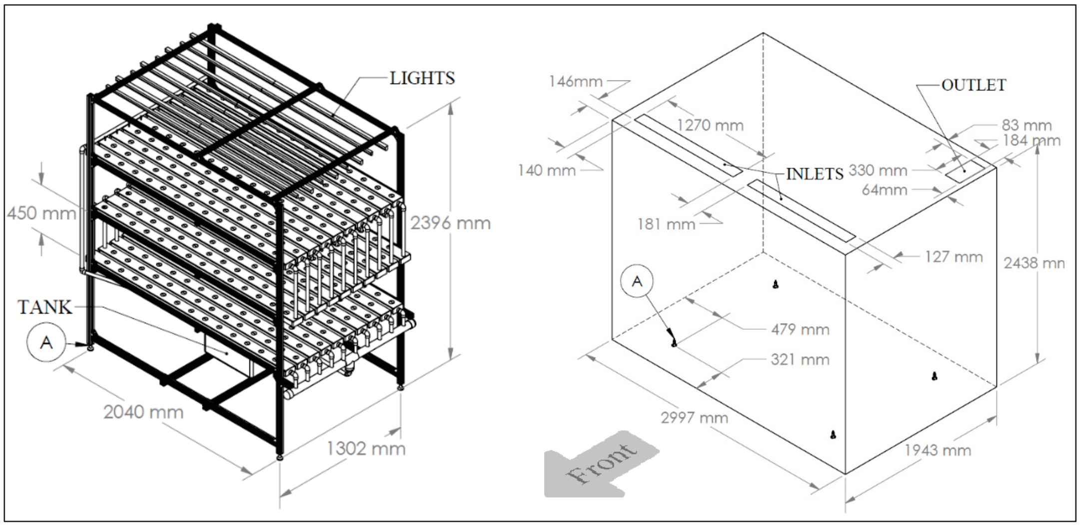

Figure 5.4 Isometric view of the hydroponic production system (left)
and production space enclosure (right)

5.4 CFD Model

A computational fluid dynamics (CFD) model of the air distribution of the CEA-HD space illustrated in Figure 5.4 was previously developed using user-defined functions (UDFs) to account for the crop airflow impingement, photosynthesis, and sensible and latent heat exchanges (Larochelle Martin & Monfet, 2024). These UDFs solve the heat balance at the leaf level in each cell using a numerical root-finding algorithm (secant method) and add a CO_2 sink. CFD crop modelling uses numerical schemes to solve the Navier-Stokes, energy and mass transport equations in the specified spatial domain. The boundary conditions of the modelled domain need to be specified in the CFD tool (Fluent 19.2). These are specified using results from the building energy model (BEM) using the EnergyPlus default CHTC algorithm (TARP algorithm), as illustrated in Figure 5.3. The BEM estimates the temperature of the inside surfaces according to the heat balance method of the thermal zone. Subsequently, using a reference bulk fluid temperature, the CFD model can be used to compute the average CHTC for each internal surface. The CHTC values computed with the CFD model are then used as inputs for the energy model. The BEM is then used to conduct a yearly simulation for the analysis (see Figure 5.3).

The CFD model needs to resolve the boundary layer using a high-resolution mesh to stay well within the viscous sublayer and, thus, properly evaluate the temperature gradient at the boundary. The dimensionless wall distance (y^+) value used in the CFD model is approximately 1 for all the enclosure surfaces in the CFD model to stay well within the linear viscous sub-layer of the boundary layer (Rincón-Casado & Sánchez de la Flor, 2018). The dimensionless wall distance is detailed in equation (5.2) where y^+ is the dimensionless wall distance, ρ is the fluid density (kg·m^{-3}), τ_w is the wall shear stress (Pa) and μ is the fluid dynamic viscosity (Pa·s). The velocity magnitude results of the CFD airflow simulation in the CEA-HD production space on selected planes are presented in Figure 5.5. Further CFD model results are shown in (Larochelle Martin & Monfet, 2024).

$$y^+ = \frac{\rho y \left(\sqrt{\frac{\tau_w}{\rho}}\right)}{\mu} \tag{5.2}$$

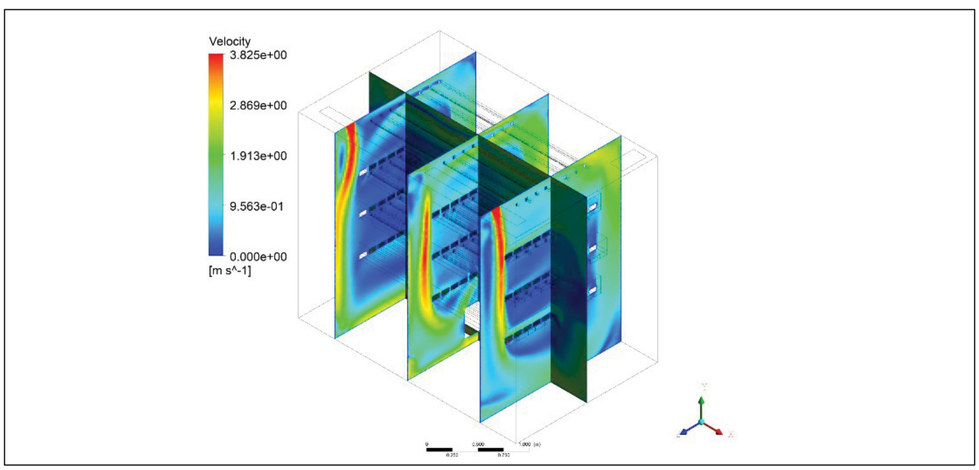

Figure 5.5 Velocity magnitude results for the CFD model
Taken from Larochelle Martin and Monfet (2024)

Post-treatment of the CFD results is necessary to extract the average boundary surface CHTC. The CFD reference CHTC values are thus derived from the temperature field results as the surface heat flux at the boundary using equation (5.3). The temperature gradient over a boundary adjacent cell yields the total heat flux for this cell, and by averaging these values, the mean CHTC for the boundary surfaces is obtained. Equation (5.3) describes the heat flux evaluated at the domain boundary using Fourier's law, and equation (5.4) represents the average surface CHTC using a reference bulk temperature (21ºC) where q_s is the surface adjacent cell heat flux (W·m^{-2}), $\overline{q_s}$ is the surface average heat flux (W·m^{-2}), k is the thermal conductivity of the fluid (W·m^{-1}·K^{-1}), T is the temperature (K), y is the absolute distance from the wall (m), h_c is the average surface heat transfer coefficient (W·m^{-2}·K^{-1}), T_{si} is the surface temperature (K) and T_a is the zone air temperature (K).

$$q_s = k \frac{\partial T}{\partial y}\bigg|_{y=0} \tag{5.3}$$

$$h_c = \frac{\overline{q_s}}{(T_{si} - T_a)} \tag{5.4}$$

5.5 Building Energy Model

The building energy model of the experimental CEA-HD production space was developed using the internal gains described in the production space section. The sensible and latent loads of the production space were computed using the EnergyPlus ideal load option. A crop energy balance model was added to the energy model using the EnergyPlus Python API and was previously verified through an inter-software comparison with the TRNSYS simulation program ("Development of a tool for modelling Controlled Environment agriculture (CEA) spaces in EnergyPlus," 2024). To account for the CFD model flow conditions over an entire year, the EnergyPlus simulation was carried out with a fixed supply airflow rate using an energy management system (EMS) program. This limitation of the proposed method is caused by the high computing power required to perform a strong coupling between the CFD model and the BEM for yearly simulation. Since the supply airflow rate is fixed, the underlying hypothesis is that the computed CFD-computed CHTC values remain constant throughout the year. The building energy model consists of a single thermal zone with a fixed supply airflow rate and does not explicitly model the HVAC system. Given the multiple options available to model the heat conduction through the enclosure in EnergyPlus, the default option (conduction transfer functions) was used for the simulation.

5.6 Results

The CHTC values computed by EnergyPlus are compared against CFD reference CHTC values to assess the variation between the different algorithms. Table 5.2 compiles the CHTC values for each of the six surfaces of the production space enclosure computed with CFD, Simple, TARP, Ceiling Diffuser, Adaptive Convection and ASTMC1340 algorithms. The surfaces are referenced according to the orientation presented in Figure 5.4. Upon examination of the values of Table 5.2, it is evident that the values computed with the Adaptive Convection algorithm are approximately within the same order of magnitude as the CFD reference values, albeit at the expense of a notably aberrant ceiling CHTC. Indeed, the forced convection flow regime in gases is expected to yield a CHTC between 25 and 250 $W \cdot m^{-2} \cdot K^{-1}$ (American Society of Heating & Air-Conditioning Engineers, 2021). The other EnergyPlus algorithms computed lower inside surfaces CHTCs than the CFD reference values, except for the Ceiling Diffuser algorithm ceiling surface. This difference can be explained by the orientation of the supply air inlet jet (see Figure 5.5).

Table 5.2 Computed inside surfaces CHTC values using computational fluid dynamics (CFD) and the EnergyPlus inside convection algorithms

Surface	CFD	E+ Simple	E+ TARP	E+ Ceiling Diffuser	E+ Adaptive Convection	E+ ASTMC 1340
Front	41.61	3.07	3.34	17.55	43.09	2.79
Right	24.62	3.07	3.34	17.55	43.04	2.79
Back	29.82	3.07	3.34	17.55	43.09	2.79
Left	34.54	3.07	3.34	17.55	43.04	2.79
Ceiling	34.42	0.95	1.96	43.80	3.44e+06	1.58
Floor	38.95	4.04	3.86	11.35	28.93	4.03

N.B. values are given in $W \cdot m^{-2} \cdot K^{-1}$

The impact of the different CHTC algorithms on the production space energy use and peak demand is presented in Figure 5.6 and Figure 5.7, respectively. The difference in the computed CHTC values has a more significant impact on the peak demand than energy use. For example, the estimated sensible peak demand varies between 1 kW and 13 kW, while the estimated sensible cooling energy use varies between 5500 kWh and 6500 kWh. The sensible cooling peak demand for the Adaptive Convection algorithm is significantly higher, linked to the aberrant value of the ceiling CHTC shown in Table 5.2.

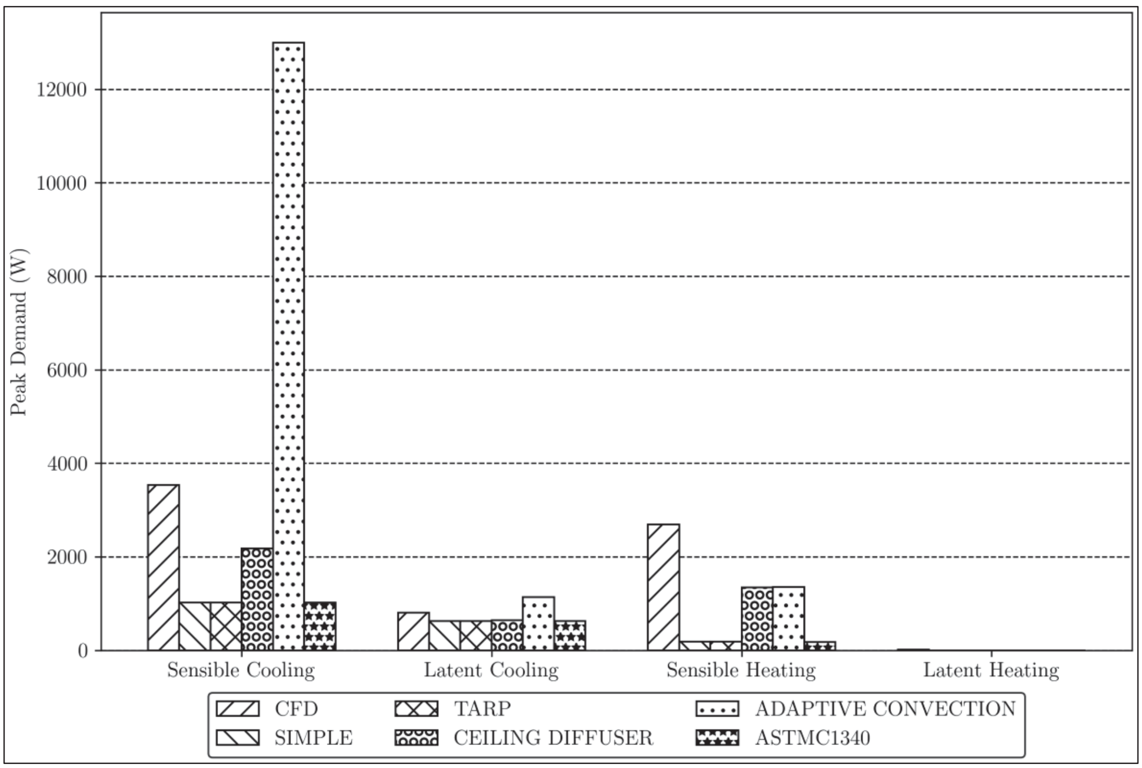

Figure 5.6 Yearly peak demand comparison by end-uses between the different CHTC algorithms

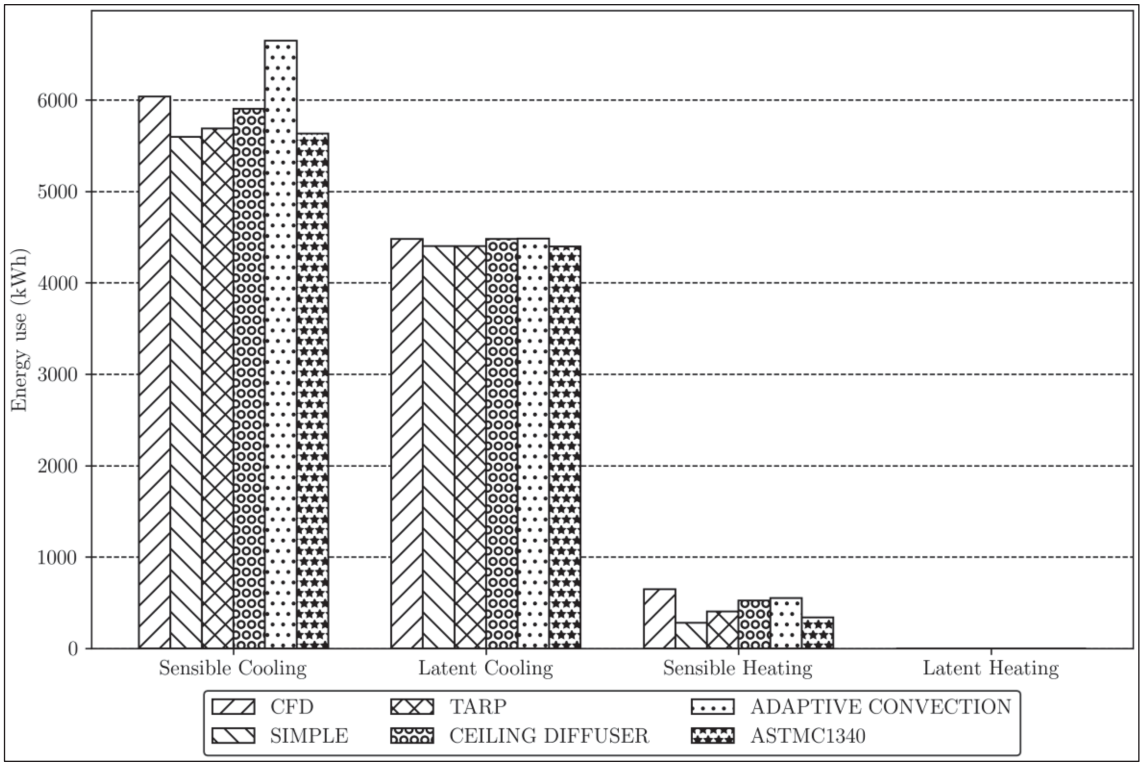

Figure 5.7 Yearly energy end-use comparison between the different CHTC algorithms

The impact of the different computed CHTC values was then assessed on the daily profiles of critical CEA-HD variables, such as the zone air temperature, relative humidity, and crop temperature, as presented in Figure 5.8. These variables are critical for solving the heat balance at the crop level, resulting in the computation of sensible and latent heat exchanges between the crops and the zone. Figure 8 shows two emerging clusters: (1) the Simple, TARP, and ASTMC1340 algorithms and (2) the Ceiling Diffuser, Adaptive Convection, and CFD-derived CHTC values. This suggests that the Simple, TARP, and ASTMC1340 algorithms might be ill-suited for modelling CEA-HD spaces based on the CFD computed CHTC values.

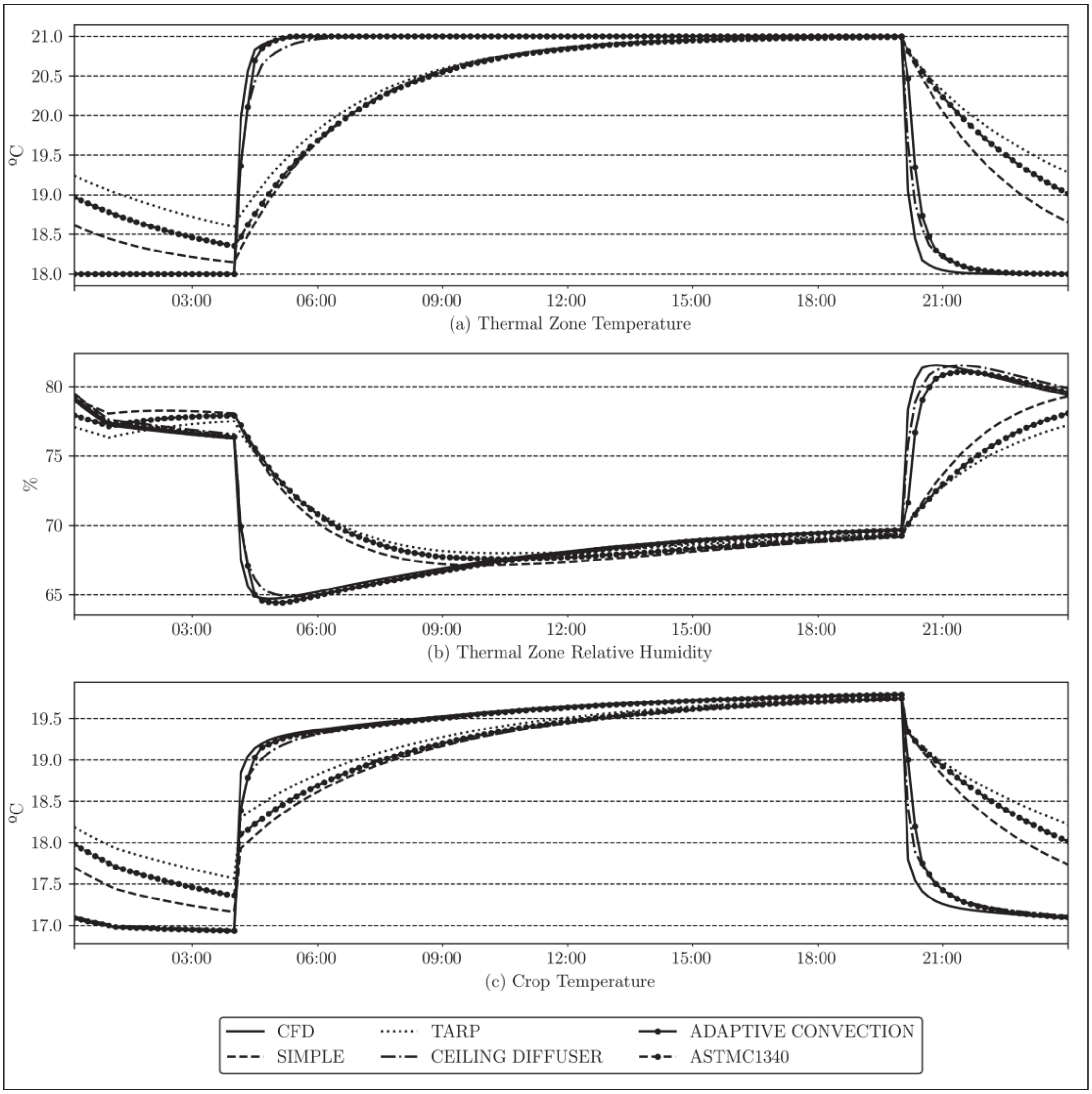

Figure 5.8 Typical day CEA-HD energy model (a) zone air temperature, (b) relative humidity and (c) crop temperature

The crop sensible and latent heat exchanges between the crops and the building zone air, both outputs of the leaf level heat balance, are presented for a typical production day in Figure 5.9. The same two clusters identified in Figure 5.8 are observed in Figure 5.9. This further supports disregarding the Simple, TARP, and ASTMC1340 algorithms for BEM of CEA-HD spaces. The peak crop cooling effect (negative crop sensible heat exchange) is underestimated at the beginning of the photoperiod by a factor of 5 for the ill-suited cluster of algorithms. Figure 5.9 also partly explains why the impact is higher on the peak demand than energy use. Indeed, the absolute discrepancies between the curves of Figure 5.9 impacting peak demand are more pronounced than the difference in area under the different curves associated with energy use.

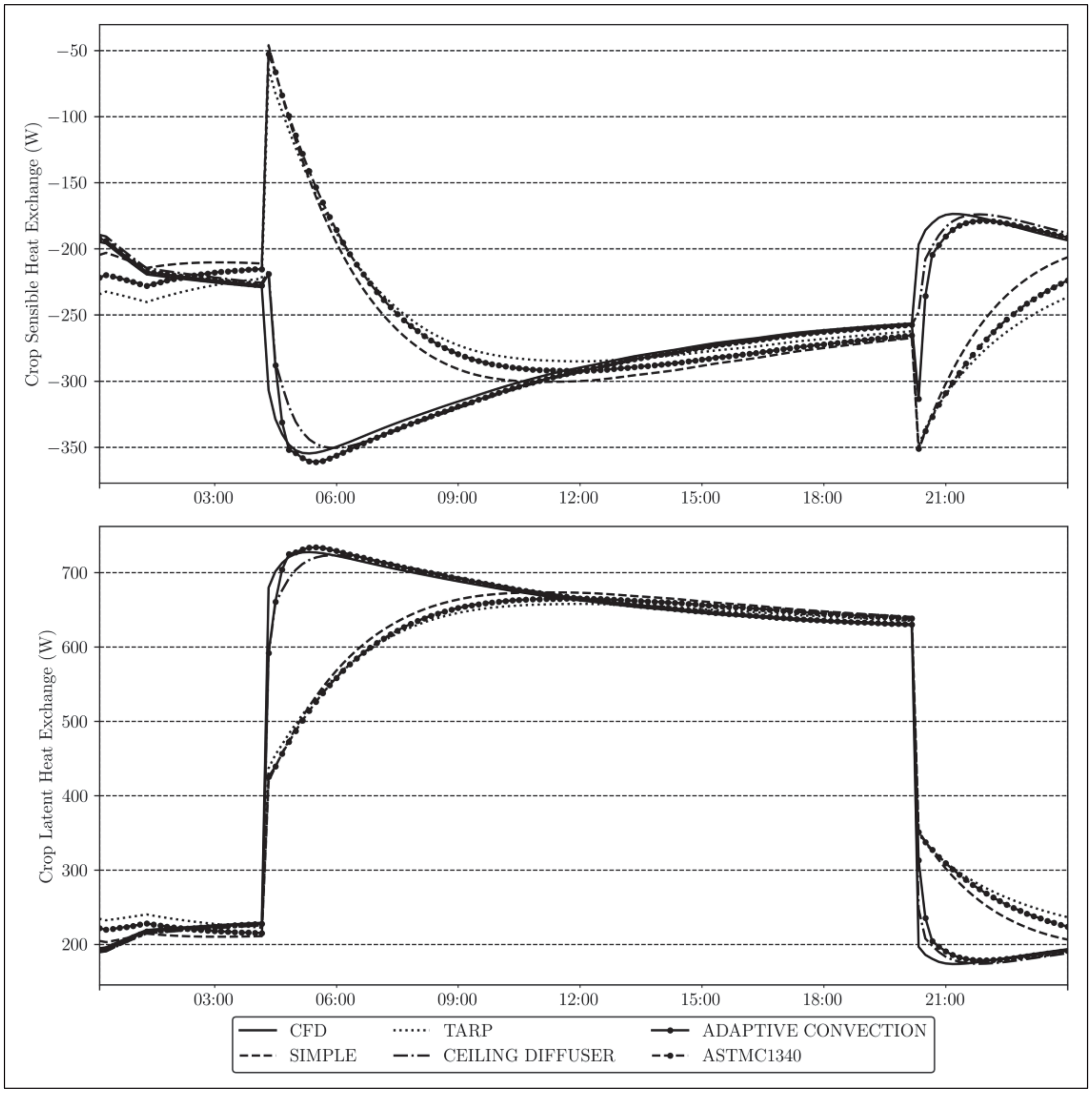

Figure 5.9 Crop sensible and latent heat exchanges between the crops and the zone air computed by the building energy model for a typical day

To meet the load requirement, the zone supply air temperature and absolute humidity fluctuated as the supply airflow rate remained fixed. The zone supply air inlet temperature and absolute humidity computed using the energy model also vary from one CHTC algorithm to another. Figure 5.10 illustrates the distribution of those two supply air variables over a yearly simulation for each inside surface CHTC algorithm. The previously identified ill-suited algorithm cluster exhibits a broader range in supply inlet temperatures with a narrower range in relative humidity. This becomes particularly relevant when using the energy model for HVAC control sequence development or performance evaluation. Indeed, using an inappropriate CHTC algorithm might yield suboptimal, inadequate rule-based control sequences and potentially adversely affect the production microclimate.

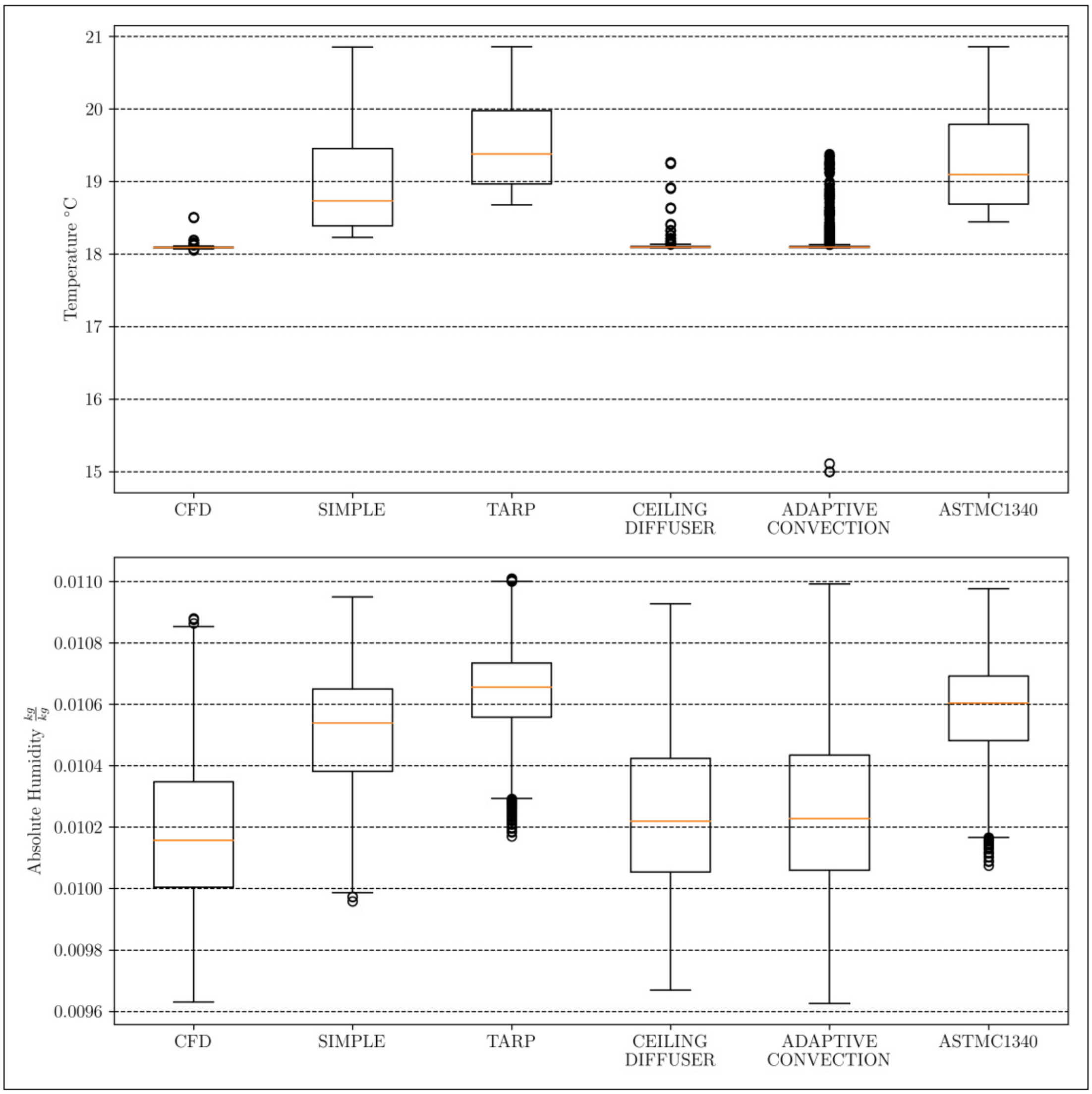

Figure 5.10 Yearly supply inlet temperature and absolute humidity results computed by the BEM

5.7 Discussion

The results presented in this paper highlight the discrepancies in peak demand, energy use, thermal zone temperature, humidity, crop temperature and the sensible and latent heat exchanges between the crops and the zone air that can be caused by an ill-advised selection of the inside surface CHTC algorithm in CEA-HD spaces energy modelling using the BPS program EnergyPlus. While CHTC values directly impact the BPS computed results, further exploration of the different assumptions used in BPS tools, such as EnergyPlus, must be performed before the widespread use of BPS for CEA-HD energy modelling. Indeed, other algorithms used for wall conduction or radiation exchanges, for example, could result in discrepancies for additional critical heat or mass transfer. Concerningly, recent research using BPS for CEA-HD energy modelling is often performed by authors outside the BPS field, leading to oversimplification of the building energy model used.

One limitation of the performed analysis is that the boundary conditions of the CFD model should ideally be dynamic and not fixed. Hence, the temperature used for the surfaces of the CFD model should vary using the results of a heat balance calculation in the thermal zone of the building energy model. Ideally, convergence between the two tools would be reached for each timestep of a yearly simulation run period. This is still very challenging, given the currently available computing power. Coupling the CFD and BEM could enhance the methodology used when advances in CFD modelling and/or computing power are made. Furthermore, particular attention to the mesh size and the governing equations is critical. As the wall adjacent mesh y+ has to be below 5 to stay within the viscous sublayer region of the boundary layer, the mesh quality becomes a critical factor impacting solution convergence. Indeed, model cell count must be increased to keep an acceptable cell aspect ratio at the boundary faces as cell sizing is reduced. Maintaining mesh quality with the small inflation layer needed at the mesh boundaries to keep an acceptable y+ value is challenging.

Fixing the supply airflow rate during the energy model simulation simplifies the real production space operating conditions. Indeed, the required airflow rate might vary depending on several factors such as lighting schedule, crop growing stage, sensible heat ratio, etc. Using a single CFD computed reference CHTC value for the year is a limitation of this paper that could be addressed in the future by extracting correlations from multiple CFD modelled production space operating conditions.

One major limitation of the proposed work is the lack of real-world measurements. As advanced as CFD models may currently be, measurements are still a critical requirement for validation. CHTC measurements are costly and complex, yet they may provide further insights into developing more precise CEA-HD inside surfaces, CHTC correlations or algorithms, or algorithm modification. Perhaps a more manageable alternative would be to validate the energy model given access to operating CEA-HD production spaces. Access to this data type is challenging as producers frequently hesitate to share information closely tied to their financial and production performance. After extensive validation, the results from the energy model offer a wide range of practical applications, including assessing the energy impacts under various production space operating conditions, enclosure compositions, HVAC control sequences, etc. This can support the development of guidelines and design tools for HVAC engineers and production space designers based on validated models.

5.8 Conclusion

This paper investigates the impact of inside surfaces convection heat transfer coefficient (CHTC) on energy metrics for a small experimental high-density controlled environment agriculture (CEA-HD) production space. The analysis used the EnergyPlus building performance simulation (BPS) tool, computational fluid dynamics (CFD) and crop modelling. The results showed that specific algorithms packaged with EnergyPlus (Simple, TARP, and ASTMC1340 algorithms) are ill-suited to model CEA-HD production spaces based on CFD computed reference values. This paper aims to serve as a foundation for comprehensive research on energy modelling of CEA-HD production spaces using BPS tools.

5.9 Disclosure statement

The authors report there are no competing interests to declare.

5.10 Data Availability Statement

The data that support the findings of this study are available from the corresponding author upon reasonable request.

DISCUSSION

Les résultats présentés dans les trois chapitres précédents incluent trois contributions à la modélisation des espaces d'agriculture en environnement contrôlé à haute densité (AEC-HD). Ces contributions comblent plusieurs lacunes de la littérature scientifique identifiées au cours de la revue de littérature. Dans cette discussion globale, les résultats des trois articles préalablement présentés sont interprétés en relation avec l'objectif principal visant à développer une méthode de modélisation énergétique des espaces d'AEC basée sur l'utilisation d'outils de simulation de la performance énergétique du bâtiment (BPS) en tenant compte de l'uniformité du microclimat de production. De plus, la comparaison des résultats avec la littérature scientifique ainsi que la principale limitation de la thèse sont adressées. Finalement, plusieurs perspectives de travaux futurs basés sur les contributions de cette thèse sont discutées.

Dans l'article #1 (CHAPITRE 3), l'intégration de plusieurs modèles associés aux plantes (résistance à l'écoulement, transpiration et photosynthèse) avec les équations de la dynamique des fluides numérique (CFD) a permis d'obtenir un modèle prédictif de la distribution spatiale des variables du microclimat de production des espaces d'AEC-HD. Le couplage de ce modèle prédictif avec un algorithme d'optimisation métaheuristique a par la suite permis de proposer une nouvelle approche d'optimisation de l'uniformisation des variables du microclimat de production avec une fonction objectif tenant compte de la variation de la vitesse de l'écoulement d'air et de l'humidité absolue dans les différents plans de production de l'espace d'AEC-HD modélisé. Ce modèle CFD est utilisé dans l'article #3 (CHAPITRE 5) pour évaluer les algorithmes de calculs des coefficients de transfert de chaleur convectifs (CHCTs) des surfaces internes du logiciel de simulation énergétique du bâtiment EnergyPlus dans le contexte de modélisation énergétique d'espaces d'AEC-HD. Les algorithmes de calcul des CHTCs des surfaces internes utilisés dans ce logiciel ont été développés à partir de corrélations empiriques obtenues avec des géométries de pièce et des configurations de systèmes de chauffage, ventilation et conditionnement de l'air différentes des installations retrouvées dans les espaces d'AEC-HD. Les résultats de simulation obtenus sont directement influencés par le choix de l'algorithme et ont un impact important tel que démontré par les résultats présentés dans l'article #3 (CHAPITRE 5). L'intégration de la résolution du bilan d'énergie à la feuille dans un logiciel de simulation énergétique du bâtiment est aussi un aspect de la modélisation énergétique des espaces d'AEC-HD ayant un impact direct sur les résultats de simulation. Cette intégration a été réalisée dans l'article #2 (CHAPITRE 4) dans un logiciel de simulation supporté, validé, gratuit et publiquement disponible par l'exploitation d'une méthode de résolution numérique efficace et efficiente en plus de proposer une interface graphique. Tel que démontré par la revue de littérature effectuée dans l'article #2 (CHAPITRE 4), la modélisation du bilan d'énergie à feuille est déficiente dans une grande proportion de la littérature scientifique actuelle. L'outil logiciel développé dans le cadre de cette thèse est une solution pérenne à cette problématique. De plus, l'utilisation de l'interface de programmation (API) Python rend l'utilisation du modèle extrêmement flexible et simplifie grandement sa modification pour l'ajout de fonctionnalités supplémentaires.

La comparaison des résultats obtenus avec la littérature scientifique est actuellement difficile puisque le domaine de la simulation énergétique des espaces d'AEC-HD utilisant les outils de simulation énergétique du bâtiment (BPS) est encore en émergence. Pour l'uniformisation des variables du microclimat de production, quelques articles ont pu être identifiés (voir section 3.6), mais les résultats expérimentaux rapportés restent d'envergure modeste, ce qui rend difficile l'identification de niveaux de performance fiables. L'accès aux données est un enjeu du domaine, car l'information publique est rare et les connaissances sont protégées par les entreprises (Jonlin & Lewellen, 2017).

La limitation principale des travaux effectués dans le cadre de cette thèse est l'absence de données expérimentale afin de valider les différents modèles proposés. Bien que les ordres de grandeur des résultats de simulations ont été vérifiés à partir de différentes sources de données, la validation à partir de données mesurées reste essentielle et devra faire l'objet de travaux futurs.

En plus de la validation expérimentale, beaucoup d'autres initiatives de recherche pourraient exploiter les contributions présentées dans cette thèse par articles. Ainsi, d'autres analyses combinant les deux modèles pourraient s'avérer intéressantes dans une perspective d'adoption des outils de simulation énergétique du bâtiment (BPS) pour la modélisation énergétique des espaces d'AEC-HD. Une meilleure évaluation de la performance énergétique lors de l'optimisation de la distribution de l'air pourrait être effectuée en utilisant le modèle énergétique développé dans l'article #2 dans le processus d'optimisation de l'article #1. Ainsi, la fonction objective viserait à maximiser l'uniformité dans l'espace de production et la vitesse de l'écoulement de l'air à la feuille tout en minimisant la consommation énergétique annuelle simulée par le modèle énergétique. Après validation expérimentale du modèle CFD et du modèle BPS, la modélisation de plusieurs types de géométries typiquement retrouvées dans les espaces d'AEC-HD pourrait mener au développement d'outils de conception des systèmes de distribution de l'air tel que des abaques, des critères prescriptifs de maintien de l'uniformité du microclimat de production, des indicateurs de performances typiques pour les systèmes de ventilation, etc.

Le modèle CFD détaillé dans l'article #1 pourrait être utilisé non seulement pour l'optimisation de la conception des systèmes de distribution de l'air, mais aussi pour l'optimisation de la conception du système de production hydroponique. Différentes géométries et différents concepts de systèmes de production pourraient être évalués en conjonction avec la conception assistée par ordinateur pour maximiser les critères de conception au niveau du microclimat de production. Des stratégies d'accumulation thermique dans le système de production pourraient être envisagées afin d'effectuer un délestage lors des heures de pointe tout en maintenant des niveaux acceptables de température, d'humidité et de dioxyde de carbone pour les plantes.

Le calcul plus précis des charges sensibles et latentes traitées par le système de chauffage, ventilation et conditionnement de l'air (CVCA) est aussi une application potentielle du modèle CFD développé dans l'article #1. En effet, une meilleure modélisation du microclimat de l'espace de production permet un calcul plus précis des charges sensibles et latentes de l'espace de production par l'évaluation locale des transferts d'énergie et de masse résultant éventuellement à un meilleur dimensionnement des équipements CVCA. Un dimensionnement optimal des équipements CVCA permet d'obtenir un gain sur l'efficacité énergétique de l'espace de production tout en minimisant les investissements nécessaires à la construction de l'enceinte de production.

Les résultats présentés dans l'article #3 sont un avertissement important concernant la modélisation énergétique des espaces d'AEC-HD avec les outils de simulation énergétiques du bâtiment (BPS) sans préalablement vérifier les hypothèses et les limites de ces outils de modélisation. L'exploration systématique des différents domaines de la simulation énergétique du bâtiment (p. ex. enveloppe, irradiation solaire, etc.) devrait permettre de mettre en lumière les lacunes et problématiques de ces outils pour la modélisation énergétique d'espaces d'agriculture en environnement contrôlé (AEC).

Le modèle énergétique développé dans l'article #2 ouvre la voie à la modélisation de nouveaux bâtiments à usages multiples comprenant des espaces de production d'AEC-HD. Ces bâtiments pourraient tirer profit de synergies énergétiques et des concepts de systèmes énergétiques novateurs. Ces synergies ont été évaluées à 341.93 $kWh \cdot m^{-2}$ par an pour l'intégration de serres sur toit au concept énergétique d'un bâtiment en climat méditerranéen (Nadal et al., 2017). Actuellement, l'impact énergétique de l'intégration d'espaces d'AEC-HD dans des bâtiments à usages multiples est encore méconnu. Ainsi, la valorisation de la chaleur dégagée par les diodes électroluminescentes, l'humidité transmise par évaporation des feuilles de la plante et l'absorption de CO_2 de l'air ambiant permettrait de chauffer, d'humidifier et d'assainir l'air vicié avant sa recirculation vers des espaces occupés durant la période hivernale. Durant la période estivale, l'espace d'AEC à haute densité devra être climatisé. Il pourra donc bénéficier de la capacité du bâtiment en climatisation pour refroidir l'espace de production. La phytoremédiation de l'air concerne la captation de particules en suspension et l'adsorption de composés organiques volatils (VOCs) de l'air pouvant provenir de la gaine de retour (c.-à-d. air vicié) et de la gaine d'air frais (c.-à-d. milieux urbains pollués). Une étude simplifiée de l'impact de plantes sur la qualité de l'air rapporte un abaissement de 1°C, une augmentation de 9-13 % de l'humidité relative et des économies de 10-15 % d'énergie dans la région de

Syracuse, NY (Carver et al., 2010). Les modèles développés dans le cadre de cette thèse permettront de préciser les résultats de cette étude.

Le couplage avec un modèle de croissance de la plante, le développement de systèmes de compostages locaux, l'intégration avec d'autres productions commerciales (p. ex. comme les effluents de bières) et l'utilisation locale des matières organiques dans l'élaboration de solutions nutritives pourraient permettre de viser d'autres objectifs de recherche au niveau de l'efficacité de l'utilisation des ressources. Le coût monétaire d'un concept de production alimentaire ou de phytoremédiation de l'air n'est pas toujours le bon indicateur pour indiquer la performance ou le potentiel, d'un domaine de recherche. Ainsi, avec la modélisation de l'utilisation des ressources et de la production alimentaire, il serait possible de viser des constructions «net-zéro ressources» ou «net-zéro déchets» plaçant l'accent de la recherche vers la consommation de ressources plutôt que sur la consommation d'énergie.

CONCLUSION

Cette thèse apporte trois contributions claires à la modélisation des espaces d'agriculture en environnement contrôlé à haute densité (AEC-HD) en utilisant des outils de simulation de la performance du bâtiment (BPS) et de dynamique des fluides numériques (CFD). Ces trois contributions sont :

1. Une méthode d'optimisation de la distribution de l'air prenant en compte l'uniformité du microclimat de production et maximisant la vitesse de l'écoulement d'air à la plante;
2. Un outil graphique permettant d'intégrer simplement la résolution du bilan d'énergie à la feuille d'une façon efficace dans un logiciel de simulation énergétique du bâtiment supporté, validé, gratuit et publiquement disponible;
3. L'évaluation de la performance des algorithmes de calcul des coefficients de transfert de chaleur convectifs (CHTCs) des surfaces internes du logiciel EnergyPlus dans le contexte de la modélisation énergétique d'espaces d'AEC-HD.

Ainsi, l'objectif principal de cette thèse par article, soit de développer une méthode de modélisation énergétique des espaces d'AEC basée sur l'utilisation d'outils de simulation de la performance énergétique du bâtiment (BPS) en tenant compte de l'uniformité du microclimat de production, a été atteint. Cependant, des travaux de recherche supplémentaires sont nécessaires pour compléter, améliorer et, surtout, valider expérimentalement les contributions apportées.

RECOMMANDATIONS

Les contributions présentées dans cette thèse permettent d'entrevoir la modélisation énergétique des espaces d'AEC-HD à l'aide d'outils de simulation de la performance énergétique du bâtiment (BPS). Toutefois, des travaux de recherche complémentaires devraient être réalisés avant l'adoption de cette méthode de modélisation :

- Valider expérimentalement les modèles proposés :
  - De la modélisation spatiale des variables environnementales selon les principes de la norme ASME V&V 20-2009 (R2021);
  - Du modèle du bilan thermique à la feuille;
  - Du modèle énergétique en suivant les lignes directrices 14-2014 de l'ASHRAE.
- Proposer des cas tests, du type ASHRAE 140, pour la vérification des outils de simulation énergétique des espaces d'agricultures en environnement contrôlé.

BIBLIOGRAPHIE

Adesanya, M. A., Na, W.-H., Rabiu, A., Ogunlowo, Q. O., Akpenpuun, T. D., Rasheed, A., Yoon, Y.-C., & Lee, H.-W. (2022). TRNSYS simulation and experimental validation of internal temperature and heating demand in a glass greenhouse. *Sustainability, 14*(14), 8283.

AeroFarms. (2024). About AeroFarms The Vertical Farming, Elevated Flavor Company. Retrieved from https://www.aerofarms.com/about-us/

Agrebi, S., Chargui, R., Tashtoush, B., & Guizani, A. (2021). Comparative performance analysis of a solar assisted heat pump for greenhouse heating in Tunisia. *International Journal of Refrigeration, 131*, 547-558.

Agritecture. (2021). *Global CEA Census Report 2021*. Retrieved from https://www.agritecture.com/census:

Ahamed, M. S., Guo, H., & Tanino, K. (2020). Modeling heating demands in a Chinese-style solar greenhouse using the transient building energy simulation model TRNSYS. *Journal of Building Engineering, 29*, 101114. doi:https://doi.org/10.1016/j.jobe.2019.101114

Akpenpuun, T., Ogunlowo, Q., Rabiu, A., Adesanya, M., Na, W., Omobowale, M., Mijinyawa, Y., & Lee, H. (2022). Building Energy Simulation model application to greenhouse microclimate, covering material and thermal blanket modelling: A Review. *Nigerian Journal of Technological Development, 19*(3), 276-286.

Al-Kodmany, K. (2018). The Vertical Farm: A Review of Developments and Implications for the Vertical City. *Buildings, 8*(2), 24. Retrieved from https://www.mdpi.com/2075-5309/8/2/24

Alamdari, F., & Hammond, G. P. (1983). Improved data correlations for buoyancy-driven convection in rooms. *Building Services Engineering Research and Technology, 4*(3), 106-112. doi:10.1177/014362448300400304

Alinejad, T., Yaghoubi, M., & Vadiee, A. (2020). Thermo-environomic assessment of an integrated greenhouse with an adjustable solar photovoltaic blind system. *Renewable energy, 156*, 1-13.

Allen, L., Prasad, P. V., & Goodman, R. (2004). Crop responses to elevated carbon dioxide. *Encyclopedia of plant and crop science*, 346-348.

Altes-Buch, Q., Quoilin, S., & Lemort, V. (2022). A modeling framework for the integration of electrical and thermal energy systems in greenhouses. *Building Simulation, 15*(5), 779-797. doi:10.1007/s12273-021-0851-2

Altmayer, E., Gadgil, A., Bauman, F. S., & Kammerud, R. C. (1983). Correlation for Convective Heat Transfer from Room Surfaces. *ASHRAE Transactions, 89 (2)*, 61-77.

Alvarez-Sánchez, E., Leyva-Retureta, G., Portilla-Flores, E., & López-Velázquez, A. (2014). Evaluation of thermal behavior for an asymmetric greenhouse by means of dynamic simulations. *Dyna, 81*(188), 152-159.

American Society of Heating, R., & Air-Conditioning Engineers, I. (2021). 2021 ASHRAE® Handbook - Fundamentals (SI Edition). In: American Society of Heating, Refrigerating and Air-Conditioning Engineers, Inc. (ASHRAE).

Amin, M. T., & Kissock, J. K. (2016). *Dynamic modeling and verification of an energy-efficient greenhouse with aquaponics.* Paper presented at the Energy Sustainability.

Appolloni, E., Orsini, F., Specht, K., Thomaier, S., Sanyé-Mengual, E., Pennisi, G., & Gianquinto, G. (2021). The global rise of urban rooftop agriculture: A review of worldwide cases. *Journal of Cleaner Production, 296*, 126556. doi:https://doi.org/10.1016/j.jclepro.2021.126556

Asa'd, O., Ugursal, V. I., & Ben-Abdallah, N. (2019). Investigation of the energetic performance of an attached solar greenhouse through monitoring and simulation. *Energy for Sustainable Development, 53*, 15-29. doi:https://doi.org/10.1016/j.esd.2019.09.001

ASHRAE. (2013a). *Fundamentals handbook*: American Society of Heating, Refrigerating and Air-Conditioning Engineers, Inc., Atlanta, GA.

ASHRAE. (2014). Guideline 14-2014 : Measurement of energy, demand, and water savings. 1-150.

ASHRAE, A. (2013b). *Standard 62.1-2013 Ventilation for acceptable indoor air quality*: American Society of Heating, Refrigerating and Air-Conditioning Engineers, Inc., Atlanta, GA.

Ataei, A. (2016). Performance optimization of a combined solar collector, geothermal heat pump and thermal seasonal storage system for heating and cooling greenhouses. *Journal of Applied Engineering Science, 14*(2), 296-305. doi:10.5937/jaes14-8749

Attar, I., & Farhat, A. (2015). Efficiency evaluation of a solar water heating system applied to the greenhouse climate. *Solar Energy, 119*, 212-224.

Attar, I., Naili, N., Khalifa, N., Hazami, M., & Farhat, A. (2013). Parametric and numerical study of a solar system for heating a greenhouse equipped with a buried exchanger.

Energy Conversion and Management, 70, 163-173. doi:https://doi.org/10.1016/j.enconman.2013.02.017

Avgoustaki, D. D., & Xydis, G. (2021). Energy cost reduction by shifting electricity demand in indoor vertical farms with artificial lighting. *Biosystems Engineering, 211*, 219-229. doi:https://doi.org/10.1016/j.biosystemseng.2021.09.006

Awani, S., Chargui, R., Kooli, S., Farhat, A., & Guizani, A. (2015). Performance of the coupling of the flat plate collector and a heat pump system associated with a vertical heat exchanger for heating of the two types of greenhouses system. *Energy Conversion and Management, 103*, 266-275. doi:https://doi.org/10.1016/j.enconman.2015.06.032

Awani, S., Kooli, S., Chargui, R., & Guizani, A. (2017). Numerical and experimental study of a closed loop for ground heat exchanger coupled with heat pump system and a solar collector for heating a glass greenhouse in north of Tunisia. *International Journal of Refrigeration, 76*, 328-341. doi:10.1016/j.ijrefrig.2017.01.030

Awbi, H. B., & Hatton, A. (1999). Natural convection from heated room surfaces. *Energy and buildings, 30*(3), 233-244.

Baek, M.-S., Kwon, S.-Y., & Lim, J.-H. (2015). Improvement of uniformity in cultivation environment and crop growth rate by hybrid control of air flow devices. *Journal of Central South University, 22*(12), 4702-4708. doi:10.1007/s11771-015-3021-9

Baek, M.-S., Kwon, S.-Y., & Lim, J.-H. (2016). Improvement of the Crop Growth Rate in Plant Factory by Promoting Air Flow inside the Cultivation. *International Journal of Smart Home, 10*(2), 63-74.

Baglivo, C., Mazzeo, D., Panico, S., Bonuso, S., Matera, N., Congedo, P. M., & Oliveti, G. (2020). Complete greenhouse dynamic simulation tool to assess the crop thermal well-being and energy needs. *Applied Thermal Engineering, 179*, 115698.

Bambara, J., & Athienitis, A. K. (2018). Energy and economic analysis for greenhouse ground insulation design. *Energies, 11*(11). doi:10.3390/en11113218

Bambara, J., Athienitis, A. K., & Eicker, U. (2021). Decarbonizing Local Mobility and Greenhouse Agriculture through Residential Building Energy Upgrades: A Case Study for Québec. *Energies, 14*(20). doi:10.3390/en14206820

Banakar, A., Montazeri, M., Ghobadian, B., Pasdarshahri, H., & Kamrani, F. (2021). Energy analysis and assessing heating and cooling demands of closed greenhouse in Iran. *Thermal Science and Engineering Progress, 25*, 101042.

Beausoleil-Morrison, I. (2002). The adaptive simulation of convective heat transfer at internal building surfaces. *Building and Environment, 37*(8), 791-806. doi:https://doi.org/10.1016/S0360-1323(02)00042-2

Beausoleil-Morrison, I., Macdonald, F., Kummert, M., McDowell, T., & Jost, R. (2014). Co-simulation between ESP-r and TRNSYS. *Journal of Building Performance Simulation, 7*(2), 133-151. doi:10.1080/19401493.2013.794864

Beausoleil-Morrison, I., & Strachan, P. (1999). On the significance of modeling internal surface convection in dynamic whole-building simulation programs. *ASHRAE Transactions, 105*, 929.

Benis, K., Reinhart, C., & Ferrão, P. (2017). Development of a simulation-based decision support workflow for the implementation of Building-Integrated Agriculture (BIA) in urban contexts. *Journal of Cleaner Production, 147*, 589-602. doi:https://doi.org/10.1016/j.jclepro.2017.01.130

Benni, S., Tassinari, P., Bonora, F., Barbaresi, A., & Torreggiani, D. (2016). Efficacy of greenhouse natural ventilation: Environmental monitoring and CFD simulations of a study case. *Energy and Buildings, 125*, 276-286.

Berroug, F., Lakhal, E. K., El Omari, M., Faraji, M., & El Qarnia, H. (2011). Thermal performance of a greenhouse with a phase change material north wall. *Energy and buildings, 43*(11), 3027-3035. doi:https://doi.org/10.1016/j.enbuild.2011.07.020

Birdsall, B., Buhl, W., Ellington, K., Erdem, A., & Winkelmann, F. (1990). Overview of the DOE-2 building energy analysis program. *Report LBL-19735m rev. w, Lawrence Berkeley Laboratory, Berkeley, CA*.

Bonachela, S., González, A. M., & Fernández, M. D. (2006). Irrigation scheduling of plastic greenhouse vegetable crops based on historical weather data. *Irrigation Science, 25*(1), 53-62.

Bonuso, S., Panico, S., Baglivo, C., Mazzeo, D., Matera, N., Congedo, P. M., & Oliveti, G. (2020). Dynamic analysis of the natural and mechanical ventilation of a solar greenhouse by coupling Controlled Mechanical Ventilation (CMV) with an Earth-to-Air Heat Exchanger (EAHX). *Energies, 13*(14), 3676.

Boulard, T., Kittas, C., Roy, J. C., & Wang, S. (2002). SE—Structures and Environment: Convective and Ventilation Transfers in Greenhouses, Part 2: Determination of the Distributed Greenhouse Climate. *Biosystems Engineering, 83*(2), 129-147. doi:https://doi.org/10.1006/bioe.2002.0114

Boulard, T., Roy, J.-C., Pouillard, J.-B., Fatnassi, H., & Grisey, A. (2017). Modelling of micrometeorology, canopy transpiration and photosynthesis in a closed greenhouse using computational fluid dynamics. *Biosystems Engineering, 158*, 110-133. doi:https://doi.org/10.1016/j.biosystemseng.2017.04.001

Bournet, P.-E., & Rojano, F. (2022). Advances of Computational Fluid Dynamics (CFD) applications in agricultural building modelling: Research, applications and challenges. *Computers and Electronics in Agriculture, 201*, 107277.

Boussinesq, J. (1877). *Essai sur la théorie des eaux courantes*: Impr. nationale.

Bradley, B., & Riley, M. (1991). Models and Features in Hot-2000 version 6.

Brisson, N., Gary, C., Justes, E., Roche, R., Mary, B., Ripoche, D., Zimmer, D., Sierra, J., Bertuzzi, P., & Burger, P. (2003). An overview of the crop model STICS. *European Journal of agronomy, 18*(3-4), 309-332.

Camci, M., Karakoyun, Y., Acikgoz, O., & Dalkilic, A. S. (2021). A comparative study on convective heat transfer in indoor applications. *Energy and buildings, 242*. doi:10.1016/j.enbuild.2021.110985

Cameron, D. (2023). Le volume de production en serre a presque doublé. Retrieved from https://www.lapresse.ca/actualites/environnement/2023-03-23/autonomie-alimentaire-au-quebec/le-volume-de-production-en-serre-a-presque-double.php

Candy, S., Moore, G., & Freere, P. (2012). *Design and modeling of a greenhouse for a remote region in Nepal.* Paper presented at the Procedia Engineering.

Carver, R., Zhang, J., & Wang, Z. (2010). Air cleaning technologies for indoor air quality (ACT-IAQ): growing fresh and clean air. *New York State Energy Research and Development Authority*, 1.

Chahidi, L. O., Fossa, M., Priarone, A., & Mechaqrane, A. (2021). Energy saving strategies in sustainable greenhouse cultivation in the mediterranean climate–A case study. *Applied Energy, 282*, 116156.

Chahidi, L. O., & Mechaqrane, A. (2021). Energetic and economic analysis for improving greenhouse energy efficiency. *Journal of Energy Systems, 5*(4), 296-305.

Chang, Y.-W., Lin, T.-S., Wang, J.-C., Chou, J.-J., Liao, K., & Jiang, J. (2011). The effect of temperature distribution on the vertical cultivation in plant factories with a WSN-based environmental monitoring system. *Advances in Biomedical Engineering, 3*, 5.

Chen, C., Li, Y., Li, N., Wei, S., Yang, F., Ling, H., Yu, N., & Han, F. (2018). A computational model to determine the optimal orientation for solar greenhouses located at different latitudes in China. *Solar Energy, 165*, 19-26.

Chen, C., Yu, N., Yang, F., Mahkamov, K., Han, F., Li, Y., & Ling, H. (2019). Theoretical and experimental study on selection of physical dimensions of passive solar greenhouses for enhanced energy performance. *Solar Energy, 191*, 46-56. doi:https://doi.org/10.1016/j.solener.2019.07.089

Choab, N., Allouhi, A., El Maakoul, A., Kousksou, T., Saadeddine, S., & Jamil, A. (2019). Review on greenhouse microclimate and application: Design parameters, thermal modeling and simulation, climate controlling technologies. *Solar Energy, 191*, 109-137. doi:https://doi.org/10.1016/j.solener.2019.08.042

Choab, N., Allouhi, A., El Maakoul, A., Kousksou, T., Saadeddine, S., & Jamil, A. (2020). Effect of greenhouse design parameters on the heating and cooling requirement of greenhouses in Moroccan climatic conditions. *IEEE Access, 9*, 2986-3003.

Clarke, J. A., & Hensen, J. L. M. (2015). Integrated building performance simulation: Progress, prospects and requirements. *Building and Environment, 91*, 294-306. doi:https://doi.org/10.1016/j.buildenv.2015.04.002

Crawley, D. B. (1997). Building energy tools directory. *Proceedings of Building Simulation'97, 1*, 63-64.

Crawley, D. B., Hand, J. W., Kummert, M., & Griffith, B. T. (2008). Contrasting the capabilities of building energy performance simulation programs. *Building and Environment, 43*(4), 661-673.

Crawley, D. B., Lawrie, L. K., Winkelmann, F. C., Buhl, W. F., Huang, Y. J., Pedersen, C. O., Strand, R. K., Liesen, R. J., Fisher, D. E., & Witte, M. J. (2001). EnergyPlus: creating a new-generation building energy simulation program. *Energy and buildings, 33*(4), 319-331.

Dahlan, N., Amiruddin, A., Luong, N. D., & Sakimin, S. Z. (2018a). Energy and Climate Analysis of Greenhouse System for Tomatoes Cultivation using CFD and Open Studio Energy Plus Software. *International Journal of Engineering & Technology, 7*(3.11), 183-186.

Dahlan, N., Sakimin, S., Faizwan, M., Ajmain, N., & Aris, A. (2018b). Automated Calibration Of Greenhouse Energy Model Using Hybrid Evolutionary Programming (EP)-Energy Plus. *Indonesian Journal of Electrical Engineering and Computer Science, 12*(2), 648-654. doi:10.11591/ijeecs.v12.i2.pp648-654

Deb, K., Pratap, A., Agarwal, S., & Meyarivan, T. (2002). A fast and elitist multiobjective genetic algorithm: NSGA-II. *IEEE transactions on evolutionary computation, 6*(2), 182-197.

Defraeye, T., Verboven, P., Ho, Q. T., & Nicolai, B. (2013). Convective heat and mass exchange predictions at leaf surfaces: Applications, methods and perspectives. *Computers and Electronics in Agriculture, 96*, 180-201. doi:https://doi.org/10.1016/j.compag.2013.05.008

Deltour, J., De Halleux, D., Nijskens, J., Coutisse, S., & Nisen, A. (1985). *Dynamic modelling of heat and mass transfer in greenhouses.* Paper presented at the Symposium Greenhouse Climate and its Control 174.

Denzer, A., Wang, L., Thomas, Y., & McMorrow, G. (2017). Greenhouse Design with Waste Heat: Principles and Practices. In *AEI 2017* (pp. 440-455).

Despommier, D. (2010). *The vertical farm: feeding the world in the 21st century*: Macmillan.

Development of a tool for modelling Controlled Environment agriculture (CEA) spaces in EnergyPlus. (2024). *(Manuscript under review)*.

Eaton, M., Shelford, T., Cole, M., & Mattson, N. (2023). Modeling resource consumption and carbon emissions associated with lettuce production in plant factories. *Journal of Cleaner Production, 384*, 135569. doi:https://doi.org/10.1016/j.jclepro.2022.135569

Engler, N., & Krarti, M. (2021). Review of energy efficiency in controlled environment agriculture. *Renewable and Sustainable Energy Reviews, 141*, 110786. doi:https://doi.org/10.1016/j.rser.2021.110786

EPRI. (2018). *Indoor Agriculture: A Utility, Water, Sustainability, Technology and Market Overview* (3002014056). Retrieved from

Fabrizio, E. (2012). Energy reduction measures in agricultural greenhouses heating: Envelope, systems and solar energy collection. *Energy and buildings, 53*, 57-63. doi:10.1016/j.enbuild.2012.07.003

Fan, R., Liu, H., Zhou, S., He, Z., Zhang, X., Liu, K., Wang, J., Yang, Q., Zheng, Y., & Lu, W. (2020). *CFD simulation of the airflow uniformity in the plant factory.* Paper presented at the IOP Conference Series: Earth and Environmental Science.

Fang, H., Li, K., Wu, G., Cheng, R., Zhang, Y., & Yang, Q. (2020). A CFD analysis on improving lettuce canopy airflow distribution in a plant factory considering the crop resistance and LEDs heat dissipation. *Biosystems Engineering, 200*, 1-12. doi:https://doi.org/10.1016/j.biosystemseng.2020.08.017

Farber, K., Farber, P., Gräbel, J., Krick, S., & Ueberholz, P. (2017). A numerical study of a greenhouse CFD simulation including radiation heat transfer and transpiration. *International Journal of Engineering Systems Modelling and Simulation, 9*(3), 161-168.

Farber, P., Gräbel, J., Krick, S., Ueberholz, P., & Farber, K. (2015). *A computational fluid dynamics investigation of flow, solar radiation, heat transfer, transpiration and condensation in a greenhouse.* Paper presented at the International Symposium on New Technologies and Management for Greenhouses-GreenSys2015 1170.

Fatnassi, H., Bournet, P. E., Boulard, T., Roy, J. C., Molina-Aiz, F. D., & Zaaboul, R. (2023). Use of computational fluid dynamic tools to model the coupling of plant canopy activity and climate in greenhouses and closed plant growth systems: A review. *Biosystems Engineering, 230*, 388-408. doi:10.1016/j.biosystemseng.2023.04.016

Fiksel, A., Thornton, J., Klein, S., & Beckman, W. (1995). Developments to the TRNSYS simulation program.

Fisher, D. E. (1995). *An experimental investigation of mixed convection heat transfer in a rectangular enclosure*: University of Illinois at Urbana-Champaign.

Fisher, D. E., & Pedersen, C. O. (1997). *Convective heat transfer in building energy and thermal load calculations* (0001-2505). Retrieved from

Fontanini, A. D., Castro Aguilar, J. L., Mitchell, M. S., Kosny, J., Merket, N., DeGraw, J. W., & Lee, E. (2018). Predicting the performance of radiant technologies in attics: Reducing the discrepancies between attic specific and whole-building energy models. *Energy and buildings, 169*, 69-83. doi:https://doi.org/10.1016/j.enbuild.2018.03.054

Fontanini, A. D., Vaidya, U., Passalacqua, A., & Ganapathysubramanian, B. (2016). Quantifying mechanical ventilation performance: The connection between transport equations and Markov matrices. *Building and Environment, 104*, 253-262. doi:https://doi.org/10.1016/j.buildenv.2016.05.019

Frankenstein, S., & Koenig, G. (2004). *FASST vegetation models*. Retrieved from

Frantz, J. M., Hand, B., Buckingham, L., & Ghose, S. (2010). Virtual grower: software to calculate heating costs of greenhouse production in the United States. *HortTechnology, 20*(4), 778-785.

Fricke, W. (2017). Water transport and energy. *Plant, cell & environment, 40*(6), 977-994. doi:https://doi.org/10.1111/pce.12848

Fuller, R. J., Aye, L., Zahnd, A., & Thakuri, S. (2009). Thermal evaluation of a greenhouse in a remote high altitude area of Nepal. *International Energy Journal, 10*(2).

Gao, X., Yang, H., Guan, Y., Bai, J., Zhang, R., & Hu, W. (2017). *Length Determination of the Solar Greenhouse North Wall in Lanzhou.* Paper presented at the Procedia Engineering.

Gary, C., Tchamitchian, M., Bertin, N., Boulard, T., Baille, A., Charasse, L., Rebillard, A., & Cardi, J. P. (1998). *SIMULSERRE: AN EDUCATIONAL SOFTWARE SIMULATING THE GREENHOUSE-CROP SYSTEM*.

Goto, E., Ishigami, Y., & Okushima, L. (2017). *Development of a greenhouse simulation model to estimate energy and resources necessary for environmental controls under various climate conditions.* Paper presented at the Acta Horticulturae.

Gouvernement du Québec. (2020). Croissance des serres au Québec. Retrieved from https://www.quebec.ca/nouvelles/actualites/details/croissance-serres

Gouvernement du Québec. (2024, 8 septembre 2023). Culture des fruits et légumes de serre (serriculture). Retrieved from https://www.quebec.ca/agriculture-environnement-et-ressources-naturelles/agriculture/industrie-agricole-au-quebec/productions-agricoles/culture-fruits-legumes-serre-serriculture

Graamans, L., Baeza, E., van den Dobbelsteen, A., Tsafaras, I., & Stanghellini, C. (2018). Plant factories versus greenhouses: Comparison of resource use efficiency. *Agricultural Systems, 160*, 31-43. doi:https://doi.org/10.1016/j.agsy.2017.11.003

Graamans, L., Tenpierik, M., van den Dobbelsteen, A., & Stanghellini, C. (2020). Plant factories: Reducing energy demand at high internal heat loads through facade design. *Applied Energy, 262*, 114544.

Graamans, L., van den Dobbelsteen, A., Meinen, E., & Stanghellini, C. (2017). Plant factories; crop transpiration and energy balance. *Agricultural Systems, 153*, 138-147. doi:https://doi.org/10.1016/j.agsy.2017.01.003

Ha, T., Lee, I.-b., Kwon, K.-s., & Hong, S.-W. (2015). Computation and field experiment validation of greenhouse energy load using building energy simulation model. *International Journal of Agricultural and Biological Engineering, 8*(6), 116-127.

Harbick, K., & Albright, L. D. (2016). Comparison of energy consumption: greenhouses and plant factories. *Acta Hortic., 1134*, 285-292. doi:10.17660/ActaHortic.2016.1134.38

Henshaw, P. (2017). Modelling changes to an unheated greenhouse in the Canadian subarctic to lengthen the growing season. *Sustainable Energy Technologies and Assessments, 24*, 31-38. doi:https://doi.org/10.1016/j.seta.2016.12.004

Herron, D., Walton, G., & Lawrie, L. (1981). *Building Loads Analysis and System Thermodynamics (BLAST) Program Users Manual. Volume One. Supplement (Version 3.0)*. Retrieved from

Hwang, P.-W., Chen, C.-H., & Chang, Y.-J. (2017). *A study on energy strategy of a plant factory using sustainable energy combined with computational fluid dynamics simulation: An innovative practice of green information systems.* Paper presented at the 2017 Computing Conference.

Iddio, E., Wang, L., Thomas, Y., McMorrow, G., & Denzer, A. (2020). Energy efficient operation and modeling for greenhouses: A literature review. *Renewable and Sustainable Energy Reviews, 117*, 109480. doi:https://doi.org/10.1016/j.rser.2019.109480

Ishigami, Y., Goto, E., Watanabe, M., Takahashi, T., & Okushima, L. (2013). *Development of a simulation model to evaluate environmental controls in a tomato greenhouse.* Paper presented at the International Symposium on New Technologies for Environment Control, Energy-Saving and Crop Production in Greenhouse and Plant 1037.

Jahangir, M. H., Ziyaei, M., & Kargarzadeh, A. (2022). Evaluation of thermal behavior and life cycle cost analysis of greenhouses with bio-phase change materials in multiple locations. *Journal of Energy Storage, 54*, 105176. doi:https://doi.org/10.1016/j.est.2022.105176

Jans-Singh, M., Ward, R., & Choudhary, R. (2021). Co-simulating a greenhouse in a building to quantify co-benefits of different coupled configurations. *Journal of Building Performance Simulation, 14*(3), 247-276. doi:10.1080/19401493.2021.1908426

Jiang, J.-A., Liao, M.-S., Lin, T.-S., Huang, C.-K., Chou, C.-Y., Yeh, S.-H., Lin, T.-T., & Fang, W. (2018a). Toward a higher yield: a wireless sensor network-based temperature monitoring and fan-circulating system for precision cultivation in plant factories. *Precision Agriculture, 19*, 929-956.

Jiang, J.-A., Liao, M.-S., Lin, T.-S., Huang, C.-K., Chou, C.-Y., Yeh, S.-H., Lin, T.-T., & Fang, W. (2018b). Toward a higher yield: a wireless sensor network-based temperature monitoring and fan-circulating system for precision cultivation in plant factories. *Precision Agriculture, 19*(5), 929-956. doi:10.1007/s11119-018-9565-6

Jin, T.-H., Shin, K.-Y., Yoon, S.-W., Im, Y.-H., & Chang, K.-C. (2017). *Simulation of thermal environment in a three-layer vinyl greenhouse by natural ventilation control.* Paper presented at the E3S Web of Conferences.

Jones, J. W., Dayan, E., Allen, L., Van Keulen, H., & Challa, H. (1991). A dynamic tomato growth and yield model (TOMGRO). *Transactions of the ASAE, 34*(2), 663-0672.

Jonlin, D. L., & Lewellen, D. J. (2017). A low-energy high managing energy use for commercial indoor cannabis cultivation. *Energy Engineering, 114*(4), 69-79.

Kalantari, F., Tahir, O. M., Joni, R. A., & Fatemi, E. (2018). Opportunities and Challenges in Sustainability of Vertical Farming: A Review. *Journal of Landscape Ecology, 11*(1), 35-60. doi:doi:10.1515/jlecol-2017-0016

Kaliakatsos, D., Nicoletti, F., Paradisi, F., Bevilacqua, P., & Arcuri, N. (2022). Evaluation of Building Energy Savings Achievable with an Attached Bioclimatic Greenhouse: Parametric Analysis and Solar Gain Control Techniques. *Buildings, 12*(12). doi:10.3390/buildings12122186

Karimipanah, T., HB, A., & Moshfegh, B. (2008). The air distribution index as an indicator for energy consumption and performance of ventilation systems. *Journal of the Human-Environment System, 11*(2), 77-84.

Katzin, D., Marcelis, L. F. M., & van Mourik, S. (2021). Energy savings in greenhouses by transition from high-pressure sodium to LED lighting. *Applied Energy, 281*, 116019. doi:https://doi.org/10.1016/j.apenergy.2020.116019

Katzin, D., van Henten, E. J., & van Mourik, S. (2022). Process-based greenhouse climate models: Genealogy, current status, and future directions. *Agricultural Systems, 198*, 103388. doi:https://doi.org/10.1016/j.agsy.2022.103388

Khalifa, A.-J. N. (1989). *Heat transfer processes in buildings.* University of Wales, College of Cardiff,

Kichah, A., Bournet, P.-E., Migeon, C., & Boulard, T. (2012). Measurement and CFD simulation of microclimate characteristics and transpiration of an Impatiens pot plant crop in a greenhouse. *Biosystems engineering, 112*(1), 22-34.

Kim, K., Yoon, J.-Y., Kwon, H.-J., Han, J.-H., Son, J. E., Nam, S.-W., Giacomelli, G. A., & Lee, I.-B. (2008). 3-D CFD analysis of relative humidity distribution in greenhouse with a fog cooling system and refrigerative dehumidifiers. *Biosystems engineering, 100*(2), 245-255.

Kimball, B. A. (1973). Simulation of the energy balance of a greenhouse. *Agricultural Meteorology, 11*(C), 243-260. doi:10.1016/0002-1571(73)90067-8

Kitaya, Y., Tsuruyama, J., Shibuya, T., Yoshida, M., & Kiyota, M. (2003). Effects of air current speed on gas exchange in plant leaves and plant canopies. *Advances in Space Research, 31*(1), 177-182. doi:10.1016/S0273-1177(02)00747-0

Koch, K., Samson, R., & Denys, S. (2019). Aerodynamic characterisation of green wall vegetation based on plant morphology: An experimental and computational fluid dynamics approach. *Biosystems Engineering, 178*, 34-51. doi:https://doi.org/10.1016/j.biosystemseng.2018.10.019

Körner, O., & Challa, H. (2003). Process-based humidity control regime for greenhouse crops. *Computers and Electronics in Agriculture, 39*(3), 173-192. doi:https://doi.org/10.1016/S0168-1699(03)00079-6

Kozai, T. (2018). Smart plant factory. *The Next Generation Indoor Vertical Farms; Springer: Singapore*, 238.

Kozai, T., Niu, G., & Takagaki, M. (2015). *Plant factory: an indoor vertical farming system for efficient quality food production*: Academic Press.

Kozai, T., Niu, G., & Takagaki, M. (2019). *Plant factory: an indoor vertical farming system for efficient quality food production*: Academic press.

Kreyszig, E. (1999). Advanced Engineering Mathematics, 8-th edition. In: John Wiley & Sons.

Kusuma, P., Pattison, P. M., & Bugbee, B. (2020). From physics to fixtures to food: current and potential LED efficacy. *Horticulture Research, 7*. doi:10.1038/s41438-020-0283-7

Labihi, A., Meslem, A., Collet, F., & Prétot, S. Transient Thermal Simulation of a Greenhouse for Tomato Plants: A Trnsys Model with Experimental Validation. *Preprint, submitted in 2023*.

Lalonde, T., Talbot, M. H., & Monfet, D. (2019). *The impacts of plants on HVAC system performances: A parametric study.* Paper presented at the Proceedings of Building Simulation 2019: 16th Conference of International Building Performance Simulation Association.

Larochelle Martin, G., & Monfet, D. (2024). High-density controlled environment agriculture (CEA-HD) air distribution optimization using computational fluid dynamics (CFD). *Engineering Applications of Computational Fluid Mechanics, 18*(1), 2297027. doi:10.1080/19942060.2023.2297027

Launder, B. E., & Spalding, D. B. (1974). The numerical computation of turbulent flows. *Computer Methods in Applied Mechanics and Engineering, 3*(2), 269-289. doi:https://doi.org/10.1016/0045-7825(74)90029-2

Lebre, B., Silva, P. D., Pires, L. C., & Gaspar, P. D. (2021). Computational Modeling of the Thermal Behavior of a Greenhouse. *Applied Sciences, 11*(24), 11816.

Ledesma, G., Nikolic, J., & Pons-Valladares, O. (2022). Co-simulation for thermodynamic coupling of crops in buildings. Case study of free-running schools in Quito, Ecuador. *Building and Environment, 207*, 108407. doi:https://doi.org/10.1016/j.buildenv.2021.108407

Lee, C.-G., Cho, L.-H., Kim, S.-J., Park, S.-Y., & Kim, D.-H. (2022). Prediction Model for the Internal Temperature of a Greenhouse with a Water-to-Water Heat Pump Using a Pellet Boiler as a Heat Source Using Building Energy Simulation. *Energies, 15*(15), 5677.

Lee, C., Cóstola, D., Loonen, R., & Hensen, J. L. (2013). *Energy saving potential of long-term climate adaptive greenhouse shells.* Paper presented at the Proceedings of Building Simulation 2013: 13th Conference of International Building Performance Simulation Association.

Lee, C., Costola, D., Swinkels, G., & Hensen, J. (2012). *On the use of building energy simulation programs in the performance assessment of agricultural greenhouses.* Paper presented at the Proceedings of the 1st Asia Conference of the International Building Performance Simulation Association. Shanghai, China.

Lee, K. H., Lee, J. H., Lee, K. H., & Song, D. (2016). Energetic and economic feasibility analysis of utilizing waste heat from incineration facility and power plant for large-scale horticulture facilities. *Applied Thermal Engineering, 105*, 577-593.

Lee, S.-y., Lee, I.-b., Lee, S.-n., Yeo, U.-h., Kim, J.-g., Kim, R.-w., & Decano-Valentin, C. (2021). Dynamic energy exchange modelling for a plastic-covered multi-span greenhouse utilizing a thermal effluent from power plant. *Agronomy, 11*(8), 1461.

Léveillé-Guillemette, F., & Monfet, D. (2018). Calibration d'un modèle énergétique et analyse économique de mesures de conservation d'énergie d'une serre communautaire à Montréal.

Liebman-Pelaez, M., Kongoletos, J., Norford, L. K., & Reinhart, C. (2021). Validation of a building energy model of a hydroponic container farm and its application in urban design. *Energy and buildings, 250*, 111192. doi:https://doi.org/10.1016/j.enbuild.2021.111192

Lim, T.-G., & Kim, Y. H. (2014). [Analysis of Airflow Pattern in Plant Factory with Different Inlet and Outlet Locations using Computational Fluid Dynamics]. *39*. doi:10.5307/JBE.2014.39.4.310

Liu, J., Jin, T.-H., & Shin, K.-Y. (2021). Parametric study on a simplified model for the estimation of the heating and the cooling loads of a closed-span greenhouse: a case study in Korea. *Journal of Mechanical Science and Technology, 35*(1), 333-341.

Lu, W., Hu, Y., Zhou, S., Zhang, X., Yuan, Q., Zhou, X., Liu, H., Hu, J., Yang, Q., Zheng, Y., & Zheng, Y. (2020). Experimental verification of a CFD model for the closed plant factory under artificial lighting. *E3S Web Conf., 213*, 03013. Retrieved from https://doi.org/10.1051/e3sconf/202021303013

Ma, J., Du, X., Meng, S., Ding, J., Gu, X., Zhang, Y., Li, T., & Wang, R. (2022). Simulation of Thermal Performance in a Typical Chinese Solar Greenhouse. *Agronomy, 12*(10). doi:10.3390/agronomy12102255

Magni, M., Ochs, F., de Vries, S., Maccarini, A., & Sigg, F. (2021). Detailed cross comparison of building energy simulation tools results using a reference office building as a case study. *Energy and buildings, 250*, 111260. doi:https://doi.org/10.1016/j.enbuild.2021.111260

Marcelis, L. F. M., Broekhuijsen, A. G. M., Meinen, E., Nijs, E. M. F. M., & Raaphorst, M. G. M. (2006). *QUANTIFICATION OF THE GROWTH RESPONSE TO LIGHT QUANTITY OF GREENHOUSE GROWN CROPS.*

Marie, T. R. J. G., Leonardos, E. D., Lanoue, J., Hao, X., Micallef, B. J., & Grodzinski, B. (2022). A Perspective Emphasizing Circadian Rhythm Entrainment to Ensure

Sustainable Crop Production in Controlled Environment Agriculture: Dynamic Use of LED Cues. *Frontiers in Sustainable Food Systems, 6*. doi:10.3389/fsufs.2022.856162

Mashonjowa, E., Ronsse, F., Milford, J. R., & Pieters, J. G. (2013). Modelling the thermal performance of a naturally ventilated greenhouse in Zimbabwe using a dynamic greenhouse climate model. *Solar Energy, 91*, 381-393. doi:10.1016/j.solener.2012.09.010

Mazzeo, D., Baglivo, C., Panico, S., & Congedo, P. M. (2021). Solar greenhouses: Climates, glass selection, and plant well-being. *Solar Energy, 230*, 222-241.

McCree, K. J. (1971). The action spectrum, absorptance and quantum yield of photosynthesis in crop plants. *Agricultural Meteorology, 9*, 191-216.

McHale, M., Friedman, J., & Karian, J. (2009). Standard for verification and validation in computational fluid dynamics and heat transfer. *The American Society of Mechanical Engineers, ASME V&V, 20*, 100.

Menter, F. (1993). *Zonal two equation kw turbulence models for aerodynamic flows.* Paper presented at the 23rd fluid dynamics, plasmadynamics, and lasers conference.

Millette, J., Sansregret, S., & Daoud, A. (2011). *SIMEB: simplified interface to DOE2 and Energy Plus–A user's perspective–Case study of an existing building.* Paper presented at the Building Simulation 2011.

Mohammadi, S., Khalife, E., Kaveh, M., Sayyah, A. H. A., Nikbakht, A. M., Szymanek, M., & Dziwulski, J. (2021). Comparison of Optimized and Conventional Models of Passive Solar Greenhouse—Case Study: The Indoor Air Temperature, Irradiation, and Energy Demand. *Energies, 14*(17), 5369.

Mohd Noh, A., Mohamad Tahir, M.A., Mat, S., & Dzulkifli, M. H. (2020). CFD simulation of temperature and airflow inside a shipping container size plant factory for optimal lettuce production. *Food Research, 4*, 56-59.

Mohsenipour, M., Ebadollahi, M., Rostamzadeh, H., & Amidpour, M. (2020). Design and evaluation of a solar-based trigeneration system for a nearly zero energy greenhouse in arid region. *Journal of Cleaner Production, 254*, 119990. doi:https://doi.org/10.1016/j.jclepro.2020.119990

Molina, J., Ponce, M., Horn, M., & Gómez, M. (2019). *Towards a sustainable bioclimatic approach for the Peruvian high Andean rural area: Evaluation of the thermal contribution of a greenhouse attached to a dwelling.* Paper presented at the Proc. ISES Sol. World Congr. 2019 IEA SHC Int. Conf. Sol. Heat. Cool. Build. Ind.

Monje, O. (1998). Predicting transpiration rates of hydroponically-grown plant communities in controlled environments.

Monteith, J. (1981). Evaporation and surface temperature. *Quarterly Journal of the Royal Meteorological Society, 107*(451), 1-27.

Muñoz-Liesa, J., Royapoor, M., Cuerva, E., Gassó-Domingo, S., Gabarrell, X., & Josa, A. (2022). Building-integrated greenhouses raise energy co-benefits through active ventilation systems. *Building and Environment, 208*, 108585. doi:https://doi.org/10.1016/j.buildenv.2021.108585

Nadal, A., Llorach-Massana, P., Cuerva, E., López-Capel, E., Montero, J. I., Josa, A., Rieradevall, J., & Royapoor, M. (2017). Building-integrated rooftop greenhouses: An energy and environmental assessment in the mediterranean context. *Applied Energy, 187*, 338-351.

Naranjani, B., Najafianashrafi, Z., Pascual, C., Agulto, I., & Chuang, P.-Y. A. (2022). Computational analysis of the environment in an indoor vertical farming system. *International Journal of Heat and Mass Transfer, 186*, 122460. doi:https://doi.org/10.1016/j.ijheatmasstransfer.2021.122460

Natarajan, G., Zaid, M., Konka, H., Srinivasan, R., Ramanathan, S. S., Ahmed, T., & Chowdhury, H. (2022). *Modeling of air distribution inside a shipping container plant factory using computational fluid dynamics (CFD).* Paper presented at the AIP Conference Proceedings.

Nayak, S., & Tiwari, G. N. (2008). Energy and exergy analysis of photovoltaic/thermal integrated with a solar greenhouse. *Energy and buildings, 40*(11), 2015-2021. doi:https://doi.org/10.1016/j.enbuild.2008.05.007

Nebbali, R., Roy, J., & Boulard, T. (2012). Dynamic simulation of the distributed radiative and convective climate within a cropped greenhouse. *Renewable Energy, 43*, 111-129.

Nelson, J. A., & Bugbee, B. (2014). Economic analysis of greenhouse lighting: light emitting diodes vs. high intensity discharge fixtures. *PLoS One, 9*(6), e99010.

Neymark, J., Judkoff, R., Kummert, M., Muehleisen, R., Johannsen, A., Kruis, N., Glazer, J., Henninger, R., Witte, M., & Ono, E. (2020). *Update of ASHRAE Standard 140 Section 5.2 and Related Sections (BESTEST Building Thermal Fabric Test Cases)*. Retrieved from

Niam, A., Muharam, T., Widodo, S., Solahudin, M., & Sucahyo, L. (2019a). *CFD simulation approach in determining air conditioners position in the mini plant factory for shallot seed production.* Paper presented at the AIP Conference Proceedings.

Niam, A., Widodo, S., Solahudin, M., Sucahyo, L., & Nurjanah, S. (2019b). *Tracer study of CO2 enrichment for shallot growth in mini plant factory with CFD approach.* Paper presented at the IOP Conference Series: Earth and Environmental Science.

Niam, A. G., Muharam, T. R., Widodo, S., Solahudin, M., & Sucahyo, L. (2019c). CFD simulation approach in determining air conditioners position in the mini plant factory for shallot seed production. *AIP Conference Proceedings, 2062*(1), 020017. doi:10.1063/1.5086564

Obyn, S., & van Moeseke, G. (2015). Variability and impact of internal surfaces convective heat transfer coefficients in the thermal evaluation of office buildings. *Applied Thermal Engineering, 87*, 258-272. doi:https://doi.org/10.1016/j.applthermaleng.2015.05.030

Ogunlowo, Q. O., Na, W. H., Rabiu, A., Adesanya, M. A., Akpenpuun, T. D., Kim, H. T., & Lee, H. W. (2022). Effect of envelope characteristics on the accuracy of discretised greenhouse model in TRNSYS. *Journal of Agricultural Engineering, 53*(3).

Okayama, T., Okamura, K., Park, J.-E., Ushada, M., & Murase, H. (2008a). A Simulation for Precision Airflow Control using Multi-Fan in a Plant Factory. *Environmental Control in Biology, 46*(3), 183-194. doi:10.2525/ecb.46.183

Okayama, T., Okamura, K., Park, J. E., Ushada, M., & Murase, H. (2008b). A simulation for precision airflow control using multi-fan in a plant factory. *Environmental Control in Biology, 46*(3), 183-194. doi:10.2525/ecb.46.183

Ouazzani Chahidi, L., & Mechaqrane, A. (2022). Greenhouse Design Selection in Moroccan Climatic Conditions. In *WITS 2020* (pp. 639-648): Springer.

Pakari, A., & Ghani, S. (2022). Regression equation for estimating the maximum cooling load of a greenhouse. *Solar Energy, 237*, 231-238. doi:https://doi.org/10.1016/j.solener.2022.04.006

Peeters, L., Beausoleil-Morrison, I., & Novoselac, A. (2011). Internal convective heat transfer modeling: Critical review and discussion of experimentally derived correlations. *Energy and buildings, 43*(9), 2227-2239. doi:https://doi.org/10.1016/j.enbuild.2011.05.002

Penman, H. L. (1948). Natural evaporation from open water, bare soil and grass. *Proceedings of the Royal Society of London. Series A. Mathematical and Physical Sciences, 193*(1032), 120-145.

Pieters, J. G., & Deltour, J. M. (1997). Performances of Greenhouses with the Presence of Condensation on Cladding Materials. *Journal of Agricultural Engineering Research, 68*(2), 125-137. doi:https://doi.org/10.1006/jaer.1997.0187

Pieters, J. G., & Deltour, J. M. (1999). Modelling solar energy input in greenhouses. *Solar Energy, 67*(1-3), 119-130.

Pineda, I. T., Lee, Y. D., Cho, J., & Lee, S. M. (2020). *Environmental impacts of heating in a conventional greenhouse and a rooftop greenhouse for fresh tomato production.* Paper presented at the ECOS 2020 - Proceedings of the 33rd International Conference on

Efficiency, Cost, Optimization, Simulation and Environmental Impact of Energy Systems.

Piscia, D., Montero, J., Bailey, B., Muñoz, P., & Oliva, A. (2013). A new optimisation methodology used to study the effect of cover properties on night-time greenhouse climate. *Biosystems engineering, 116*(2), 130-143.

Piscia, D., Montero, J., Melé, M., Flores, J., Perez-Parra, J., & Baeza, E. (2011). *A CFD model to study above roof shade and on roof shade of greenhouses.* Paper presented at the International Symposium on Advanced Technologies and Management Towards Sustainable Greenhouse Ecosystems: Greensys2011 952.

Pocock, T. (2016). Advanced lighting technology in controlled environment agriculture. *Lighting Research & Technology, 48*(1), 83-94. doi:10.1177/1477153515622681

Rabiu, A., Na, W.-H., Akpenpuun, T. D., Rasheed, A., Adesanya, M. A., Ogunlowo, Q. O., Kim, H. T., & Lee, H.-W. (2022). Determination of overall heat transfer coefficient for greenhouse energy-saving screen using Trnsys and hotbox. *Biosystems Engineering, 217*, 83-101.

Rao, S. S. (2019). Modern Methods of Optimization. In *Engineering Optimization Theory and Practice* (pp. 633-672).

Rasheed, A., Kim, H. T., & Lee, H. W. (2022). Modeling-Based Energy Performance Assessment and Validation of Air-To-Water Heat Pump System Integrated with Multi-Span Greenhouse on Cooling Mode. *Agronomy, 12*(6), 1374.

Rasheed, A., Kwak, C. S., Kim, H. T., & Lee, H. W. (2020a). Building energy and simulation model for analyzing energy saving options of multi-span greenhouses. *Applied Sciences, 10*(19), 6884.

Rasheed, A., Kwak, C. S., Na, W. H., Lee, J. W., Kim, H. T., & Lee, H. W. (2020b). Development of a building energy simulation model for control of multi-span greenhouse microclimate. *Agronomy, 10*(9), 1236.

Rasheed, A., Lee, J. W., & Lee, H. W. (2017). Development of a model to calculate the overall heat transfer coefficient of greenhouse covers. *Spanish Journal of Agricultural Research, 15*(4). doi:10.5424/sjar/2017154-10777

Rasheed, A., Lee, J. W., & Lee, H. W. (2018). Development and Optimization of a Building Energy Simulation Model to Study the Effect of Greenhouse Design Parameters. *Energies, 11*(8), 2001. Retrieved from https://www.mdpi.com/1996-1073/11/8/2001

Rasheed, A., Na, W. H., Lee, J. W., Kim, H. T., & Lee, H. W. (2019). Optimization of greenhouse thermal screens for maximized energy conservation. *Energies, 12*(19), 3592.

Rasheed, A., Na, W. H., Lee, J. W., Kim, H. T., & Lee, H. W. (2021). Development and validation of air-to-water heat pump model for greenhouse heating. *Energies, 14*(15), 4714.

Reynolds, O. (1895). IV. On the dynamical theory of incompressible viscous fluids and the determination of the criterion. *Philosophical Transactions of the Royal Society of London. (A.), 186*, 123-164. doi:doi:10.1098/rsta.1895.0004

Rincón-Casado, A., & Sánchez de la Flor, F. J. (2018). 3D internal forced convection heat-transfer correlations from CFD for building performance simulation. *Engineering Applications of Computational Fluid Mechanics, 12*(1), 553-566. doi:10.1080/19942060.2018.1476267

Rincón-Casado, A., Sánchez de la Flor, F. J., Chacón Vera, E., & Sánchez Ramos, J. (2017). New natural convection heat transfer correlations in enclosures for building performance simulation. *Engineering Applications of Computational Fluid Mechanics, 11*(1), 340-356. doi:10.1080/19942060.2017.1300107

Roy, J., Pouillard, J., Boulard, T., Fatnassi, H., & Grisey, A. (2013). *Experimental and CFD results on the CO2 distribution in a semi closed greenhouse.* Paper presented at the International Symposium on New Technologies for Environment Control, Energy-Saving and Crop Production in Greenhouse and Plant 1037.

Roy, J. C., Boulard, T., Kittas, C., & Wang, S. (2002). Convective and ventilation transfers in greenhouses, part 1: The greenhouse considered as a perfectly stirred tank. *Biosystems Engineering, 83*(1), 1-20. doi:10.1006/bioe.2002.0107

Saberian, A., & Sajadiye, S. M. (2019). The effect of dynamic solar heat load on the greenhouse microclimate using CFD simulation. *Renewable Energy, 138*, 722-737.

Sayyah, A. H. A., Mohammadi, S., Nikbakht, A. M., & Khalife, E. (2020). Modeling and Design a Special Type of Passive Solar Greenhouse in Cold Climate by TRNSYS. *Journal of Agricultural Sciences, 26*(4), 488-498.

Scott, N. R., Rutzke, C. J., & Albright, L. D. (2005). Energy conversion options for energy-efficient controlled environment agriculture. *HortScience, 40*(2), 287-292.

Semple, L., Carriveau, R., & Ting, D. S. K. (2017a). Assessing heating and cooling demands of closed greenhouse systems in a cold climate. *International Journal of Energy Research, 41*(13), 1903-1913.

Semple, L., Carriveau, R., & Ting, D. S. K. (2017b). A techno-economic analysis of seasonal thermal energy storage for greenhouse applications. *Energy and buildings, 154*, 175-187. doi:10.1016/j.enbuild.2017.08.065

Semple, L. M., Carriveau, R., & Ting, D. S. K. (2018). Potential for large-scale solar collector system to offset carbon-based heating in the Ontario greenhouse sector. *International Journal of Sustainable Energy, 37*(4), 378-392. doi:10.1080/14786451.2016.1270946

Sliney, D. H. (2016). What is light? The visible spectrum and beyond. *Eye, 30*(2), 222-229. doi:10.1038/eye.2015.252

Standard Practice for Estimation of Heat Gain or Loss Through Ceilings Under Attics Containing Radiant Barriers by Use of a Computer Program. [1 online resource]. Retrieved from https://doi.org/10.1520/C1340_C1340M-10R21

Stanghellini, C. (1987). *Transpiration of greenhouse crops: an aid to climate management*: Wageningen University and Research.

Strachan, P., Kokogiannakis, G., & Macdonald, I. (2008). History and development of validation with the ESP-r simulation program. *Building and Environment, 43*(4), 601-609.

Talbot, M.-H., & Monfet, D. (2020). Estimating the impact of crops on peak loads of a Building-Integrated Agriculture space. *Science and Technology for the Built Environment, 26*(10), 1448-1460. doi:10.1080/23744731.2020.1806594

Talbot, M.-H., & Monfet, D. (2024). Analysing the influence of growing conditions on both energy load and crop yield of a controlled environment agriculture space. *Applied Energy, 368*, 123406. doi:https://doi.org/10.1016/j.apenergy.2024.123406

Talbot, M.-H., Monfet, D., Lalonde, T., & Haillot, D. (2021). *Impact of modelling thermal phenomena in a high-density controlled environment agriculture (CEA-HD) space*. Paper presented at the Proceedings of Building Simulation 2021: 17th Conference of IBPSA.

Tei, F., Scaife, A., & Aikman, D. P. (1996). Growth of Lettuce, Onion, and Red Beet. 1. Growth Analysis, Light Interception, and Radiation Use Efficiency. *Annals of botany, 78*(5), 633-643. doi:10.1006/anbo.1996.0171

Thomas, Y., Wang, L., & Denzer, A. (2017). *Energy savings analysis of a greenhouse heated by waste heat.* Paper presented at the Building Simulation Conference Proceedings.

Tian, C., Shao, Z., Wang, R., Yan, Y., Wang, X., & Ren, A. (2022). Optimal Design of Integrated Energy Supply System for Continuous Greenhouse Effect: A Study on Carbon Emission and Operational Cost. *Planning and Operation of Hybrid Renewable Energy Systems*, 845637128.

Torres Pineda, I., Cho, J. H., Lee, D., Lee, S. M., Yu, S., & Lee, Y. D. (2020). Environmental impact of fresh tomato production in an urban rooftop greenhouse in a humid continental climate in South Korea. *Sustainability, 12*(21), 9029.

Treethidtaphat, W., Kittipiyakul, S., Kaemarungsi, K., & Isshiki, T. (2015). *An investment decision support tool for horticulture with an adaptive energy management system.* Paper presented at the 2015 6th International Conference of Information and Communication Technology for Embedded Systems (IC-ICTES).

UN. (2015). World population prospects: The 2015 revision, key findings and advance tables. *Working PaperNo*.

University of Wisconsin--Madison. Solar Energy, L. (1975). *TRNSYS, a transient simulation program*: Madison, Wis. : The Laboratory, 1975.

Vadiee, A., & Martin, V. (2012). Energy management in horticultural applications through the closed greenhouse concept, state of the art. *Renewable and Sustainable Energy Reviews, 16*(7), 5087-5100. doi:https://doi.org/10.1016/j.rser.2012.04.022

Vadiee, A., & Martin, V. (2013). Energy analysis and thermoeconomic assessment of the closed greenhouse – The largest commercial solar building. *Applied Energy, 102*, 1256-1266. doi:https://doi.org/10.1016/j.apenergy.2012.06.051

Vadiee, A., Yaghoubi, M., Martin, V., & Bazargan-Lari, Y. (2016). Energy analysis of solar blind system concept using energy system modelling. *Solar Energy, 139*, 297-308. doi:https://doi.org/10.1016/j.solener.2016.09.039

Villarreal-Guerrero, F., Kacira, M., Fitz-Rodríguez, E., Kubota, C., Giacomelli, G. A., Linker, R., & Arbel, A. (2012). Comparison of three evapotranspiration models for a greenhouse cooling strategy with natural ventilation and variable high pressure fogging. *Scientia Horticulturae, 134*, 210-221. doi:https://doi.org/10.1016/j.scienta.2011.10.016

Walton, G. N. (1983). Thermal analysis research program reference manual.

Wang, Y., Du, J., & Li, D. (2020). *An investigation into PAR (Photosynthetically active radiation) and energy performances in small-scale greenhouses in Northern China.* Paper presented at the Proceedings of the ISES Solar World Congress 2019 and IEA SHC International Conference on Solar Heating and Cooling for Buildings and Industry 2019.

Ward, R., Choudhary, R., Cundy, C., Johnson, G., & McRobie, A. (2015). *Simulation of plants in buildings; incorporating plant-Air interactions in building energy simulation.* Paper presented at the 14th International Conference of IBPSA-Building Simulation 2015, BS 2015, Conference Proceedings.

Watson, D. J. (1947). Comparative physiological studies on the growth of field crops: I. Variation in net assimilation rate and leaf area between species and varieties, and within and between years. *Annals of botany, 11*(41), 41-76.

Weidner, T., Yang, A., & Hamm, M. W. (2021). Energy optimisation of plant factories and greenhouses for different climatic conditions. *Energy Conversion and Management, 243*, 114336. doi:https://doi.org/10.1016/j.enconman.2021.114336

Wetter, M., Benne, K., Tummescheit, H., & Winther, C. (2023). Spawn: coupling Modelica Buildings Library and EnergyPlus to enable new energy system and control applications. *Journal of Building Performance Simulation*, 1-19.

Wilcox, D. C. (1988). Reassessment of the scale-determining equation for advanced turbulence models. *AIAA journal, 26*(11), 1299-1310.

Wilcox, D. C. (1993). *Turbulence modeling for CFD*. La Canada, Calif.: DCW Industries.

Wohlfahrt, G., & Gu, L. (2015). The many meanings of gross photosynthesis and their implication for photosynthesis research from leaf to globe. *Plant, cell & environment, 38*(12), 2500.

Yang, G., Shi, H., Xu, D., Shen, Z., Zhang, Z., Shen, H., & Wang, Z. (2021). *Research on simulation of energy consumption of ground water-source heat pump air conditioning system in plant factory.* Paper presented at the IOP Conference Series: Earth and Environmental Science.

Yang, W., Du, J., & Li, D. (2020). *A Simulation Study of Typical Greenhouses in Beijing: PAR (Photosynthetically Active Radiation) Performances and Energy Consumption.* Paper presented at the PROCEEDINGS OF BUILDING SIMULATION 2019: 16TH CONFERENCE OF IBPSA.

Yeo, U.-H., Lee, S.-Y., Park, S.-J., Kim, J.-G., Choi, Y.-B., Kim, R.-W., Shin, J. H., & Lee, I.-B. (2022). Rooftop Greenhouse: (1) Design and Validation of a BES Model for a Plastic-Covered Greenhouse Considering the Tomato Crop Model and Natural Ventilation Characteristics. *Agriculture, 12*(7), 903. Retrieved from https://www.mdpi.com/2077-0472/12/7/903

Yildirim, N., & Bilir, L. (2017). Evaluation of a hybrid system for a nearly zero energy greenhouse. *Energy Conversion and Management, 148*, 1278-1290. doi:https://doi.org/10.1016/j.enconman.2017.06.068

Zhang, G., Fu, Z., Yang, M., Liu, X., Dong, Y., & Li, X. (2019a). Nonlinear simulation for coupling modeling of air humidity and vent opening in Chinese solar greenhouse based on CFD. *Computers and Electronics in Agriculture, 162*, 337-347. doi:https://doi.org/10.1016/j.compag.2019.04.024

Zhang, L., Xu, P., Mao, J., Tang, X., Li, Z., & Shi, J. (2015). A low cost seasonal solar soil heat storage system for greenhouse heating: Design and pilot study. *Applied Energy, 156*, 213-222. doi:https://doi.org/10.1016/j.apenergy.2015.07.036

Zhang, X., Zhang, F., Li, M., Zhang, Z., & Liu, W. (2019b). Design and applications of multichannel photosynthetic photon flux density sensor for artificial lighting. *Optical Engineering, 58*, 1. doi:10.1117/1.OE.58.2.027105

Zhang, Y., & Kacira, M. (2018). *Analysis of environmental uniformity in a plant factory using computational fluid dynamics (CFD) analysis*.

Zhang, Y., & Kacira, M. (2020). Comparison of energy use efficiency of greenhouse and indoor plant factory system. *European Journal of Horticultural Science, 85*(5), 310-320.

Zhang, Y., & Kacira, M. (2022). Analysis of climate uniformity in indoor plant factory system with computational fluid dynamics (CFD). *Biosystems Engineering, 220*, 73-86. doi:https://doi.org/10.1016/j.biosystemseng.2022.05.009

Zhang, Y., Kacira, M., & An, L. (2016). A CFD study on improving air flow uniformity in indoor plant factory system. *Biosystems engineering, 147*, 193-205. doi:https://doi.org/10.1016/j.biosystemseng.2016.04.012

Zhen, S., van Iersel, M., & Bugbee, B. (2021). Why far-red photons should be included in the definition of photosynthetic photons and the measurement of horticultural fixture efficacy. *Frontiers in Plant Science, 12*, 1158.

Zhou, S., Liu, H., Fan, R., He, Z., Zhang, Y., Chen, Y., Sun, X., Zhou, X., Yang, Q., & Zheng, Y. (2020a). *Temperature field simulation using CFD in the plant factory.* Paper presented at the IOP Conference Series: Earth and Environmental Science.

Zhou, S., Zhang, X., He, Z., Liu, H., Liu, K., Chen, Y., Peng, F., Yang, Q., Zheng, Y., & Lu, W. (2020b). *Experimental validation of CFD model with the air velocity and temperature in the plant factory.* Paper presented at the IOP Conference Series: Earth and Environmental Science.